DESIGN OPTIMISATION OF A CANE HAULAGE VEHICLE

Simon L. Cowling

Submitted in fulfillment of the requirements for the degree of

Master of Science in Engineering

In the

Mechanical Engineering Programme

University of KwaZulu-Natal.

15 February 2008

Supervisor: Prof. G. Bright

Co-Supervisor: Prof. P. Lyne

External Co-Supervisor: Prof. E. Morozov

Acknowledgments

I wish to thank my supervisors Prof. G. Bright, Prof. E. Morozov and Prof. P. Lyne for their support and guidance, as well as Mr. John Pilcher, for sharing his many years of experience and assisting with this project.

I thank my family and friends for their understanding and support.

I gratefully acknowledge the support of the South African Sugar Research Institute (SASRI), a bursary from the National Department of Transport via the Eastern Centre of Transport Development (ECOTD) and a grant from the National Research Foundation (South Africa) to enable this research to be undertaken.

Lastly, I would like to thank the staff at the Faculty of Engineering, U.K.Z.N., and everyone else who assisted in any way with this project.

Preface

I, Simon Linden Cowling, hereby declare that the whole of this dissertation is my own work and has not been submitted in part or in whole to any other University. Where use has been made of the work of others, it had been duly acknowledged in the text.

_____ _____

(Signature of Candidate) Date

_____ _____

(Signature of Supervisor) Date

Abstract

The sugar industry transports in excess of 20 million tons of sugarcane per annum, equating to approximately 800 000 road consignments. This entails substantial expenditure on vehicle capital and operational costs.

There exists substantial scope to redesign vehicle configurations to reduce the vehicles tare mass and optimise the process of cane transportation. These modifications could potentially save the industry approximately R136 million per annum, and in addition will increase a vehicles lifespan, performance and speed.

This project is one aspect of a larger project organised by the South African Sugarcane Research Institute, with the general aim of optimising the entire sugarcane transportation system. Aspects of this particular project include literature research as well as field investigation into the various sugarcane transportation systems in South Africa and throughout the world. The design of a cane haulage vehicle will be analysed and optimised, using tools such as finite element analysis.

The aims of this project include the investigation of the engineering design issues with respect to vehicle/trailer configurations, and the design of an optimised cane haulage vehicle which increases the efficiency of raw sugarcane transportation in South Africa.

Table of Contents

List of Figures

List of Tables

List of Symbols

b	Flange width
$\mathbf{c}$	Objective function vector
d	Web depth
l	Length of trailer section
m	Average mass per unit length
t_f	Flange thickness
t_w	Web thickness
w	Trailer width
$\mathbf{x}$	Design variable vector
D	Distance from the kingpin to the centre of the rear truck axle unit
E	Modulus of elasticity
G	Distance from the trailer connection frame to the centre of the rear truck axle unit
H	Height of trailer
P	Payload
R	Reaction at suspension unit
α	Angle between inclined section of trailer
ρ	Density
σ_T	Tensile strength
σ_y	Yield strength

Chapter 1 - Introduction

1.1 Introduction

1.1.1 The South African Sugar Industry

The South African sugar cane industry consists of 47 000 registered cane-growers, producing about 21 million tons of raw sugar cane per season from 14 mill supply areas [1]. This results in approximately 2.5 million tons of high quality sugar per annum produced by the six mill operating companies. Approximately 50% of this is sold through the Southern Africa Custom's Union (SACU). The remainder is exported to numerous markets in Africa, the Middle East, North America and Asia; contributing R2 billion to the country's foreign exchange earnings [2].

Sugar cane is grown and processed in many areas in South Africa, its geographical focus extending from North Pondoland in the Eastern Cape through KwaZulu-Natal to Mpumalanga [3]. In addition to producing high quality sugar, some sugar mills produce a variety of downstream products, including ethyl alcohol and furfural [3].

1.1.2 Project Background

Research into cost analysis on transportation and other relevant costs of sugar cane production reveals that transportation has become a significant factor affecting the production costs of sugar [4]. The South African sugar industry transports in excess of 20 million tons of raw sugar cane per annum, resulting in approximately 800 000 road consignments. This entails substantial expenditure on vehicle capital and operational costs.

The South African Sugar cane Research Institute (SASRI) has implemented a full-scale investigation into the transport of raw sugar cane in an attempt to reduce the cost. The project includes many aspects of the entire transportation system, including logistics optimisation through the use of satellite vehicle tracking and scheduling, central tyre inflation systems, performance based standards and tare mass reduction

through design optimisation, which is the main focus of this thesis.

Tare mass reduction in a vehicle body can substantially reduce the costs associated with transport [5, 6]. Fuel economy alone has been shown to increase in the range of 0.034 kilometres/litre to 0.050 kilometres/litre, per 1000kg reduction in tare mass [7, 8]. Related industries (for example the South African timber industry) have obtained large reductions in transportation costs through decreasing the tare mass of haulage vehicles.

To investigate the effect of tare mass reduction on the cost of transportation in this particular case, a simulation is carried out using HTM TransSolve. HTM TransSolve is a logistics software package, used for various transport and logistics-related calculations [9]. A simple simulation of a haulage vehicle collecting cane from a farm and delivering to a mill 16.2 kilometres away is run. The fixed costs, such as license fees and overheads, are constant and the simulation is run with a standard trailer loaded to legal capacity, and a trailer with a tare mass reduced by 8.54% loaded to legal capacity (see Appendix I). The results showed that the total cost of transportation was reduced from 19.67 Rand/ton to 18.53 Rand/ton, or a saving of 5.8%, which is substantial when the volume of cane transportation is considered. This figure is an indication of the possible cost reduction, as factors such as distance, cane density, vehicle finance and offloading time all affect the overall cost of transportation.

The aim of this project is to investigate the current status of vehicles utilised for raw sugar cane transportation, and to optimise and analyse the selected design using finite element analysis (FEA). The finite element method has become an important tool for analysing vehicle structures, and has proven to be extremely valuable to the heavy vehicle industry [10]. FEA has been used in various design aspects of heavy vehicles, for example [11, 12], and to successfully reduce the tare mass of heavy vehicles [6, 13] with weight savings ranging from 11% to 25%.

1.2 General Methods of Sugar Cane Transportation

1.2.1 Introduction

Methods of sugar cane transportation vary according to many factors, including a particular region's infrastructure, road regulations and topography. The two primary methods are road and rail haulage. Loading and offloading methods vary from region to region, and also depend on the type of haulage vehicle.

1.2.2 U.S.A.

Sugar cane is grown in 16 states across the U.S.A., and is mechanically harvested. The primary modes of transport are large highway trailers and rail. Cane is typically removed from the field with four-wheel drive tractors, hauling about 16 tons using a 4 wagon load. The cane is then loaded onto highway trailers or railway cars, carrying about 20 tons each. The cane is offloaded using various systems, including one where the entire semi-trailer rig is tilted backwards to remove the cane.

1.2.3 Australia

Sugar is one of Australia's largest export crops, and is cultivated along the coastline of Northern Queensland and Northern New South Wales. Cane is mechanically planted and harvested. The primary method of transportation is rail, with a narrow gauge railway line network that connects the growing areas directly to the mills. The cane is loaded onto rail cars from the field and offloaded at the mill. This results in a harvest to crush delay of no more than 16 hours, which is highly desirable as the sugar content of the cane decreases after it has been cut, resulting in decreased yield.

1.2.4 Brazil

Brazil produces more than 300 million tons of sugar per annum, cultivated mainly in the north-eastern coastal region. The cane is harvested using mechanical and manual

methods, and is primarily transported with road haulage vehicles. Road regulations such as axle load limits tend to be less strictly enforced, resulting in overloaded vehicles and decreased transportation costs. A unique aspect of the Brazilian sugar cane transportation system is that ethanol manufactured at downstream plants at sugar mills is added to the fuel used to power the trucks, resulting in a more economical transportation system.

1.2.5 Malawi

Sugar is primarily grown in the south-central regions of Malawi, and is harvested manually. Due to the fact that the majority of transportation occurs over private land, large road trains that would be illegal on public roads are extensively used in Malawi.

1.2.6 South Africa

Sugar cane in South Africa is primarily manually harvested. This can be attributed to the abundance of relatively low cost labour, and the steep topography of the cane fields which limits accessibility of large harvesting machinery. The cane is either burnt prior to cutting, or is harvested green. Burning removes the leaves, tops and shoots, allowing for a higher density cargo.

After cutting, the cane is either laid in windrows (long continuous rows), or placed into bundles of approximately 5 tons, which are secured with chains. A three-wheeled mobile crane loads the cane (similar to a smaller version of those used to those used to shift scrap-metal and other bulk items), either loose from the windrows or bundled into the transport vehicles.

The manner in which cane is transported to the mill depends on the location of the field with respect to the mill, and the infrastructure and terrain between the two. Generally, the cane is taken from the field to a loading zone with agricultural tractors and trailers, where it is loaded onto large road going truck-trailer combination. If the terrain permits, a large road going truck-trailer combination will be directly loaded

infield. If the cane field is close to a mill, the cane can be directly transported with agricultural tractors. Rail transportation is also used, but is severely limited by the steep terrain that occurs in many of the growing areas.

The cane is offloaded through a number of methods, which vary from mill to mill. The most common is the Hilo unloading mechanism (see Figure 1.1.) The truck is positioned between a wall and the offloading mechanism. The side of the trailer is clamped, and a lifting rig is lowered and hooked under the spiller bar. Chains, which are attached to the spiller bar, run underneath the cane and are attached to the other side of the trailer. As the lifting rig and spiller bar are raised, the cane is spilled over the side of the trailer onto a conveyer.

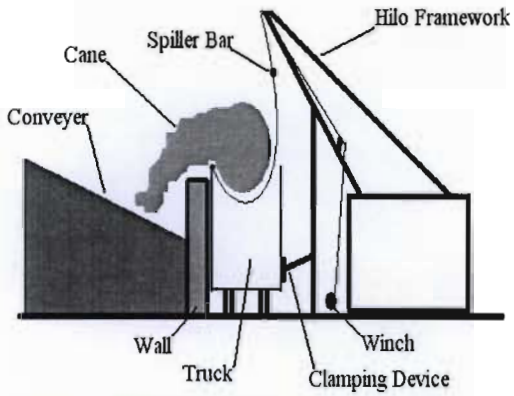

Figure 1.1 Schematic of an unloading station

An important aspect of the design arises from the lack of consistency with respect to the dimensions of the offloading apparatus. Generally the lifting rig lengths, spillage heights and placement of the hooks on the lifting rig vary from mill to mill, and some mills spill to the left while others spill to the right.

1.3 Current Vehicles Designs

1.3.1 Introduction

There are many vehicles currently being used in the transportation of sugar cane in South Africa. These include simple agricultural tractors with trailers, semi tri-axle

trailers (tridems), tandem/tandem interlink semi-trailers and rigid drawbar vehicles. The most common configurations are shown in Figures 1.2-1.4.

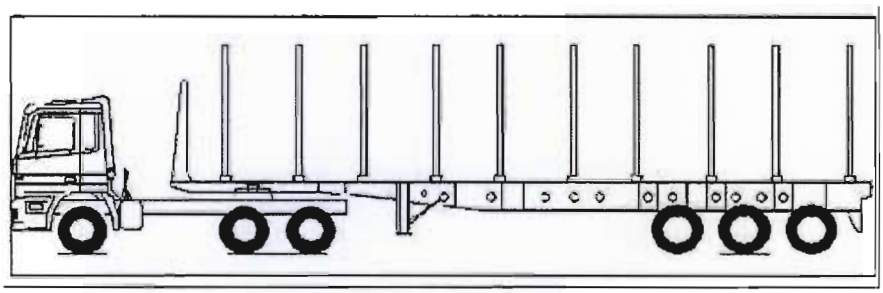

Figure 1.2 A typical tridem configuration

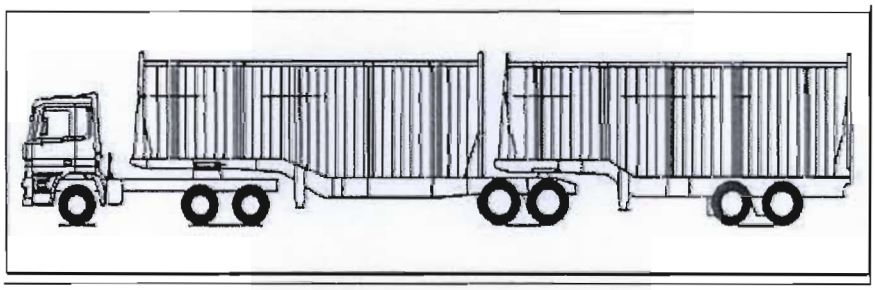

Figure 1.3 A typical tandem/tandem interlink configuration

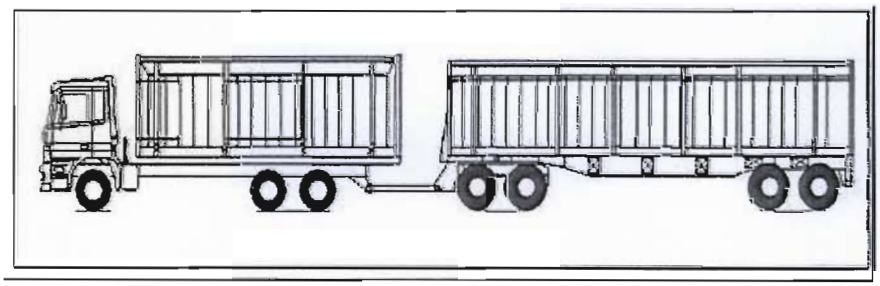

Figure 1.4 A typical rigid drawbar configuration

Tandem/tandem semi-trailer and rigid drawbar vehicles are capable of transporting large quantities of cane over large distances economically. The method of offloading these vehicles is predominantly through the use of a spiller bar system, shown in Figure 1.1. Although this system increases the tare mass of the vehicle, the majority

of sugar mills have infrastructure in place that can only unload this type of vehicle, with the exception of bundled cane.

1.3.2 Vehicle Mass Analysis

Ten vehicles from various manufacturers that are currently in use in South Africa were analysed to determine the mass of various components and the maximum payload. The results of this analysis are summarised in Table 1.1. The payload index is defined as the maximum payload divided by the tare mass of the vehicle, and is used as a rough measure of transport efficiency.

Table 1.1 Vehicle mass analysis

Truck	Tare (Kg)	Payload (Kg)	Payload Index	Type
1	19930	38870	1.95	Rigid Drawbar
2	22786	33214	1.46	Tand/Tand I-Link
3	23160	32840	1.42	Tand/Tand I-Link
4	17842	40000	2.24	Tand/Tand I-Link(timber)
5	18388	30170	1.64	Tridem Spiller
6	22119	33881	1.53	Tand/Tand I-Link
7	19740	36260	1.84	Rigid Drawbar
8	12380	28000	2.26	Tridem (timber)
9	19954	36046	1.81	Tand/Tand I-Link
10	23575	32500	1.38	Tand/Tand I-Link
Avg (of cane vehicles only)	21206	34223	1.63	

A single tri-axle trailer was ruled out as a possibility because, although they can be effective for short haulage distances, they generally cannot haul the same quantity of cane, and they are not as effective for medium to long distances as tandem/tandem interlink and rigid drawbar vehicles. Two timber haulage vehicles were included in the analysis for comparison, and generally tend to have a higher payload index due to the nature of the cargo. Timber vehicles require only light retaining bolsters on the sides of the chassis to hold the cargo, whereas sugar cane vehicles require a form enclosure to retain the sugar cane. From Table 1.1, it can be seen that a rigid drawbar

can transport a larger quantity of cane when compared to a tandem/tandem interlink. The harvesting season occurs through a relatively short period of the year. The horse of a tandem/tandem semi-trailer can be used for other goods transportation during the rest of the year, and the trailer is easily adaptable to accommodate other products. This resulted in a tandem/tandem semi-trailer, as in Figure 1.3, forming the basis of the design.

1.3.3 Mass Breakdown Analysis

To analyse the mass, and therefore the possible mass savings, of each component of a truck chassis, a mass breakdown analysis is performed for 10 cane haulage vehicles currently in use in South Africa (see Appendix II). The mass breakdown of a typical tandem/tandem interlink is shown in Figure 1.5.

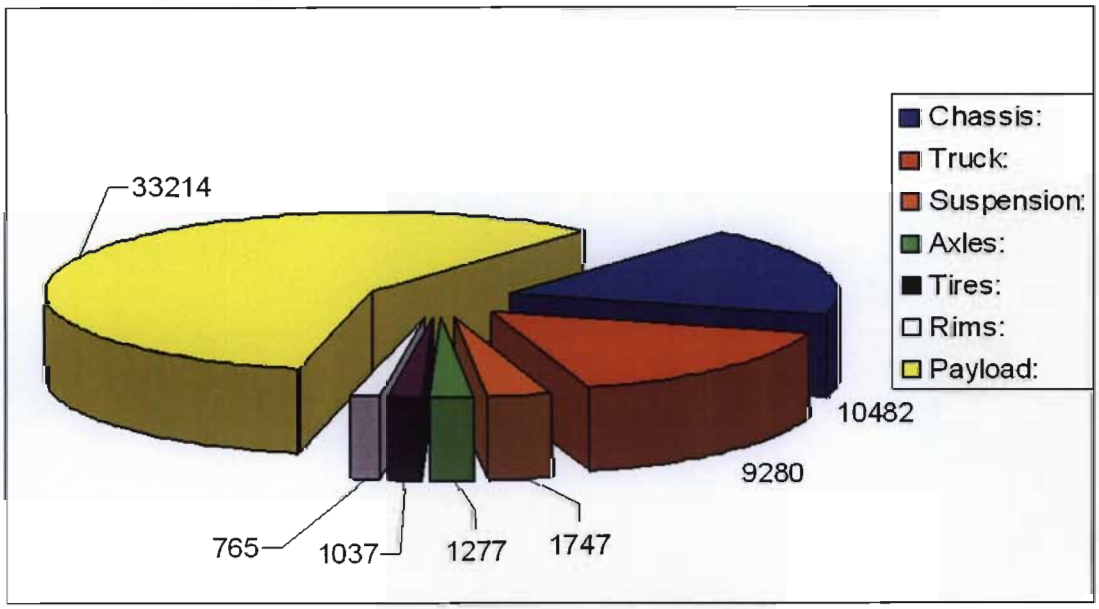

Figure 1.5 Mass breakdown of a typical interlink vehicle

From Figure 1.5, it is evident that the trailer chassis and truck make up the majority of the tare mass of the vehicle. The truck, or prime mover, is a standardised unit, and is not the focus of this project. The main aim is to reduce the tare mass of the overall vehicle. The greatest potential mass saving is through reducing the mass of the trailer chassis. The other components could yield potential tare mass reduction through the

use of lightweight components, such as aluminium rims and hollow axles.

1.4 Vehicle Operation Conditions (Harvest-to-Mill Delivery System)

1.4.1 Introduction

Vehicle operation conditions have been analysed using the data obtained from the field trips to the Sezela Sugar Mill which is operated by Illovo Sugar Limited, and is located on the South Coast of KwaZulu-Natal. The mill processes about two million tons of raw sugar cane per year, accounting for approximately 10% of the sugar produced by the South African sugar industry [14]. The mill also features a downstream plant which produces various products such as furfural and nematicide.

The purpose of the visit is to observe the offloading process and obtain data relating to the transportation of raw sugar cane from the surrounding areas to the mill.

1.4.2 Offloading Procedure

The mill has three Hilo spiller offloading stations. Two stations offload directly onto feed conveyers that deliver the cane straight to the mill. The other offloads cane onto a dump zone that acts as a buffer to ensure a continuous supply of cane to the mill in the event of a disruption in delivery. This yard operation also handles bundles of cane.

A gantry crane is also used to offload certain trucks that do not have spiller bars and chains. These include agricultural tractors with trailers and trucks carrying cane which is bundled in chains. It must be noted that this offloading process is by far the minority practice at Sezela (less than 5% in 2005).

A truck approaches the spilling station and comes to a halt. The operator then shifts a hydraulic mechanism forwards that clamps the trailer ensuring it will not tip over

during spilling. A bar with a number of steel hooks is then lowered under the spiller bar and raised until the spiller bar is firmly hooked. On the control towers signal, the operator lifts the spiller bar, which spills the raw cane over onto a conveyer which leads into the mill.

1.4.3 Comparison of Bolster and Frame-Type trailers

It was noticed that during the offloading procedure the trailers that had a bolster structure appeared easier to offload and needed less force to lift the spiller bar than trailers that had a frame-type structure.

(a) (b)

Figure 1.6 A bolster-type trailer (a), and a frame-type trailer (b)

Observing Figure 1.6(a) above, it can be noted that the bolster-type trailer has no horizontal or diagonal cross-members. While observing the offloading of various frame-type trailers (Figure 1.6(b)), cane was visibly getting stuck in the framework, thus increasing the force required to spill the cane. The geometric shape of the bolsters also seemed to influence the offloading process. The curved profile ensures that the cane slips out easier than if it were a sharp right-angle.

The fact that there is minimal area in contact with the cane, coupled with the lack of horizontal and diagonal cross-members, indicates that a bolster-type structure should be much easier to unload, with less stress on the unloading equipment and the trailer itself.

There are many factors that influence the amount of force required to spill the cane.

These include the way in which the cane is harvested (cut burnt or green), the manner in which the cane is loaded into the trailer and the size of the cane, in addition to geometry of the trailer.

If a number of different readings of the forces required to spill a trailer are taken from various frame and bolster-type trailers with varied cane conditions, it is hypothesised that the averages will show that the forces required to spill a bolster-type trailer are less than those required to spill a frame-type trailer.

To verify this, readings were taken from the two load cells which are located on the unloading structure. The load cells are calibrated on a regular basis using large water-filled plastic containers, and are used to indicate the forces acting on the spiller bar during the offloading process. The readings were taken for both the front and back trailers, and from each of the load cells.

Six readings for the front and back are taken from each type of trailer, and are summarised in Table 1.2:

Table 1.2 - Load cell readings for various bolster-type and frame-type trailers.

Trailer type	Bolster-type		Frame-type	
Trailer	Front (kN)	Back (kN)	Front (kN)	Back (kN)
	441.45	588.60	686.70	892.71
	480.69	451.26	804.42	794.61
	510.12	618.03	480.69	588.60
	382.59	500.31	794.61	696.51
	421.83	618.03	716.13	618.03
Load cell readings	510.12	519.93	588.60	716.13
Mean	457.80	549.36	678.52	717.76

The average readings for the front and back trailers are notably higher than the figures for bolster-type trailers. The readings for each individual trailer differ significantly, with an average percentage variance of 14.62%. The average differences between the readings for the bolster-type and frame-type trailers are 32.53% and 23.46% for the front and back trailers respectively. In spite of the relatively high variance, the average figures do confirm the previous hypothesis that the bolster-type trailers

require less force exerted on the spiller bar than the frame-type trailers.

1.4.4 Weigh Bridge Data

Every truck that delivers cane to the Sezela mill has a transponder and delivery card associated with it. This allows the mill management to track incoming cane and keep a thorough record of all deliveries, including a truck identification number, species of cane, the grower, the area it came from, when it was harvested, the quality of the cane and the mass of the payload.

Data for the past eight years was kindly made available through the cane procurement management at Sezela Mill.

There are many factors that influence payload. The main factor is the type of vehicle that delivers the cane. A small proportion of cane is delivered by agricultural tractors and trailers, but this is negligible when compared to the amount delivered on large trucks. The way in which the cane is harvested also affects the payload; burnt cane has a higher density than trashed cane because excess organic material is burnt off before cutting, and is not transported along with the cane. Various other factors such as the cultivar of the sugar cane and the manner in which it was grown (soil quality, moisture et cetera), also affect the payload.

The average payload is calculated by simply averaging the mass of cane delivered for each period. The results are shown in Figure 1.7.

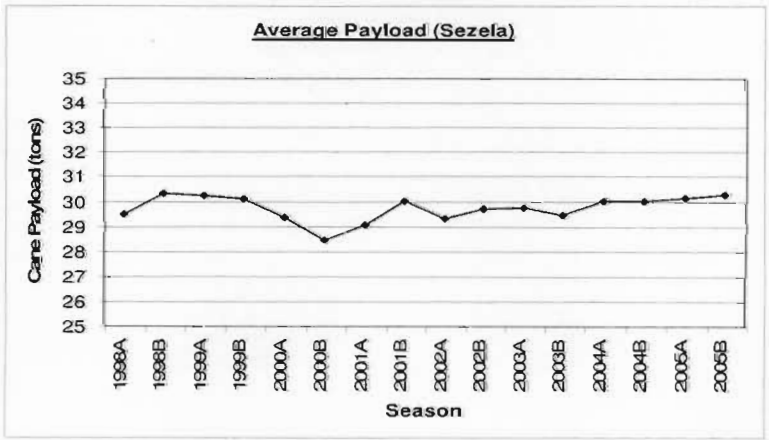

Figure 1.7 – Graph showing the average payload at Sezela mill

The overall average payload for the past eight years is 29.74 tons, and has varied by 6.25% during that period. From Figure 1.7, it can be concluded that the average payload at Sezela Mill has remained static for the past eight years, and hasn't increased by a substantial amount.

1.5 Conclusions

The configuration selected to form the basis of the design is a tandem/tandem interlink, with a bolster-type structure. This vehicle was selected because of the flexibility associated with it. The trailers can be unhitched from the prime mover for repair or servicing of either one, while the other is still in service. The prime mover can also be used with different trailers during the period in which harvesting is not taking place, and the trailers can be adapted to carry alternative cargo.

The bolster structure ensures that the cane slips out easily during offloading. This reduces the required force exerted by the offloading mechanism, lowering detrimental effects on the chassis structure during offloading.

The vehicle is primarily designed to travel from a loading zone to a mill. This is an important aspect of the design as the uneven surfaces typical of cane fields can result in high torsional stresses in the chassis. The roads in actual cane fields are often un-surfaced, and have large potholes and washed out sections, which cause on side of front or back of the vehicle to ride higher than the other.

Chapter 2 - Trailer Design Methods

2.1 Introduction

The objective of this chapter is to investigate various methodologies of trailer design, and to identify the materials and standard components used in the design.

The investigation into standards and design guidelines and methods is conducted in order to provide load cases and reserve factors used in semi-trailer design. The forms of information include standards and regulations, heavy vehicle research and information obtained from manufacturers.

Various materials and standard components, such as suspension systems, are investigated and compared, with the aim of selecting the most appropriate for the design.

2.2 Design Methodologies

The aim of this section is to investigate the methods utilised in heavy vehicle design, with regards to the structural capacity of the trailer chassis and other components, as well as the loads used for trailer design.
An extensive literature review in [15] revealed that there is very limited applicable design data which adequately defines the criteria by which trailers should be designed.
Various forms of information are investigated in this section, including standards, heavy vehicle research and information obtained from trailer manufacturers.

2.2.1 Standards

The aim of this section is to identify standards containing information in the form of recommended practices or legal requirements for the structural integrity of trailer chassis and design loads or safety factors utilised during the design process. Standards from

South Africa and international standards bodies are investigated.

South African Standards

Standards South Africa, a division of the South African Bureau of Standards, publishes a number of standards relating to heavy vehicles and semi-trailers. These include SANS 20073 [16], which relates to the lateral protection provisions of goods vehicles and semi-trailers, VC 8059 [17], which relates to specifications of pneumatic tyres for commercial vehicles and their trailers, and SANS 20104 [18], which stipulates the required markings on heavy vehicles. The standards generally relate to certain components of heavy vehicles, not the trailer chassis structure.

The South African Road Traffic Act [19] has a number of requirements that must be met for a vehicle to be roadworthy. The requirements dealing with heavy vehicles include: geometric considerations (maximum vehicle length, width, height and wheel base), maximum axle loads and braking performance. None of these stipulates the required design load capacity, or gives any insight into structural requirements for semi-trailer chassis.

International Standards

A search of European Union Council Directive documents revealed several Council Directives relating to heavy vehicles. These include Council Directives 96/53/EC [20], 2000/40/EEC [21] and 70/221/EEC [22], which deal with general heavy vehicle dimensions, and front and rear under-run protection. While the documents relating to under-run protection provide loads that the structure must withstand, these are purely from an accident related perspective. A United Nations Uniform Provisions document, Regulation No. 55 [23], concerns the adoption of uniform prescriptions for the mechanical coupling of heavy vehicles. The document describes a comprehensive testing procedure, including test forces to be applied to the coupling devices while attached to the trailer chassis.

The New Zealand Heavy Vehicles Rule [24] sets safety requirements and standards for systems and components in vehicles operating in New Zealand. It states that the chassis and body of a vehicle must be of adequate strength for all conditions of loading and operation for which the vehicle was constructed, and load cases and structural requirements are mentioned regarding chassis attachments, but no load cases or structural requirements are mentioned for the actual chassis. The rule mentions that a vehicle must have a chassis rating if the vehicle is required to have a certificate of loading under the Land Transport Rule: Vehicle Standards Compliance 2002 [25]. This relates to axle limits and a certificate issued by a certified person, but does not define methods for determining the actual load capacity of a vehicle chassis. Schedules 1 and 2 of [24] are detailed bolster attachment codes, which define load cases for both static and dynamic conditions, with allowable stress and stress ranges. This information will be used for the bolster design, but is not applicable to the trailer chassis.

Similarly, Australian Design Rules [26] address certain aspects of heavy vehicle design, with focus on components (such as axles and landing gear), light positions, general trailer dimensions and other aspects unrelated to chassis strength. Australian Standards make provisions for various aspects of heavy vehicles. These include AS 4235-1994 [27] and AS 2174.2-1994 [28], which address the attachment of kingpins and fifth-wheels, but there are no standards or guidelines for trailer chassis construction.

A search for applicable standards published by the International Organisation for Standardisation (I.S.O.) and the Society of Automotive Engineers (S.A.E.) revealed documents that principally relate to heavy vehicle performance and testing [29-38], and coupling components [39-45].

The American National Standards Institute publishes several standards related to heavy vehicle design. The most applicable is ANSI N14.30-1992 [47], which defines the design practice for vehicles used in the highway transport of weight-concentrated radioactive loads. The standard states that structural members of the semitrailer must withstand the

greater of a static load of 2.5 times the maximum load of any load case, or a cyclic fatigue factor multiplied by a dynamic design factor.

The military specification MIL-S-28550D (YD) [48] is a drop frame semitrailer specification approved for use by American naval facilities engineering command. The document states that a stress analysis must be carried out for the complete trailer main frame, loaded with a uniformly distributed load equal to the rated payload of the trailer imposed on the total length of the platform. The stress analysis must include shear force and bending moment diagrams, and maximum fibre stress in the main chassis rails. The strength of the flooring, cross-members and outside frame is not included in the analysis, but the weight of the components is included in the total load imposed on the main frame. The American Federal specification for commercial bolster semitrailers, KKK-S-2768 [49], describes a similar stress analysis requirement, with the load uniformly distributed over the body load area. The American Federal standard KKK-S-2806 [50] for bottom dump semitrailers states that the rated payload and the sprung weight of the semitrailer shall not impose a fibre stress greater than 50 percent of the yield strength of the material used when the semitrailer is operating under general mobile conditions.

2.2.2 Heavy Vehicle Research

Recent advances in heavy vehicle simulation have resulted in a number of different fields, each with their own objectives. The purpose of the investigation of vehicle dynamics is to determine the loads acting on the chassis that arise from dynamic situations.

The areas addressed are static and dynamic chassis frame simulation, ride quality assessment and vehicle-infrastructure interaction. The investigation is not a full literature view, but rather highlights the possible applicable data that can be obtained from such studies.

Static and Dynamic Chassis Frame Simulation

A method for analysing commercial vehicle structures using a hybrid method is presented in [51]. The method is based on finite element models of joints and analytically derived beam elements for the cross-members and main chassis members. This is expanded in [52] where nine load cases are defined. The load cases are mentioned, but no procedure or method is described to calculate the loads.

In [53], finite element and analytical models of a semitrailer excited by road surfaces are compared. The semitrailer is modelled as a rigid body in the analytical model, and as a flexible beam in the finite element model. The models are subjected to random road excitations. The natural frequencies and power spectral density of the two models are compared, and the mode shapes of the finite element model are determined.

A study of trailers and semitrailers is carried out in [54]. Finite element method is used to determine the maximum stress and calculate fundamental frequencies. Both static and dynamic forces are considered. A uniformly distributed load equivalent to the sum of the tare mass and payload mass is applied to the load carrying deck. For the dynamic analysis, a vertical sinusoidal impulse equivalent to gravitational acceleration is applied to the support. The results of the analyses show the areas of maximum stress and frequency response. The maximum calculated stress compared to the yield strength of the material reveals safety factors of 2.59, 1.85 and 1.33 for the trailer, tandem semitrailer and tridem semitrailer respectively.

A finite element study of a solid body truck frame is conducted in [55]. The results are compared with measurements from static loading experimentation. The results of the finite element study showed good correlation with the measurements for out-of-plane and torsional load cases. Significant discrepancies occurred when comparing the results of in-plane loads due to the exclusion of the effect of elastic buckling of the side members in the finite element model.

A study of the effect of modifying a tactical trailer is carried out in [56]. The original design is modified by raising the kingpin, creating a gooseneck structure. The effects of the modification are analysed using a rigid-body model created with Dynamic Analysis and Design System (DADS) software. A series of driving manoeuvres are simulated, and stability of the vehicle and dynamic loads are investigated. The dynamic loads are then applied to a finite element model to investigate structural integrity. The information from the study is of limited value as the vehicle is of a different type, and intended for off-road use. In addition to this, the trailer chassis is modelled as a rigid body and chassis flexure is not considered.

Ride Quality Assessment

In [57], a 2D finite element model is used to optimise the dynamic behaviour of a semitrailer. The comfort index is optimised using NASTRAN to calculate frequency response.

[58] compares results of ride comfort and endurance for four different semitrailer tractor models. Results for parameters such as wheel forces and payload acceleration are presented, but the effects of these on the chassis are not stated.

An analytical model for the evaluation of ride quality is presented in [59]. A Gaussian random road profile simulating the effects of an irregular road surface is used as the input for determining the frequency response at the driver's seat. The ride quality of the payload is mentioned, but not thoroughly discussed.

The interaction between an articulated vehicle and road surface undulations is investigated in [60]. The effects of frictional forces, bump-stops, wheel hop and road characteristics for loaded and unloaded vehicles are considered.

The vibration and ride quality of an articulated dump truck are analysed in [61]. A 24 degree-of-freedom ADAMS/View, 50 degree-of-freedom ADAMS/Car and Matlab

models are used. The results for whole body vibration are compared with measurements from physical tests. It was found that the simpler ADAMS/View model correlated better with the experimental results than the ADAMS/Car model. An optimisation study of the suspension system is conducted, with the aim of improving ride comfort.

Vehicle-Infrastructure Interaction

The dynamic loading of road surfaces by heavy vehicle tandem suspensions is investigated in [62]. Measurements are compared with a two degree-of-freedom nonlinear model. Comparisons of vertical wheel loads for three types of heavy vehicle suspension on rough and smooth roads are made.

A comprehensive technical report on dynamic vehicle infrastructure interaction [63] presents a wide range of data, both measured and obtained from heavy vehicle simulations. Although the focus is on the damage induced in bridges, roads and other structures, data concerning wheel forces is also presented. Measured wheel forces, including the effect of body bounce, for various vehicles travelling over road variations are discussed.

Similarly, [64] presents a range of data for leaf-spring and air suspension road interaction. A fourth-order Runge-Kutta computational method is used is used to solve the nonlinear system. Wheel forces, including peak wheel forces occurring over sinusoidal bumps and ditches in the road profile, are presented.

A pitch-plane model for articulated heavy vehicles, including the effects of tyres and suspension, is presented in [65]. The dynamic loads from road irregularities are evaluated and stress values for the road structure are calculated.

Similar studies of vehicle road interaction are presented in [66-68], in which various suspension systems are investigated, and dynamic tyre forces and their impact on roads

are calculated.

2.2.3 Experimental Testing of Heavy Vehicles

A significant quantity of research regarding experimental testing of heavy vehicles has been conducted. The focus of this research is primarily to compare theoretical or simulated results with actual measurements, and to investigate the forces acting on vehicle components and the effects of forces imposed by heavy vehicles on infrastructure.

Measurements of Wheel Forces and Chassis Accelerations

Research concerning the measurement of wheel forces is primarily conducted to investigate the damage to roads caused by heavy vehicles, and to verify simulation models of vehicle-road interaction. This is covered previous sections, and the wheel forces presented in [62, 63, 66-68] do provide some insight into the type and frequency of loading events, but it is difficult to quantify the actual loads experienced by the chassis from wheel force data.

The acceleration of the front chassis is measured in [60] to compare the results obtained from various models. The results are limited as the acceleration is measured over a single obstacle, and does not represent a typical load cycle. In addition to this, the measurements are taken with the objective of optimising ride quality.

Heavy Vehicle Chassis Testing and Measurement

The strain history of a high-capacity heavy duty trailer, carrying a 300 ton payload over a typical route, is recorded in [69]. It was found that the recorded results correlated well with design calculations. The measured fluctuating stresses are small compared to the high static stresses. This is mainly due to the large payload and low speed required for the heavy payload. The results presented are not indicative of a typical semitrailer because of

the difference in operating conditions.

The static and dynamic testing of a semitrailer designed to meet ANSI N14.30-1992 [44] is described in [70]. The semitrailer is designed to carry a 24 900kg payload and withstand a 2.5g vertical load. For mass optimisation, high strength steel is used. Strength of materials and finite element analyses techniques were used in the design of the trailer chassis, subjected to vertical and torsional loads. The static test involved loading the trailer to double its capacity for two hours. Strain gauges were placed in areas of highest predicted stress. The results of the test correlated well with calculated values. The dynamic testing was conducted by fitting strain gauges and accelerometers to the chassis, and performing a set of prescribed manoeuvres. The trailer did not show any signs of failure; however the values obtained from the dynamic test are not publicly available.

An attempt to determine a dynamic design factor through statistical analysis is made in [71]. The static load case is multiplied by the dynamic design factor resulting in a design load incorporating dynamic effects. Dynamic strain is recorded at various positions on a semi-trailer chassis, and the vehicle is driven over various surfaces. Statistical analysis is used to analyse the results of the measurements. The calculated design factors range from 1.2 for a smooth road to 2.4 for a paved surface.

2.2.4 Industry Design Methods

To determine the methods truck manufacturers use to estimate the design loads and dynamic effects on semi-trailer chassis for design purposes, various manufacturers and specialists in the field of trailer design, were contacted and interviewed. Due to the competitive nature of the business, most manufacturers are not willing to divulge their exact methods. The following sections present a summary of information obtained from local and international trailer manufacturers, and from [15].

Local Manufacturers

John Pilcher Designs produces designs for primarily agricultural equipment, including sugar cane and timber haulage vehicles. A safety factor of 3.0 to yield strength is used during the design process, and is typically applied to the static load case of 1g for the main chassis rails and cross-members.

Transpec (Natal) CC manufacture various truck bodies and semi-trailers. A reserve factor of 2.0 to 2.5 is used, depending on customer requirements and specifications.

AFRIT, recognised as a leader in low tare mass trailers in South Africa, use a dynamic model based on customer requirements, the nature of the payload and the expected typical road surface, to determine reserve factors. These typically vary from 1.4 for light-use to 2.8 for heavy industrial vehicles. The specific load cases to which this factor is applied were not made available.

Correspondence with Mr. A. Vach, a consultant in heavy vehicle design, stressed the importance of load assumptions, and revealed that generally, a safety factor of 2.5 to yield is adequate for semi-trailers.

International Manufacturers

Haulmark trailers, an Australian manufacturer, use a dynamic design factor that varies from 2.5 to 3.0, depending on the usage and the expected life of the trailer [15].

Correspondence with Mr. A. Leedahl, an agricultural equipment designer, revealed that for agricultural semi-trailers, which are required to travel in-field, a relatively large safety factor. This safety factor, which typically varies from 3.0 to 5.0, is necessary because of the large loads generated by the uneven ground surface.

American manufacturers Wabash Int. and East MFG use dynamic design factors of 2.5

and 2.0 to 3.0 respectively. At Wabash Int., the factor is applied to a loading scenario dependent on the use of the trailer. East MFG applies the factor to worst case legal loads [15].

AV Engineering, based in Czech Republic, use a dynamic vehicle model to estimate the forces acting on a trailer chassis generated during various dynamic manoeuvres. These loading events are than used to determine the life expectancy of a particular trailer, rather than for static design.

2.2.5 Conclusions

The investigation revealed that while many standards related to trailers exist, a standard relating to the strength of the chassis, the loads imposed on it, and a reserve factor or dynamic design factor, is lacking. The bolster attachment code of [21] will be used for the bolster calculations.

The publications regarding static and dynamic simulation revealed various methods of modelling heavy vehicles, but lacked solid design data regarding the effect of dynamic loads on the chassis. The load cases mentioned in [52] will be used, in conjunction with a dynamic design factor.

The principle area of focus for studies regarding ride quality are the forces and vibration experienced by the truck cab or driver when subjected to forces arising from irregular road surfaces. The natural frequencies of the vehicles structures are also discussed, but the forces generated by dynamic movement of the payload, and the chassis response to this effect, are not thoroughly investigated.

The publications regarding vehicle infrastructure interaction presented wheel forces generated by dynamic movement of a heavy vehicle, with the aim of relating the wheel forces to road damage. Due to the complex nature of suspension and tyre systems, it is

difficult to relate these forces to the forces acting on the vehicle chassis.

It was anticipated that dynamic simulation of heavy vehicles would provide data regarding the loads imposed on the vehicles. The results presented in the publications did not provide thorough quantification of the loads imposed on the chassis, but rather focused on results applicable to the particular objective of the study.

The data obtained from experimental test measurements proved to be useful. Although the measured wheel forces are difficult to directly relate to chassis forces, they provide some insight into the type and frequency experienced by heavy vehicles. The dynamic design factor suggested from the statistical analysis of strain data in [71] correlates with values used by manufacturers, although the vehicle in the study has a smaller span than the vehicle in this study.

The information obtained from many of the manufacturers revealed that design of trailers has developed mainly through experience and trial-and-error methods. The lack of a design standard that specifically deals with the strength and capacity of trailer chassis substantiates this. While some manufacturers carry out dynamic analyses and consider fatigue life, most of the manufacturers multiply the static load cases by a factor, which is large enough to ensure that fatigue failure will not occur.

The information obtained from manufacturers and the research in this section suggests a design factor ranging from 2.0 to 3.0. A design factor of 2.75 is adopted for this study. The factor is selected from the upper section of the range due to the severe operating conditions often experienced by this particular type of vehicle. The resulting tare mass of the vehicle is linked to the design factor; the higher the design factor, the higher the tare mass. Once the initial design is complete, the design factor will be reviewed after initial analyses and fatigue considerations have been completed.

2.3 Materials

In an effort to reduce the tare mass of semi-trailers, manufacturers have investigated and implemented both evolutionary design optimisation and the use of alternative materials in their designs [8]. A higher strength material results in a decrease of the required sections of load bearing members, hence a decrease in the overall mass.

The choice of a suitable engineering material involves many factors, including mechanical properties, physical properties and economic considerations [72]. The factors considered in this study are the tensile strength, fatigue strength, stiffness, density, cost, manufacturability and availability of the material. The tensile strength, fatigue strength, stiffness and density indicate the possible mass savings obtainable from the material. The semi-trailer structure requires a certain amount of stiffness and strength, but the selected material must also meet manufacturability and economic constraints. The values of the ratios of modulus of elasticity/density and yield strength/density are often used to compare the possible weight savings of materials in an automotive context [73, 74]. Due to the cyclic nature of the loading, fatigue strength of the material must be taken into account. The main concern with respect to manufacturability of metallic materials in this case is weldability. The cost and availability of materials is also important as there is no point in specifying a material which results in a large decrease in tare mass if the cost of the trailer is not justified by the savings made by the reduction in tare mass.

Many materials have been used in the construction of semi-trailers, including mild steel, high-strength low-alloy steels, aluminium alloys and composite materials. The purpose of this section is to provide a simple comparison between the materials, resulting in the selection of the material to be used in the design.

2.3.1 Aluminium Alloys

Pure aluminium is relatively low in strength, but when alloyed and heat-treated, its

strength rivals that of mild steel and HSLA steel [72]. Aluminium has been used in many heavy vehicle applications, including chassis components, and has resulted in large tare mass savings [75-77].

One of the main advantages of aluminium is its low density, however the lower modulus of elasticity results in larger deflections, and aluminium semi-trailer structures are often designed to deflection constraints rather than yield strength constraints [75]. Aluminium tends to have a relatively poor fatigue performance, especially with regard to welds, and special precautions must be taken into account during welding [78]. Aluminium also has good corrosion resistance due to the formation of a thin oxide layer on exposed surfaces.

2.3.2 Fibre Reinforced Composites

Fibre reinforced composites generally consist of a fibre (glass, carbon or aramid for example) in a plastic matrix. They are characterised by very high tensile strengths and stiffnesses.

The use of fibre reinforced composites in the heavy vehicle industry is increasing, primarily because they provide substantial advantages, including considerable mass reduction due to high strength and stiffness, and corrosion resistance [15]. Examples of composite semi-trailers, including glass and aramid fibre composites, can be found in [77, 79-81].

The high cost associated with composite materials is prohibitive in this case. Steel is significantly less expensive per unit volume compared to fibre reinforced composites [82]. The use of composite materials also results in an increase of the complexity of manufacturing processes.

2.3.3 Steels

Steel is an alloy of iron that contains between 0.02% and 2.11% carbon by weight, and

other components including manganese, chromium, nickel, vanadium and molybdenum [83]. There are countless varieties of steel, which vary in their compositions and properties. Traditionally, steel is the most conventional material used in automotive and heavy vehicle construction. The steels investigated in this study range from mild steel to high-strength steels, and include the steels most commonly used in semi-trailer structures.

Mild Steel

Mild steel, or structural steel, is one of the most common engineering materials, and has seen extensive use in semi-trailers. The yield strength of mild steel depends on the grade, and generally varies from 280-450 MPa [84]. The main advantages of mild steel are that it is relatively cheap and easy to manufacture [78]. Compared to many other materials, it has a low strength to weight ratio, and is prone to corrosion damage.

Domex

Domex is the trade name of a high-strength low-alloy steel intended for engineering and automotive applications manufactured by SSAB. The steel is hot-rolled, and has a yield strength ranging from 240-700 MPa, depending on the grade [85]. The steel is weldable, corrosion-resistant and has a good fatigue life [86]. Domex steel has been extensively used in the production of low tare mass trailers [87, 88].

3CR12 High Chromium Steel

3CR12 is a steel with 12% chromium nominal content, and a yield strength of 320 MPa [89]. It is used in sugar processing plants, bus frames and other applications involving high corrosion and abrasion environments [90].

The most attractive property of 3CR12 is its corrosion resistance, due to the formation of a tough iron-chromium oxide layer that develops on exposed surfaces.

ROQ-tuf AM

ROQ-tuf is the trade name of a locally manufactured high-strength steel. The steel is quenched, tempered and calcium treated [91]. The steel is weldable by conventional methods, and is used in many applications, including dump truck bodies, mobile cranes and other structural applications.

2.3.4 Comparative Analysis

The most suitable materials from each type are selected and compared using a selection matrix. The properties of the ten most suitable materials are shown in Table 2.1. The properties are obtained from [15, 73, 78, 83-86, 89, 91]. Where applicable, the yield stress is taken in the direction of rolling or primary direction. The values for composite materials are for typical examples of the type of material, and tensile strength is used instead of yield strength.

Table 2.1 Mechanical properties of materials

Material	$E\ (GPa)$	$\sigma_Y\ (MPa)$	σ_T (MPa)	$\rho\,(kg/m^3)$	$\frac{E\times10^3}{\rho}$	$\frac{\sigma_Y\times10^2}{\rho}$	Elongation (%)	Poisson's ratio
Al-7075-T6	71.70	503.00	572.00	2800.00	25.61	17.96	12.00	0.33
Al-6061-T6	68.90	276.00	310.00	2700.00	25.52	10.22	11.00	0.33
Al-2024-14	73.00	324.00	469.00	2770.00	26.35	11.70	19.00	0.33
E-glass	75.00	na	3500.00	2580.00	29.07	135.66	4.00	0.23
T-300 Carbon	235.00	na	3200.00	1750.00	134.29	182.86	1.40	0.25
DuPont Kevlar 29	65.00	na	2800.00	1440.00	45.14	194.44	4.00	0.34
Mild Steel (350W)	205.00	350.00	480.00	7850.00	26.11	4.46	18.00	0.29
Mild Steel (400WA)	205.00	450.00	550.00	7850.00	26.11	5.73	18.00	0.29
Domex 500MC	210.00	500.00	550.00	7870.00	26.68	6.35	12.00	0.30
Domex 700MC	210.00	700.00	750.00	7870.00	26.68	8.89	12.00	0.30
3CR12	200.00	320.00	450.00	7740.00	25.84	4.13	18.00	0.30
ROQtuf AM 700	205.00	700.00	780.00	7850.00	26.11	8.92	18.00	0.30

The materials are arranged in a selection matrix (see Table 2.2), and are rated relative to each other to enable a comparison. The materials are rated on the modulus of elasticity and strength to density ratio, fatigue resistance, corrosion resistance, availability,

manufacturability and cost. The maximum and minimum scores are +3 and -3 respectively.

Table 2.2 Material selection matrix

Material	7075	6061	2024	E-glass	Carbon	Kevlar 29	350W	400WA	500MC	700MC	3CR12	ROQtuf
E/ρ	0	0	+	+	+++	++	0	0	+	+	0	+
σ/ρ	+	+	+	++	+++	+++	-	0	0	+	-	+
Fatigue	-	-	-	+	++	++	0	0	+	+	0	0
Corrosion	++	++	++	+	+	+	-	-	0	0	++	0
Availability	+	0	+	-	--	---	++	++	+	+	0	++
Manufact.	0	0	0	--	--	--	++	++	++	++	+	+
Cost	0	0	0	-	--	---	++	++	+	+	+	+
Total	3	2	4	1	3	0	4	5	6	7	3	6

2.3.5 Conclusions

Aluminium is an overall attractive material, with good strength to weight ratios and corrosion resistance; however the poor fatigue life associated with aluminium structures coupled with the harsh operating environments of sugar cane haulage vehicles results in its exclusion as a possibility.

Composite materials have the potential for large tare mass reductions, but the high cost and complex manufacturing processes eliminate the possibility of producing an economically viable composite sugar cane haulage vehicle.

The various types and grades of steel generally scored the highest in the selection matrix, with the mild steels scoring the lowest due to poor corrosion resistance and strength to weight ratios. The highest scoring material is Domex 700MC. This is due to a combination of high tensile strength, relatively good fatigue properties, adequate corrosion resistance and ease of manufacturing, resulting in the selection of Domex

700MC as the material for the semi-trailer design.

2.4 Standard Components

2.4.1 Axles

The selection of axles for a heavy vehicle depends on many factors, including the nature of the payload, the type of vehicle and its intend use. In this case the choice of axles for the semi-trailer is limited by the maximum mass load stipulated the South African Road Regulations [19], and the maximum track width determined by the off-loading apparatus at the mills.

The semi-trailers will be constructed with double-axles at the front and rear, and fitted with dual tyres, allowing a maximum mass load of 18 000 kg per unit. The maximum allowable track width determined by the offloading apparatus is 1930 mm, resulting in a maximum axle shaft length of 1000 mm, although this does vary from mill to mill.

While square cross-section axles tend to have a higher capacity, round cross-section axles are generally lighter. In this case round axles with a track width of 1930 mm will be used [92].

2.4.2 Suspension

The purpose of suspensions systems is to limit vehicle vibrations, reduce the effect of road unevenness on the chassis and to ensure steering and handling stability. Typical suspensions used for cane haulage vehicles include air, walking beam, steel leaf and hydraulic suspension.

Air suspension usually costs more to implement than other types of suspension, but has been shown to reduce damage to roads and increase tyre life. It performs well on relatively even roads but its application to slightly rough roads (such as those

encountered at loading zones) is limited.

Walking beam and hydraulic suspension are generally used for in-field applications. The suspension is designed in a way that allows for large deflections of a single wheel without excessive stress on the suspension and axle components. These systems can be expensive to implement, and do not generally perform well at high-way speeds.

Leaf spring suspensions are used for many heavy vehicle applications, and are generally simpler and lower in cost than other systems. The performance of leaf spring suspension in harsh off-road applications is lower than that of some other systems. However the cane haulage vehicle is only intended for moderate off-road use, therefore leaf spring suspension will be used in the design. The selected suspension (part No. CS-002) can be found in [92].

2.4.3 Rims

Aluminium rims have been used as a means to reduce the tare mass of heavy vehicles, and can result in mass savings of up to 300kg [7, 93]. Although the initial cost is higher when compared to steel rims, aluminium rims will be used in the design to reduce tare mass.

2.5 Conclusions

The investigation into trailer design methods revealed that there is limited data regarding the structural design of semi-trailers, especially with regard to design loads. The load cases mentioned in [52] will be used, in conjunction with the dynamic design factor established in section 2.2., for the static load generated by the payload. The loads defined in the bolster attachment code of [24] will be used for the design of the bolsters.

The comparison of various materials revealed that high-strength low-alloy steels are the most advantageous materials in this specific case. The selected material is DOMEX

700MC due to a combination of high tensile strength, relatively good fatigue properties, adequate corrosion resistance and ease of manufacturing.

The selected axles and suspension are solid round axles and spring-leaf suspension. These components were selected on the basis of a combination of low weight, simplicity and cost effectiveness. Aluminium rims are selected due to the mass saving obtained through their use.

Chapter 3 - Optimisation of Geometric Vehicle Parameters

3.1 Introduction

The aim of this chapter is to determine the optimum values for the lengths of the chassis, and calculate the initial section dimensions of the main chassis beam. Geometric optimisation of the lengths of articulated vehicles has been previously conducted [94], although the principle focus is the determination of the number of drive axles and vehicle configuration. The lengths of the semi-trailer will be optimised to reduce the maximum bending moment occurring in the chassis, hence reduce the required section modulus and mass of the chassis.

A typical interlink configuration can be represented as a model composed of various lengths (see Figure 3.1). The front trailer is suspended by the fifth-wheel on the prime mover and the suspension assembly attached to the rear of the trailer. The second trailer is supported by a fifth-wheel mounted on the back of the front trailer, and the second suspension assembly.

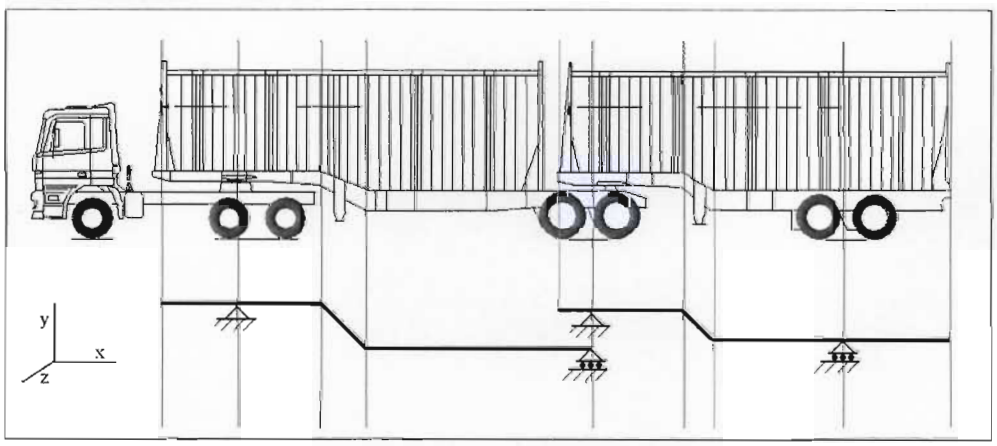

Figure 3.1 Interlink combination model

The front section must be high enough to sit above the fifth-wheel and the rear section is

low to increase payload and lower the centre of gravity, there-by improving handling and roll-over threshold [95]. The geometry must thus form a step, with the high section in front dropping down to a low section in the middle and rear.

The various lengths of the trailer chassis affect critical parameters such as axle loads, payload and the forces acting on the chassis members. The front trailer generally tends to have a greater span between supports because the second fifth-wheel and the swing clearance of the second trailer must be accommodated. The fifth-wheel and suspension allow rotation about the Z-axis, so the supports are modelled as simple pinned joints. Bending moments and shear force diagrams for a typical interlink configuration (with a downward acting force equivalent to the payload multiplied by the design factor obtained from Section 2.2.4) are shown in Figure 3.2.

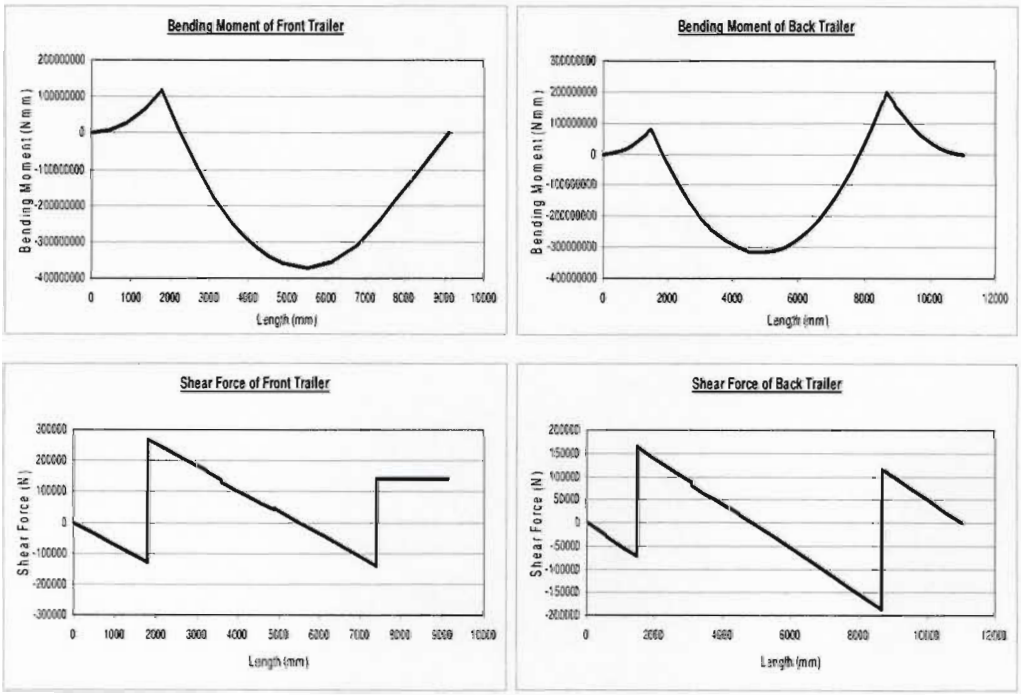

Figure 3.2 Bending moment and shear force diagrams of a typical interlink configuration

From the results in Figure 3.2, it can be noted that the bending moment of the front trailer is greater than the rear trailer, due to the increased span between the supports.

3.2 Optimisation problem formulation

A general optimisation problem may be formulated as: $\min\{f_1(x), f(x_2),..., f(x_l)\}$, where $f_1(x), f(x_2),..., f(x_l)$ are objective functions of the design variable vector, x. Values of x are limited to a domain D that is bounded by n inequality constraints and m equality constraints, such that:

$$D = \{x : g_j(x) \leq 0, h_k(x) = 0,\ j = 1,2,...,n\ \ k = 1,2,...,m\}$$

If the objective function and the constraints are linear functions of the design variables, the problem may be reduced to:

$$\min\{f\ (x) = \mathbf{c}^T \mathbf{x}\},$$

Subject to the set of constraints:

$$\mathbf{Ax}=\mathbf{b},$$
$$\mathbf{Gx} \leq \mathbf{h},$$
$$\mathbf{x}_L \leq \mathbf{x} \leq \mathbf{x}_U$$

Where:

$\mathbf{x} = \{x_1, x_2,..., x_i\}^T$ is a vector containing the i design variables

$\mathbf{c} = \{c_1, c_2,..., c_i\}^T$ is the objective function vector

$\mathbf{A}$ is an $m \times i$ matrix

$\mathbf{G}$ is an $n \times i$ matrix

$\mathbf{b} = \{b_1, b_2,..., b_m\}^T$ is the vector of equality limits

$\mathbf{h} = \{h_1, h_2, ..., h_n\}^T$ is the vector of inequality limits

$\mathbf{x}_L = \{x_{L1}, x_{L2}, ..., x_{Ln}\}^T$ is the vector of the lower limits of the design variables

$\mathbf{x}_U = \{x_{U1}, x_{U2}, ..., x_{Un}\}^T$ is the vector of the upper limits of the design variables

The lengths of the various sections of the trailers are the design variables (see Figure 3.3). Noting that the largest bending moment, and hence the highest stress, occurs in the suspended span in the front trailer, the objective function for the geometric optimisation of the interlink configuration is the sum of the lengths contributing to the distance between the two supports of the front trailer. For the purpose of clarity, the beams are shown separately, but in reality, the points *h* and *f* are coincident, and are pinned together via a fifth-wheel coupling, transferring vertical loads, but no moment.

H_f and H_b are the heights of the front and back trailers respectively, taken from the rear section of the chassis beams. α_f and α_b are the angles between the inclined section of the chassis beam and the horizontal of the front and back trailers.

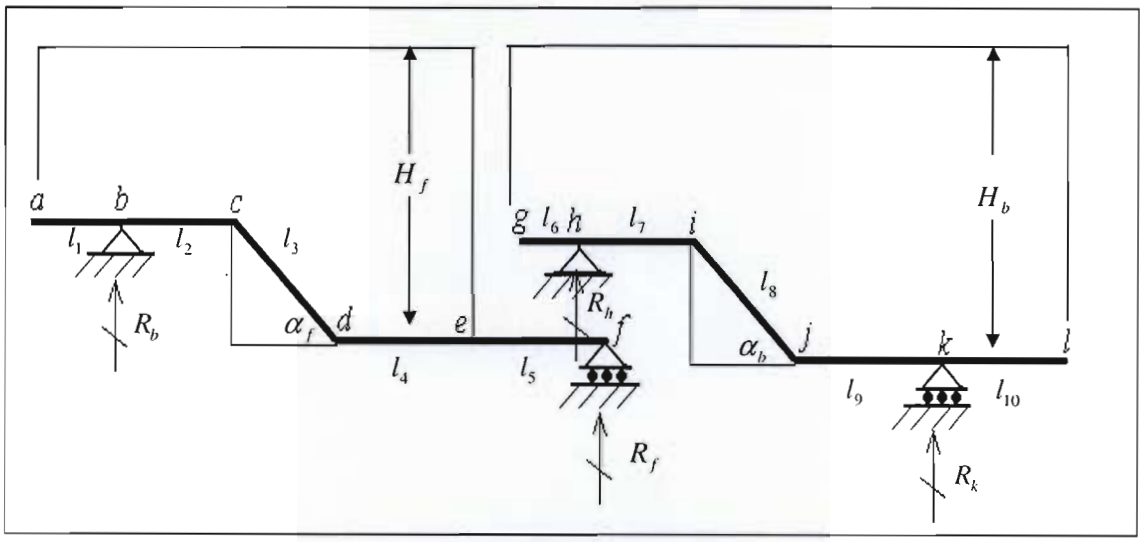

Figure 3.3 Diagram showing variables of the model

The vertical lengths, $l_3 \sin\alpha_f$ and $l_8 \sin\alpha_b$, are defined by the distance above the ground of the prime mover's fifth-wheel, and the geometry of the suspension and wheels. Basic dimensions are obtained from the Mercedes-Benz Actros 3340S-33, which is commonly used for sugarcane transportation (Figure 3.4).

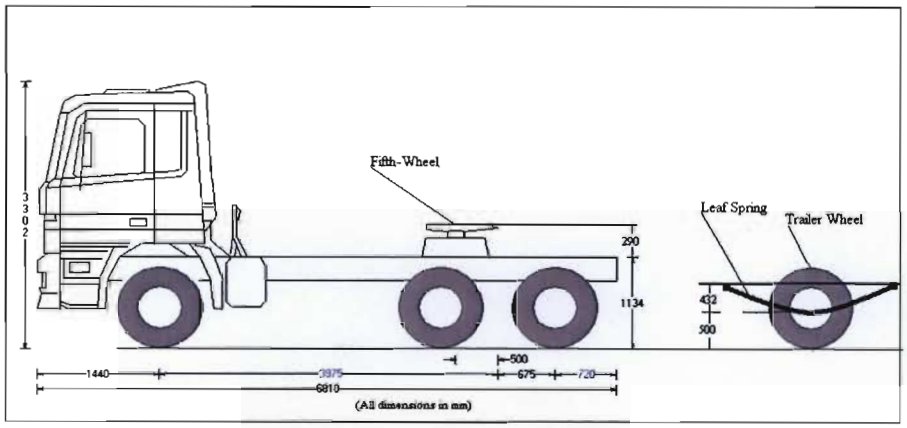

Figure 3.4 Mercedes-Benz Actros 3340S-33

The design variable and objective function vectors can be expressed as:

$$\mathbf{x} = \begin{Bmatrix} l_1 \\ l_2 \\ l_3 \cos\alpha_f \\ l_4 \\ l_5 \\ l_6 \\ l_7 \\ l_8 \cos\alpha_b \\ l_9 \\ l_{10} \end{Bmatrix} \qquad \mathbf{c} = \begin{Bmatrix} 0 \\ 1 \\ 1 \\ 1 \\ 1 \\ 0 \\ 0 \\ 0 \\ 0 \\ 0 \end{Bmatrix}$$

The constraints on the lengths of the trailers are determined by road legislation, payload requirements and the geometry of the tractor, swing clearance, as well as various

standardised components. The applicable constraints implied by legislation in the form of The Road Traffic Act are summarised in Table 3.1 [19].

Table 3.1 Constraints imposed by the Road Traffic Act

Regulation	Description	Value	Implication
351(f)	Overall Length of a Combination Vehicle	22.0m	$4915 + l_2 + l_3 \cos\alpha_f + l_4 + l_5 + l_7 + l_8 \cos\alpha_b + l_9 + l_{10} \leq 22000mm$
353(b)	Maximum Overall Width	2.6m	$w \leq 2600mm$
354(b)	Maximum Overall Height	4.3m	$H_f + 932 \leq 4300$ $H_b + 932 \leq 4300$
355(b)(i)	Maximum Semi-Trailer Wheelbase	10.0m	$l_2 + l_3 \cos\alpha_f + l_4 + l_5 \leq 10000mm$
356(1)(a)	Maximum Front Overhang	1.8m	$l_1 \leq 1800mm$ $l_6 \leq 1800mm$
226 (2)(c)	Maximum Rear Overhang	60% of body length	$(l_6 + l_7 + l_8 \cos\alpha_b + l_9 + l_{10})0.6 \geq l_{10}$
240(d)(ii)	Maximum Massload of a double axle	18000kg	$R_f + R_h \leq 176.85kN$ $R_k \leq 176.85kN$
-237(2)	Maximum Overall Gross Mass	56000kg	$Tractor\_Weight + R_b + R_f + R_h + R_k \leq 549.36\text{kN}$

The payload can be expressed as a function of the volume capacity of the trailers and the density of the raw sugarcane. The density of sugarcane varies according to the type of cane and the manner in which it is harvested and packed. An average value of 301 kg/m^3 is used. The truck is designed with a payload of at least 40000kg to account for varying densities of cane, although the actual legal limit could be less than this due to the tare mass of the prime mover and trailers, and the 56 ton overall mass limit. This results in a constraint which can be expressed as:

$$P = \rho w[(l_1 + l_2)(H_f - l_3 \sin\alpha_f) + (l_3 \cos\alpha_f (H_f - \frac{1}{2}(l_3 \sin\alpha_f))) + (l_4 H_f) + (l_6 + l_7)(H_b - l_8 \sin\alpha_b)$$
$$+ (l_8 \cos\alpha_b (H_b - \frac{1}{2}(l_8 \sin\alpha_b))) + (l_9 + l_{10})H_b] \geq 40000kg$$

where P is payload (kg)

ρ is cane density $(\frac{kg}{mm^3})$

w is trailer width (mm)

There must be sufficient swing clearance between the prime mover and the first trailer, and the first and second trailers, to insure there is no interference during turning manoeuvres. The swing clearance between the first trailer and the prime mover can be visualised as in Figure 3.5.

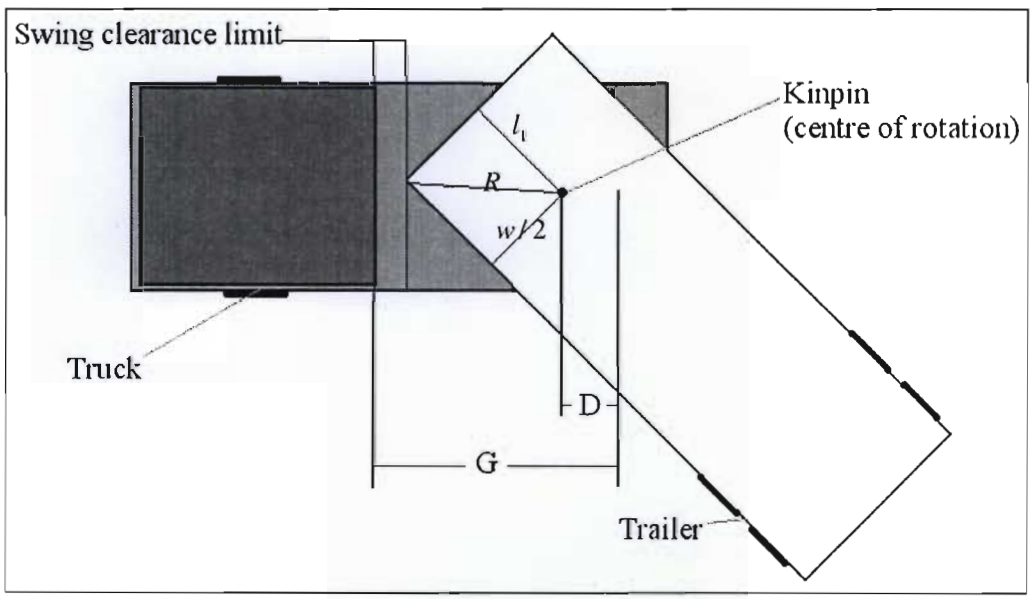

Figure 3.5 Diagram indicating swing clearance parameters

The swing clearance between the front trailer and prime mover can be expressed as:

$$G - R - D \geq 300$$

where

G is the distance from the trailer connection frame to the centre of the rear truck axle unit.

$$R = \sqrt{\left(l_1^{\,2} + \left(\frac{w}{2} \right)^2 \right)}$$

D is the distance from the kingpin to the centre of the rear truck axle unit.

300 is swing clearance limit indicated in the diagram (mm).

The inequality results in a constraint which is not linear with respect to l_1. Plotting $R \; vs. \; l_1$ (see Figure 3.6) reveals that the function is almost linear between a range of 400mm, which is the smallest practical value, and 1800mm, which is the legal maximum.

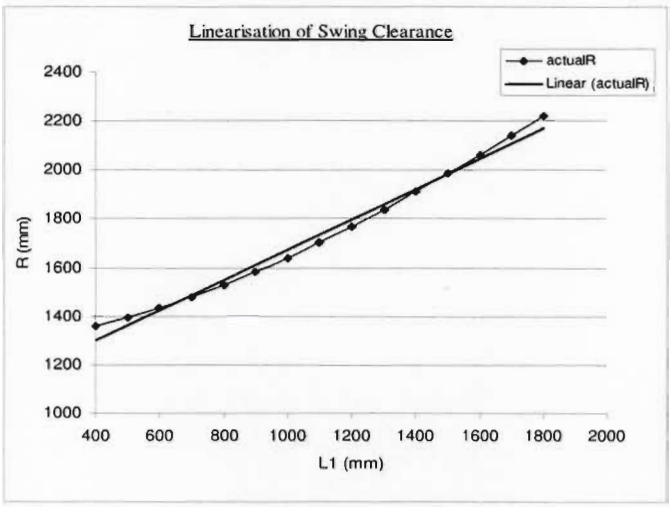

Figure 3.6 Graph of R vs. l_1

A linear approximation is obtained using the least squares method, with less than 5% error throughout the 400-1800mm range. The linear approximation is used to implement the swing clearance constraint between the prime mover and the first trailer. The

remaining swing clearance constraints are calculated with the same method, and can generally be expressed as:

$$ax_i - bx_j \leq c$$

where

x_i, x_j are the relevant design variables

a, b, c are constants

The equations for the values of the reactions are non-linear with respect to the design variables. For example, R_k is expressed as:

$$R_k = w\rho g[-x_6(H_b - h_b)0.5x_6 + x_7(H_b - h_b)0.5x_7 + x_8(H_b - h_b/2)(x_7 + 0.5x_8) + x_9(H_b)(x_7 + x_8 + 0.5x_9) + x_{10}(H_b)(x_7 + x_8 + x_9 + 0.5x_{10})\ ]/(x_7 + x_8 + x_9)$$

The model was initially optimised without the reaction constraints. This resulted in a set of values for the design variables that did not meet the reaction criteria. In addition to this, the effect of the kingpin placement, as well as the effect of having the second fifth-wheel not directly above the first trailer axle unit (points h and f are not coincident), is not taken into account.

A new model is introduced that includes the prime mover, variable kingpin placement (x_{12}), and non-coincident placement of points h and f (x_6), (see Figure 3.7). The variable x_6 is allowed to take positive and negative values to allow the second fifth-wheel to sit either in front of or behind the first trailer axle unit.

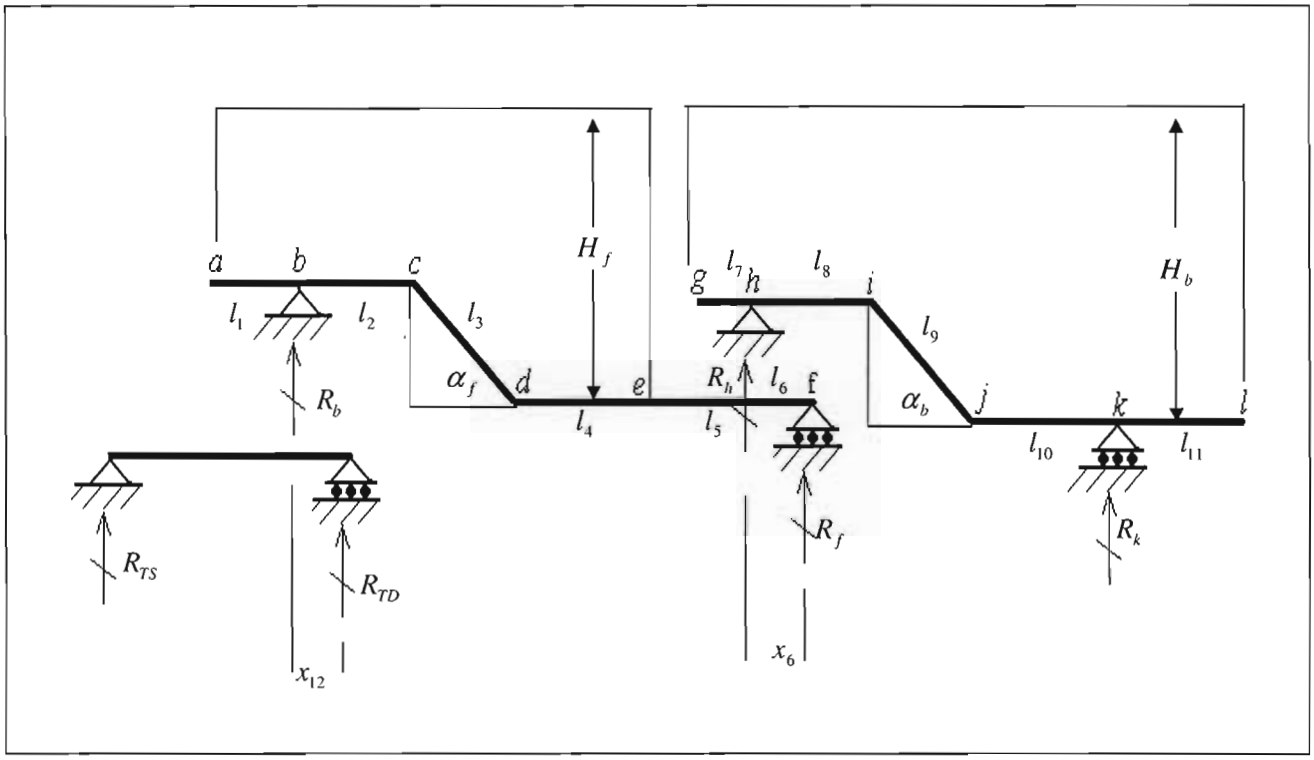

Figure 3.7 Model of an interlink combination including prime mover

R_{ts} and R_{td} are the reactions at the steering and drive axle units respectively. The mass of the actual chassis is taken into account, using a parameter $m\left(\frac{kg}{mm}\right)$, which is the average mass per unit length, and is calculated by dividing the approximate tare mass of the trailer by the total length of the chassis. The approximate tare mass of the trailer is obtained from the difference between the allowable gross mass and the sum of the payload and prime mover masses.

The reaction equations cannot be directly substituted into the B matrix for inequality constraints because of the nonlinearity with respect to the design variables. The equations are linearised by introducing coefficients c_j such that:

$$R_j(\mathbf{x}) \approx \left(c_{1,j}x_1 + c_{2,j}x_2 + \ldots c_{i,j}x_i \ldots + c_{12,j}x_{12} + B_j \right)$$

where

R_j is the reaction at point j

$$c_{i,j} = R_j(x_i + \Delta/2) - R_j(x_i - \Delta/2)$$

$$B_j = R_j - \left(c_{1,j}x_1 + c_{2,j}x_2 + \ldots c_{i,j}x_i \ldots + c_{12,j}x_{12}\right)$$

In this case there no equality constraints, so the optimisation problem can be expressed as:

$$\min\{f\ (x) = \mathbf{c}^T\mathbf{x}\},$$

subject to:

$$\mathbf{Gx} \leq \mathbf{h},$$
$$\mathbf{x}_L \leq \mathbf{x} \leq \mathbf{x}_U$$

Where:

$$\mathbf{c} = \begin{Bmatrix} 0 \\ 1 \\ 1 \\ 1 \\ 1 \\ 1 \\ 0 \\ 0 \\ 0 \\ 0 \\ 0 \\ 0 \end{Bmatrix} \quad \mathbf{x} = \begin{Bmatrix} l_1 \\ l_2 \\ l_3 \cos\alpha_f \\ l_4 \\ l_5 \\ l_6 \\ l_7 \\ l_8 \\ l_9 \cos\alpha_h \\ l_{10} \\ l_{11} \\ l_{12} \end{Bmatrix} \quad \mathbf{x}_L = \begin{Bmatrix} 400 \\ 1000 \\ 1000 \\ 1000 \\ 1000 \\ -700 \\ 400 \\ 1000 \\ 1000 \\ 1000 \\ 1000 \\ 0 \end{Bmatrix} \quad \mathbf{x}_u = \begin{Bmatrix} 1800 \\ 5000 \\ 5000 \\ 5000 \\ 5000 \\ 1000 \\ 1800 \\ 5000 \\ 5000 \\ 5000 \\ 5000 \\ 700 \end{Bmatrix}$$

$$\mathbf{h}=\left\{16585 \quad 10000 \quad 10000 \quad \left(\frac{-40000}{w\rho}\right) \quad 1000 \quad 1708.7 \quad -1321.3 \quad -2163.3 \quad -1321.3 \quad (R_{kU}-(B_k-R_{kL})) \quad (B_k-R_{kL})\right.$$
$$\left.(R_{fU}-B_f) \quad (B_f-R_{fL}) \quad (R_{tdU}-B_{td}) \quad (B_{td}-R_{tdL}) \quad (R_{tsU}-B_{ts}) \quad (B_{ts}-R_{tsL}) \quad \begin{pmatrix}61600-B_k-B_f\\-B_{td}-B_{ts}\end{pmatrix}\right\}^T$$

Taking $\sum c=(c_k+c_f+c_{td}+c_{ts})$:

$$G=\begin{Bmatrix}
0 & 1 & 1 & 1 & 1 & 0 & 0 & 1 & 1 & 1 & 1 & 0\\
0 & 1 & 1 & 1 & 1 & 1 & 0 & 0 & 0 & 0 & 0 & 0\\
0 & 0 & 0 & 0 & 0 & 0 & 0 & 1 & 1 & 1 & 0 & 0\\
-(H_f-h_f) & -(H_f-h_f) & -(H_f-h_f/2) & -(H_f) & 0 & 0 & -(H_b-h_b) & -(H_b-h_b) & -(H_b-h_b/2) & -(H_b) & -(H_b) & 0\\
-1 & -1 & -1 & -1 & 0 & 0 & 1 & 1 & 1 & 1 & 1 & 0\\
0.6447 & 0 & 0 & 0 & 0 & 0 & 0 & 0 & 0 & 0 & 0 & 1\\
0 & 0 & 0 & 0 & -1 & 0 & 0.6447 & 0 & 0 & 0 & 0 & 0\\
0 & -1 & 0 & 0 & 0 & 0 & 0 & 0 & 0 & 0 & 0 & 0.8115\\
0 & 0 & 0 & 0 & 0 & 0.6447 & 0 & -1 & 0 & 0 & 0 & 0\\
0 & c_{k,1} & c_{k,2} & \cdots & & c_{k,i} & & & & & \cdots & c_{k,12}\\
0 & -c_{k,1} & -c_{k,2} & \cdots & & -c_{k,i} & & & & & \cdots & -c_{k,12}\\
0 & c_{f,1} & c_{f,2} & \cdots & & c_{f,i} & & & & & \cdots & c_{f,12}\\
0 & -c_{f,1} & -c_{f,2} & \cdots & & -c_{f,i} & & & & & \cdots & -c_{f,12}\\
0 & c_{td,1} & c_{td,2} & \cdots & & c_{td,i} & & & & & \cdots & c_{td,12}\\
0 & -c_{td,1} & -c_{td,2} & \cdots & & -c_{td,i} & & & & & \cdots & -c_{td,12}\\
0 & c_{ts,1} & c_{ts,2} & \cdots & & c_{ts,i} & & & & & \cdots & c_{ts,12}\\
0 & -c_{ts,1} & -c_{ts,2} & \cdots & & -c_{ts,i} & & & & & \cdots & -c_{ts,12}\\
0 & \sum c_1 & \sum c_2 & \cdots & & \sum c_i & & & & & \cdots & \sum c_{12}
\end{Bmatrix}$$

Where R_{jU} , R_{jL} are the upper limit and lower limits of R_j respectively.

3.3 Optimisation Program

SCILAB is an open source scientific software package, used for numerical computation [96]. SCILAB V4.1 running on a Linux operating system is used for computing optimum values for the design variables. SCILAB provides the Linpro function for the optimisation of linear programming problems, with both equality and inequality constraints [99]. The Linpro function is based on a FORTRAN program plcbas.f [98]. The algorithm calculates a direction of decent, which can have null, positive or negative curvature, from a reduced Hessian matrix $\mathbf{H}_k$,where subscript k is iteration number [99]. The reduced Hessian is calculated using partial Cholesky factorisation [100].

The structure of the SCILAB code can be seen in Figure 3.8. The lengths are initially optimised without the reaction constraints using the Linpro function before the loop begins, and coefficients for the reaction constraints are calculated (see Appendix III for the full code).

The optimal values of the design variables are then calculated using the Linpro function, with the inclusion of the reaction constraints. The set of values for the design variables is stored, and the new reactions are calculated and stored.

The reactions constraints are checked using a Boolean matrix $(\mathbf{R})$, which is used as the control for the 'while' loop, where:

$$\mathbf{R} = \begin{Bmatrix} R_k \geq R_{kU} & R_k \leq R_{kL} \\ R_f \geq R_{fU} & R_f \leq R_{fL} \\ R_{td} \geq R_{tdU} & R_{td} \leq R_{tdL} \\ R_{ts} \geq R_{tsU} & R_{ts} \leq R_{tsL} \\ R_k + R_f + R_{td} + R_{ts} \geq 61600 & false \end{Bmatrix}$$

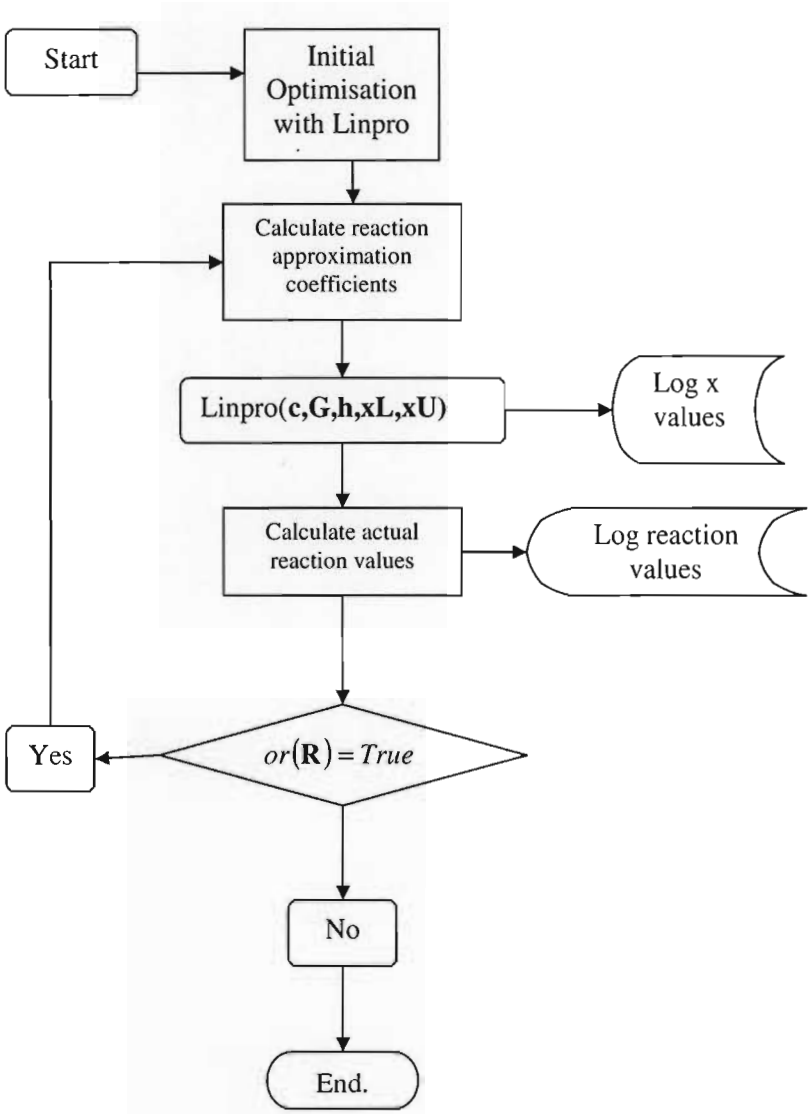

Figure 3.8 Structure of the optimisation program

The loop repeats itself until every component of the **R** matrix is false. If the reaction constraints are not met, the reaction coefficients are re-calculated with the new design variable values. The process is repeated until the reaction constraints are met.

3.4 Results

The results of the initial optimisation to calculate the starting point for the loop are shown in Figure 3.9. At iteration 1, a feasible point in the domain is calculated. The value of the objective function (shown with a dashed line) remains approximately constant until iteration 6, where x_2 and x_5 decrease. This, compensated by increases in other design variables to meet the constraint conditions, results in a decrease of the objective function.

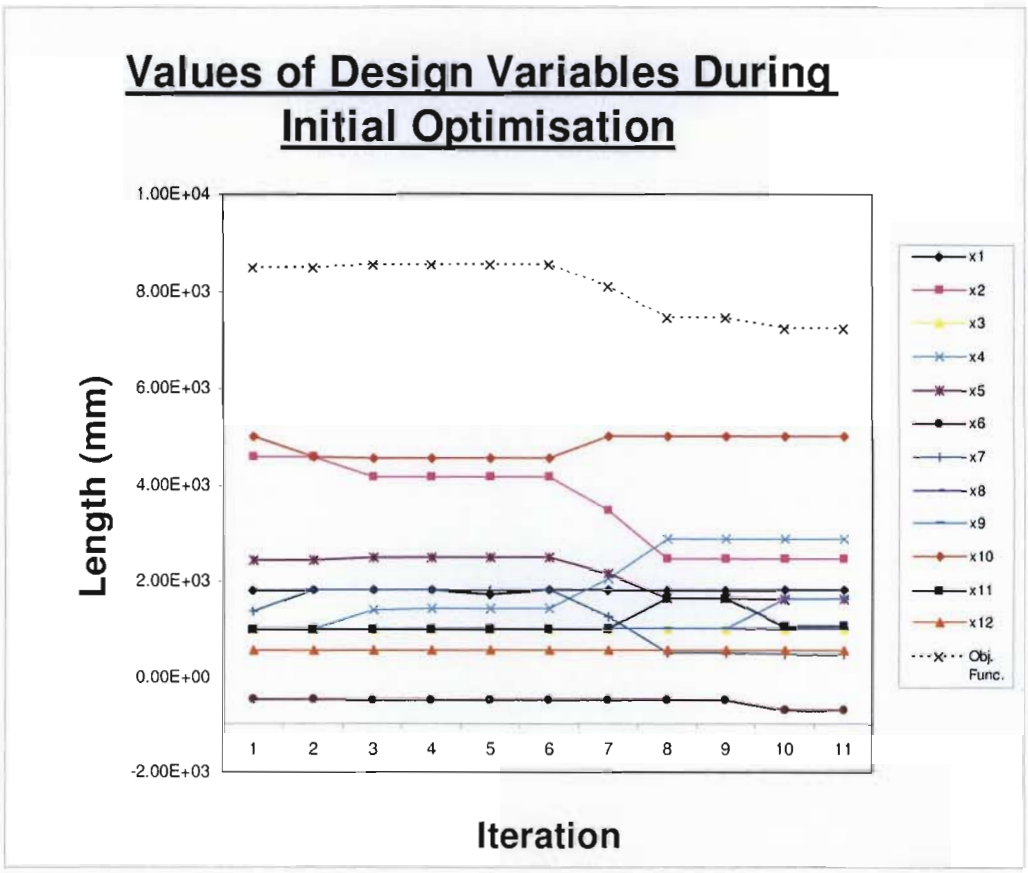

Figure 3.9 Initial optimisation values of the objective function and design variables

The value of the objective function decreases until iteration 10, where it converges, and the minimum is found. The values of the design variables at iteration 11 are then used to

calculate the initial reaction constraint coefficients. The value of $or(\mathbf{R})$ reached false after 26 passes of the while loop. The values of the reactions are plotted in Figure 3.10.

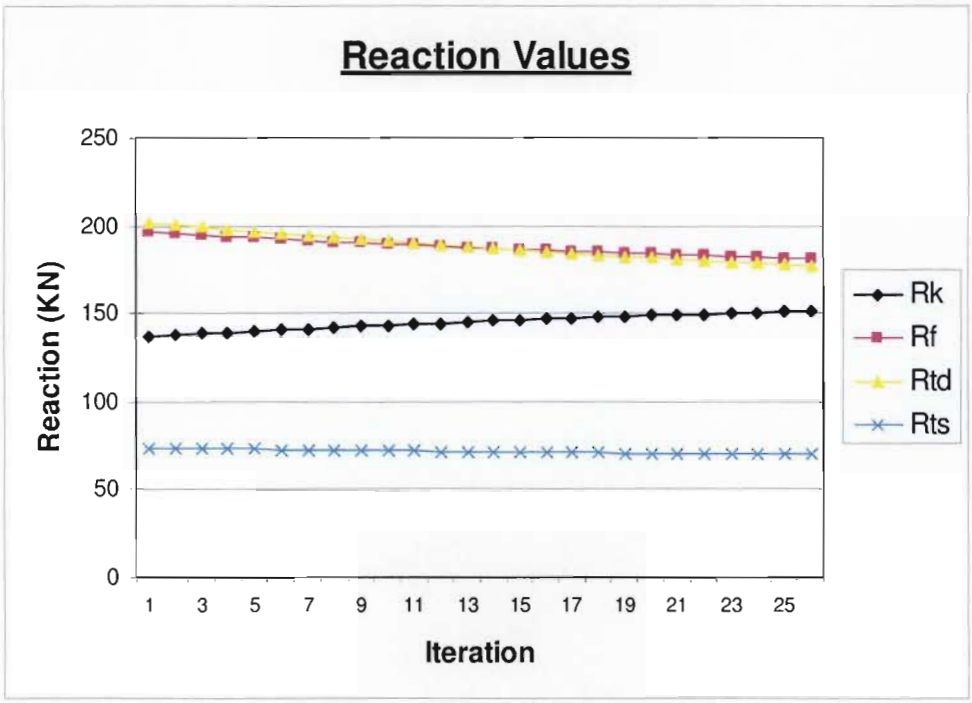

Figure 3.10 Reaction values during iterations

Initially the values of R_f and R_{td} are too high, and the value of R_k is too low. The weight distribution is gradually shifted towards the rear with each pass of the loop until the reactions are all in the allowable range.

The values of the design variables are plotted in Figure 3.11. The values of $x_1, x_2, x_4, x_5, x_6, x_8, x_{10}$ and x_{12} remain approximately constant from the initial optimisation, with x_6 taking a negative value. The value of x_9 decreases and x_{11} increases, transferring weight distribution onto the rear axle until the reaction conditions are met.

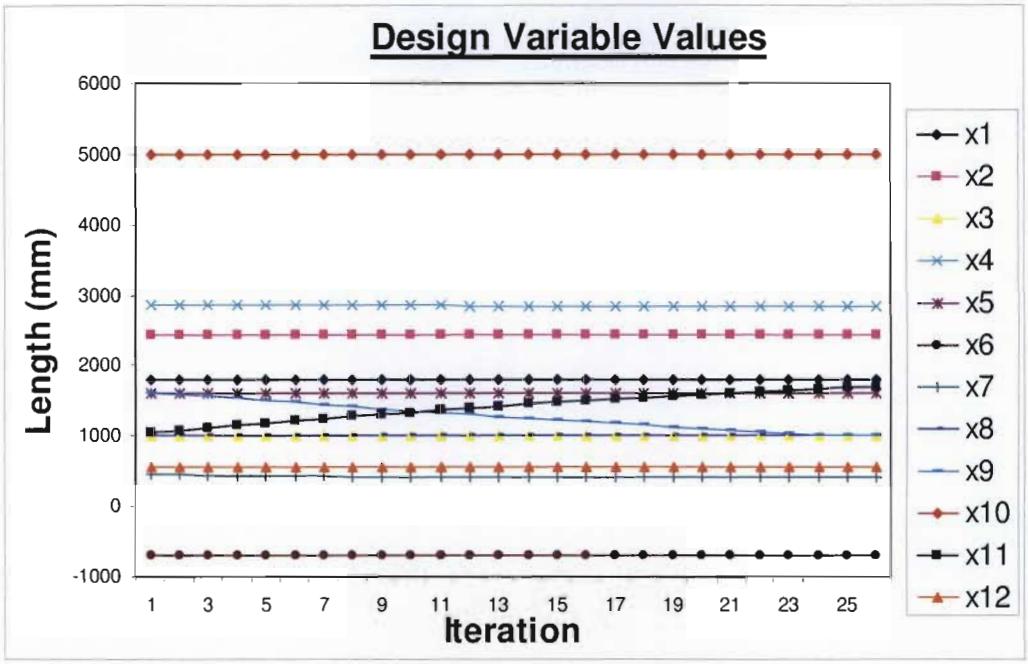

Figure 3.11 Graph of design variables during optimisation.

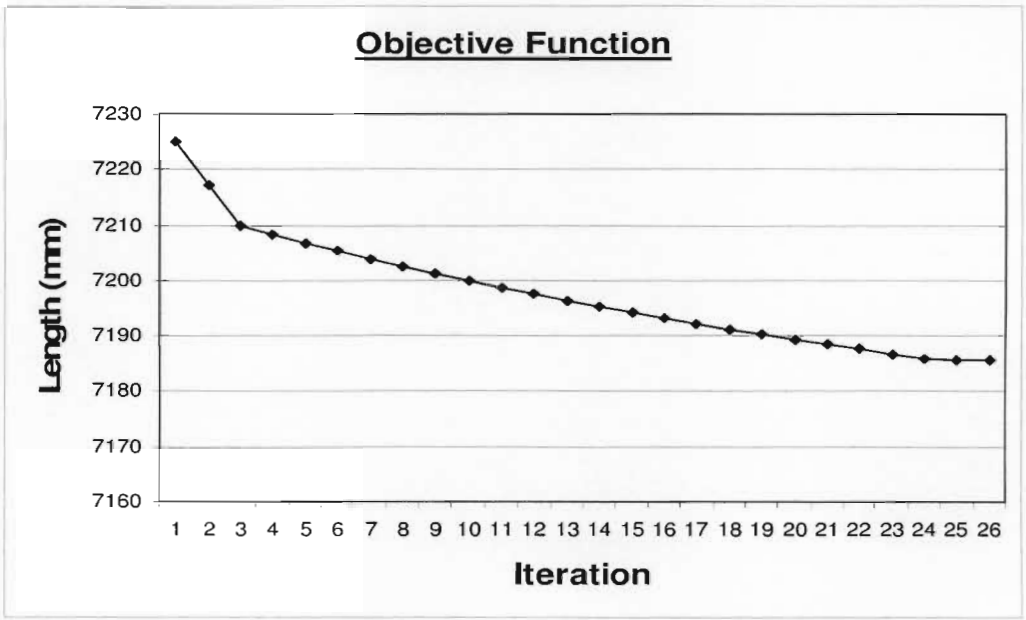

Figure 3.12 Graph of objective function during optimisation.

The objective function decreases slightly while the loop is running, but the overall trend is a more or less constant value, changing 0.54% from the iteration 1 to iteration 26. This is because the objective function is minimised during each loop, and the objective function is not dependant on variables x_9 and x_{11}, which are varied in order to meet the reaction constraints.

3.5 Geometric Parameter Optimisation Conclusions

The small variations in the design variables during the initial optimisation indicate that the feasible domain is relatively small. This is due to the number and nature of constraints, resulting in a tightly bounded domain.

A set of optimised values for the design variables was obtained. The optimum values for the length of the chassis were checked for validity, and resulted in an achievable interlink combination design (Figure 3.13).

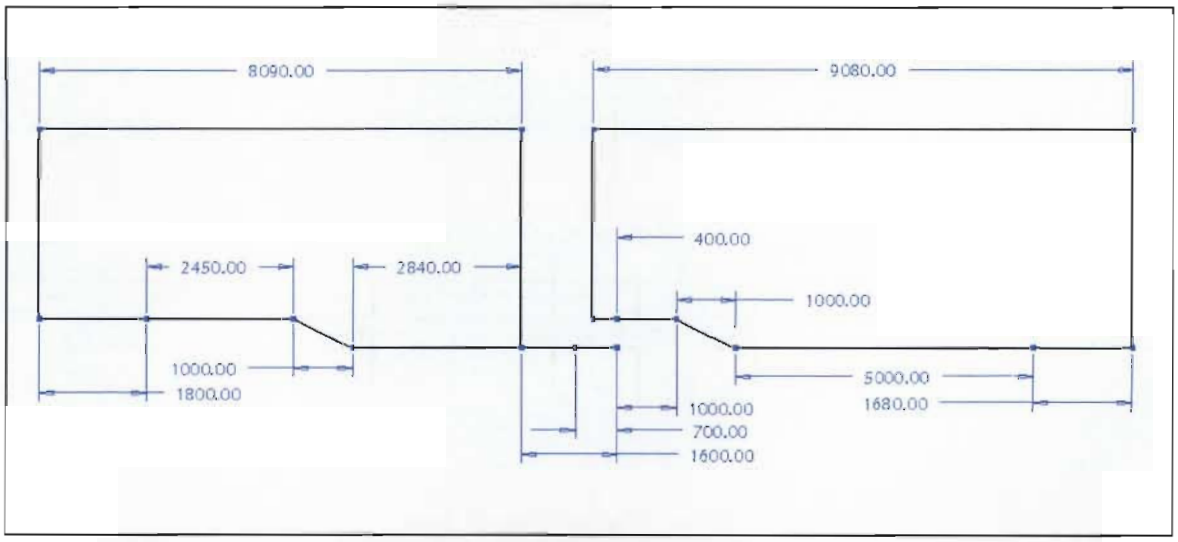

Figure 3.13 A sketch of the optimised values for the lengths of the trailers

The bending moments of the optimised trailer configuration are shown in Figure 3.14. The bending moment of the optimised rear trailer is larger than the initial trailer. Most

trailer manufacturers tend to use similar section dimensions for the front and back trailers, indicating that back trailers are probably over designed for most configurations.

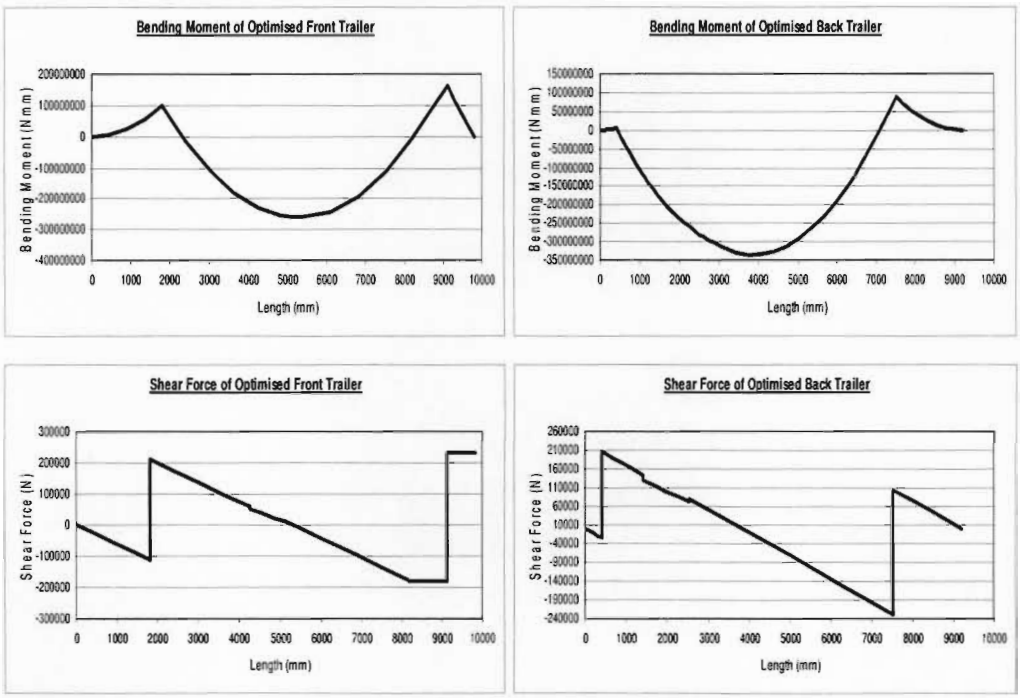

Figure 3.14 Bending moment and Shear force diagrams of the front and back trailers with optimised lengths.

The principle result of the optimised lengths is a reduction in the bending moment of the front trailer. Comparing Figures 3.2 and 3.14, the bending moment of the front trailer has been reduced from 371.3 kNm to 259.8 kNm, or a 30.04% decrease. This results in a decrease in the required section modulus of the main chassis beams and a reduction in the overall tare mass of the vehicle, while still meeting payload requirements.

3.6 Initial Section Optimisation

The main chassis beam is a welded I-beam, with variable web depth (d) and constant flange width (b), flange thickness (t_f) and web thickness (t_w), (see Figure 3.15). The flange width is fixed due to the attachment requirements of standard suspension components. To determine the initial optimum section values, the required web depth of each section of the beam is calculated for sets of web and flange thickness in a range of 2-16mm.

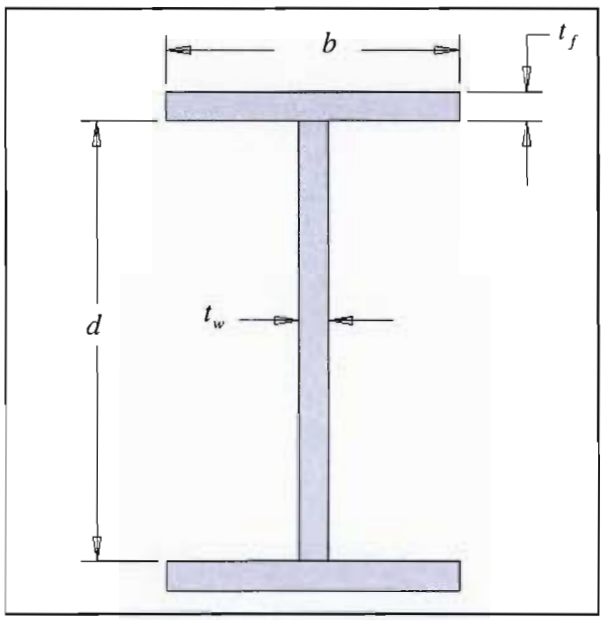

Figure 3.15 Sketch of a typical welded I-beam.

For each set of flange and web thicknesses, the required web depth is calculated with a MATLAB program (see Appendix IV). The web-depth has an initial minimum value of 200mm for equipment attachment purposes. The minimum required web depth is calculated for elastic moment capacity, shear capacity, combined moment and shear capacity, shear-buckling of the web, and shear, normal and combined fatigue of the welds.

The static load moment, shear, and combined capacity is calculated using the dynamic design factor of 2.75 from Chapter 2. Elastic moment capacity, rather than plastic moment capacity is used because it is more conservative, and ideally the full plastic

moment will never occur during operation. Shear-buckling of the web is included because of the high depth-thickness ratio of this kind of beam often results in static failure through buckling of the web before failure due to inadequate moment or shear capacity. The procedure outlined in Eurocode 03 [101] for welded plate girders is used to determine shear-buckling capacity.

The method outlined in [101] for determining cumulative fatigue damage in welded plate girders with the Palmgren-Miner sum is used to calculate the required section for fatigue considerations. It is used in conjunction with an adaptation of a block loading cycle for semi-trailers from [15] and [78]. The block loading sequence diagram is shown in figure 3.16, and consists of 2 million cycles at 1.4g, simulating minor road irregularities, 120 000 cycles at 1.9g, simulating potholes and washed-out dirt road sections, and 80 000 cycles at 2.2g simulating major road irregularities.

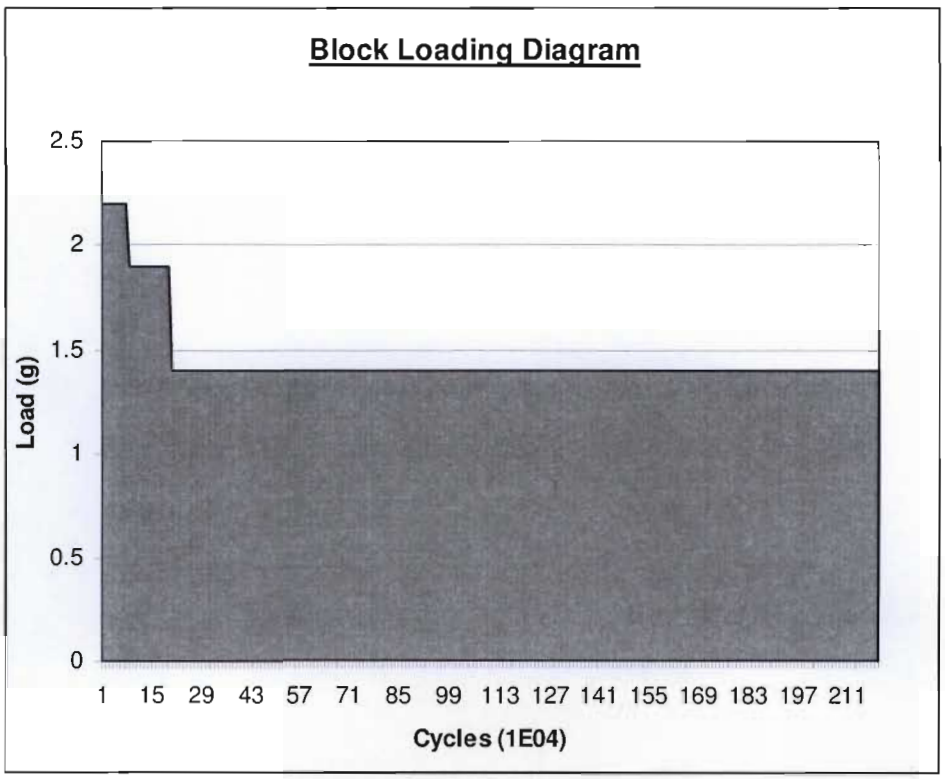

Figure 3.16 Block loading diagram for fatigue criteria

For the static loading cases, moment capacity is generally the limiting factor (shear-buckling of the web is the limiting factor when the slenderness of the web increases), but fatigue failure through cracks developing in the welds is the overall limiting factor. Figures 3.17 and 3.18 show the effect of flange and web thickness on the overall mass and maximum required web depth respectively.

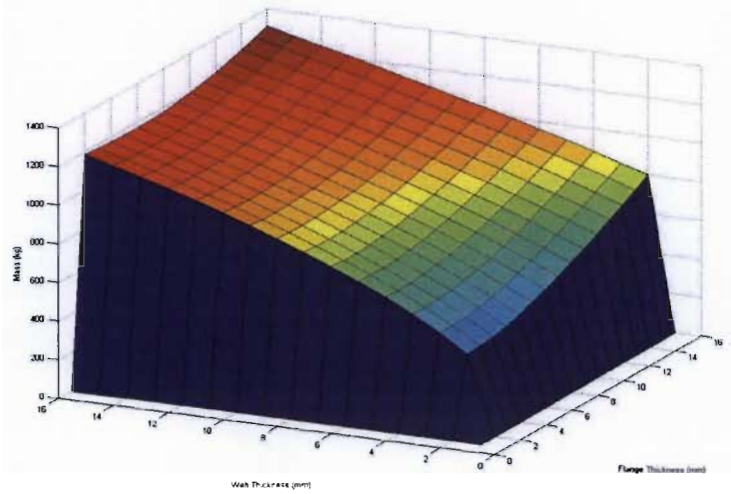

Figure 3.17 Graph showing the effect of flange and web thickness on mass.

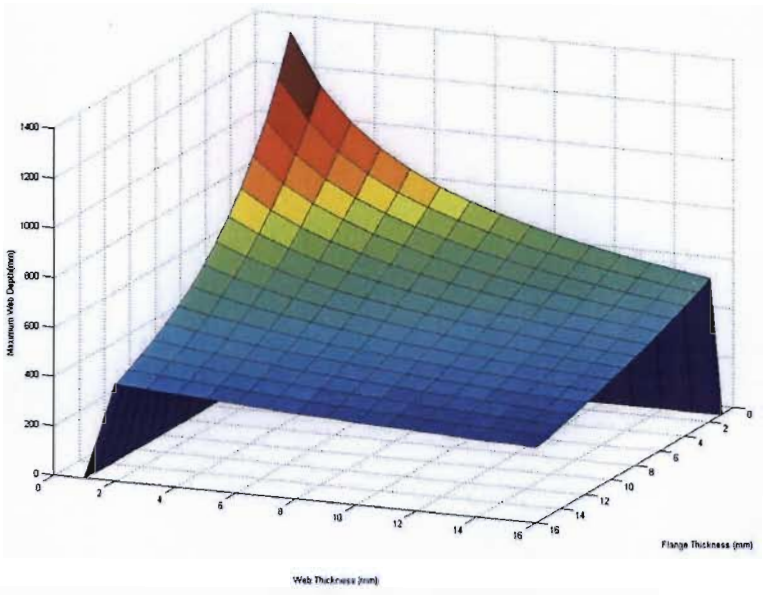

Figure 3.18 Graph showing the effect of flange and web thickness on maximum web depth.

The lowest mass occurs at the point where the flange and web thicknesses are low, but requires a large maximum web-depth (note that the graphs are oriented differently

to enable observation). As the thickness of the web decreases, the efficiency of material usage increases, resulting in a lower mass, but this is limited by the increase in web-depth.

An investigation showed that the yield strength of the material does not affect the overall mass of the chassis beam for a range of 400 MPa – 700 MPa. This is because the fatigue strength of welds in this particular range of high-strength, low-alloy steels is independent of parent material strength [86, 101]. At a value of 400 MPa, static criteria become the limiting factor. For this reason the main chassis beam will be constructed from Domex 500MC high-strength, low-alloy steel.

The sets of values with large differences between flange and web-depth thicknesses are excluded due to welding requirements. The initial section values are chosen as the values in the allowable range that result in the lowest mass, which is a flange thickness of 12mm, and a web thickness of 10mm. The minimum required values of web-depth for each section are used to create the initial beam profile. The resulting front and back beam profiles, with adaptations for manufacturing considerations, and fifth-wheel and suspension components, are shown in figures 3.19(a) and 3.19(b).

Figure 3.19(a) View of front trailer chassis beam.

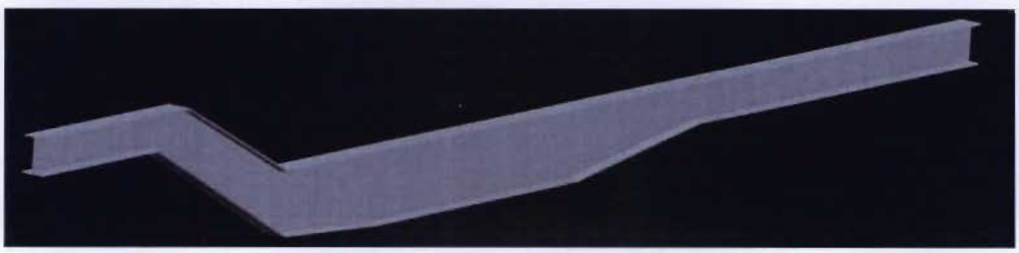

Figure 3.19(b) View of back trailer chassis beam.

Chapter 4 - Finite Element Analysis of Main Chassis Beam

4.1 Introduction

The finite element method has been used in the design and analysis of various components and structures in heavy vehicles, and has become an important tool for heavy vehicle designers [10]. Finite element analysis of heavy vehicles is conducted to determine stress levels in various components [6, 11, 54, 55], to calculate frequency response [53, 57, 61, 102], and to investigate various structural permutations [6, 12, 13]. Examples of finite element analysis in heavy vehicle industry can be found in [76, 103- 110].

The finite element software that is used to analyse the vehicle structure and components is Pro/Mechanica. The software is part of the Pro/Engineer package developed by Parametric Technology Corporation. The structural and thermal simulation package (pro/Mechanica) is a multi-discipline CAE (Computer Aided Engineering) tool that enables the multi - physical behaviour of a model to be simulated [111].

Pro/Mechanica uses *p*-version finite element method, which has been shown to be a robust, and in some cases, more efficient method than *h*-version FEM techniques [112-116]. The primary difference between the *p*- and *h*-versions, is that h-versions use a fixed polynomial degree of element, usually linear, quadratic or cubic, and *p*-version uses a varying polynomial degree of elements [117]. For increased accuracy and convergence, the mesh of *h*-version methods is refined, while the mesh of *p*-version methods is fixed and the degree of the elements is increased [118]. Figure 4.1 shows a typical *h*-type mesh, and Figure 4.2 shows a typical *p*-mesh.

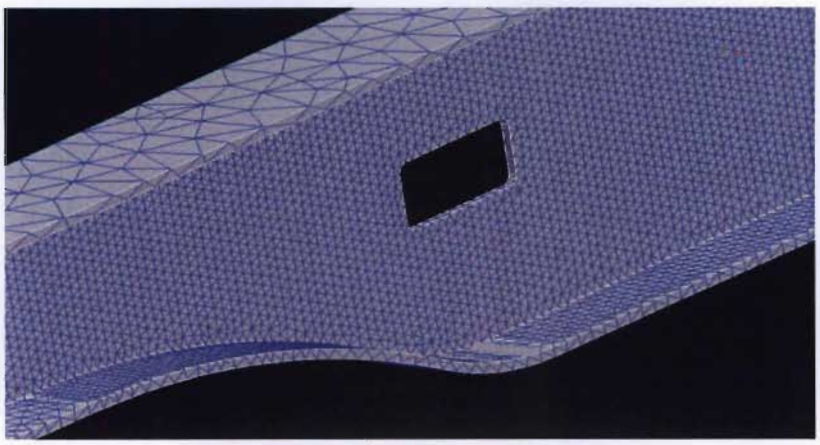

Figure 4.1 Typical *h*-type mesh

Figure 4.2 Typical *p*-type mesh

A higher order polynomial can follow underlying geometry with increased accuracy, and eliminate effects such as faceting on the edges of FE models. The nature of *p*-meshing results in a mesh with fewer elements in comparison to an equivalent h-mesh (see Figures 4.1 and 4.2). References [119-126] give further details and examples of finite element analysis based on the use of *p*-version.

4.2 Load Cases

The primary load on the main chassis rails is a vertical load equivalent to the payload multiplied by the dynamic design factor (DDF) of 2.75 obtained in Chapter 2. In addition to this, the load cases outlined in [52] are also investigated. The load cases are:

I. Static load of Stationary vehicle

II. Braking

III. Accelerating

IV. Cornering

V. Torsion

VI. Maximum load on front and rear axles

VII. Drawbar loads

VIII. Asymmetrical longitudinal loads

In [127], the torsional design aspects of long wheelbase vehicles, such as semi-trailers, are investigated. The author concludes that the most critical loads are those induced by twisted ground plane (one side of the truck travelling over a bump) and lateral cornering acceleration. These correspond to cases IV and V. Effects such as torsion induced through mal-distributed payload and uneven turning forces were found to be insignificant when compared with cases IV and V. Due to the nature of the payload, it is unlikely that the payload will be concentrated over a single axle set, as in the case of concentrated loads that occur in the cases such as heavy machinery transportation. The loads cases considered in this study are I - IV, and V. The cross-braces and other structural members are responsible for resisting a significant amount of torsional forces. For this reason, this chapter will focus on load cases I - III, and load cases IV and V will be investigated using a beam model of the entire structure in Chapter 5.

The static loads consist of a uniformly distributed load on the top surface of the upper flange equivalent to the payload and the payload multiplied by the DDF. An additional load is imposed on the surface where the fifth wheel attaches to the front trailer, which is equivalent to the reaction at the fifth-wheel plate on the rear trailer.

The loads for braking are determined by the requirements for braking performance specified in [19]. For heavy motor vehicles capable of exceeding 35 km/h, the minimum required deceleration is 4.4 m/s^2. The load is calculated by using a factor of 2 applied to the braking force to account for emergency stops and uncertainties in braking forces. The downward acting component of the payload is included, resulting

in loads of 1g and -0.897g in the vertical and horizontal directions respectively. Both loads are applied simultaneously in the same way as the static load.

The accelerating loads are calculated in a similar way to the braking loads, using the acceleration capability performance values from [128], and a factor of 2 to account for uncertainties in acceleration. The corresponding road vehicle class is class 2, but the acceleration capability standard of a class 1 vehicle is used because it is slightly conservative. A class 1 vehicle requires a time to travel 100m from rest of 20 seconds. The resulting required acceleration is 1 m/s^2 , which results in loads of 1g and 0.102g in the vertical and horizontal direction respectively. Both loads are applied simultaneously in the same way as the static load.

The torsional load from cornering is taken as 0.3g as in [127], in combination with the static load of the payload. The load from ground plane twist from uneven road profiles will be achieved by a forced displacement (of 400mm) of the points on one side of the suspension spring model.

4.3 Main Chassis Beam Model

The main chassis beam is modelled with solid elements for the flanges and shell elements for the web. Initially, the beam was constrained by means of fixed surface constraints to simulate the areas where the fifth-wheel and suspension support the beam. This was found to be inaccurate because in reality, the suspension and fifth-wheel allow the attached sections to rotate, and in the case of the suspension, a certain amount of vertical displacement is allowed. The fixed surface constraints resulted in intense stress concentration at these locations, and deflections that did not appear to be realistic (Figure 4.3).

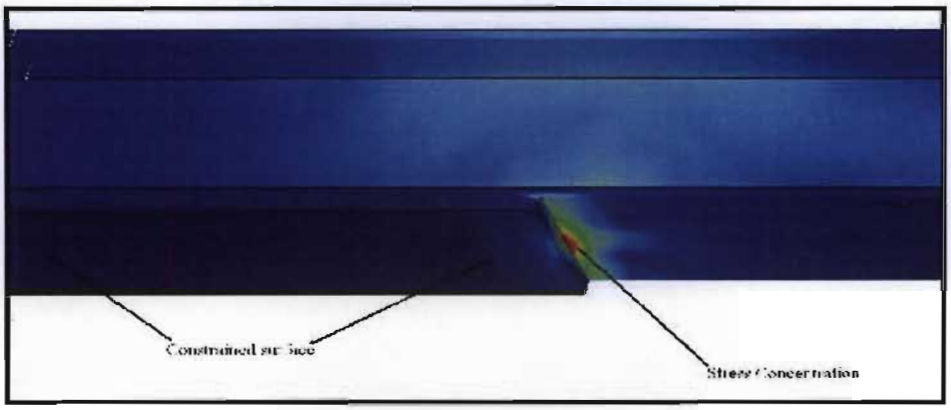

Figure 4.3 Stress concentration at the constrained surface

The problem is overcome by using simple spring representations of the fifth-wheel and suspension. The springs that represent the suspension have values equivalent to the spring deflection rate of the specified suspension. The springs have large torsional constants (1 000 000 mmN/rad), to prevent twisting of the chassis under the loads. To provide lateral stability, the springs representing the suspension are attached to either side of the suspension mounting plate and meet at a single point below, which is fixed in six degrees of freedom. The springs representing the fifth-wheel are attached at each corner of the fifth-wheel plate, and meet at a point which allows rotation in the same way as the fifth-wheel.

These constraints resulted in a deformation that appears to be closer to the actual deformation that would be experienced by a beam in a truck under this type of loading (Figure 4.4).

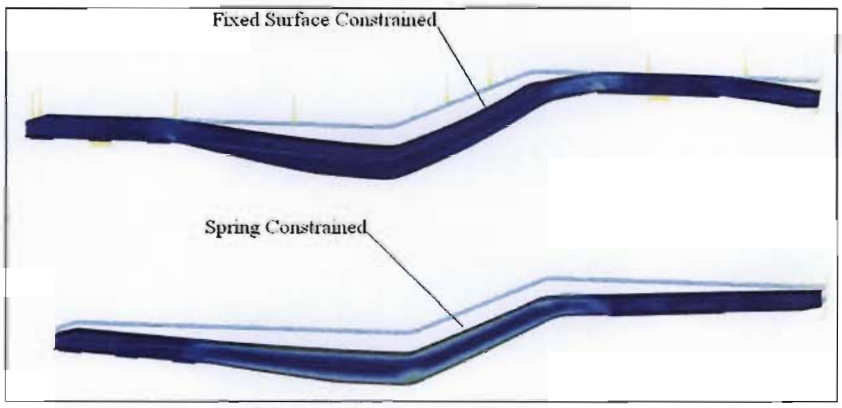

Figure 4.4 Comparison of beam deformations

A view of the front chassis beam model is shown in Figure 4.5. The flanges are modelled with 1355 solid tetrahedral elements, and the web is modelled with 35 tri and 49 quad shell elements.

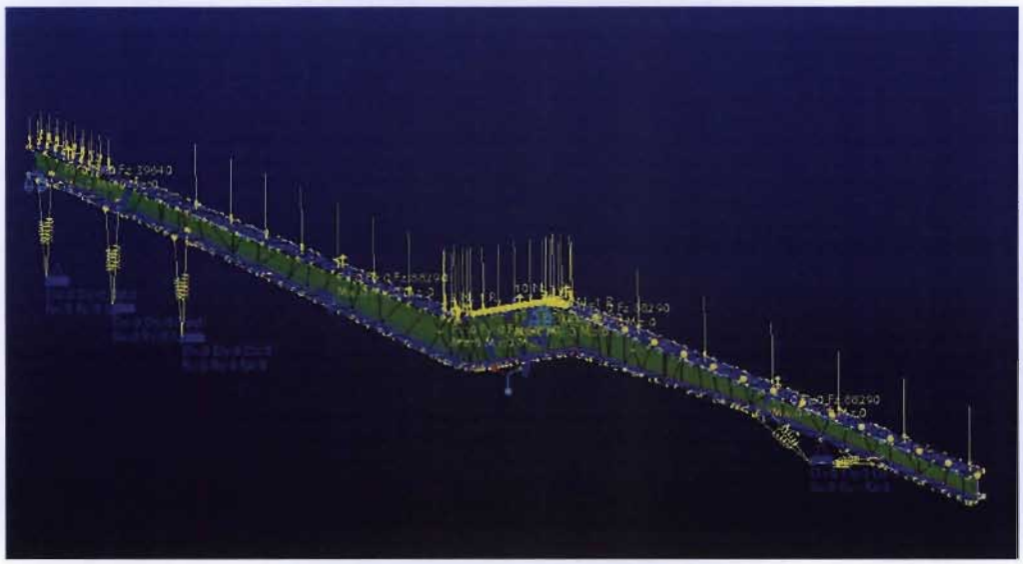

Figure 4.5 The model of the front chassis beam.

The beam is constrained through 10 spring elements and 4 points. Measures of principle and Von Mises stresses are created on the web and flanges. The back chassis beam is modelled in the same way, with 1525 solid tetrahedral, 54 tri shell and 83 quad shell elements.

4.3.1 Sensitivity Analysis of Rounded Corners

Initial analyses showed high stress concentrations occurring at the corners of the step geometry. To lessen the effect of the step geometry on the stress that occurs in the beam, the corners are rounded. A global sensitivity analysis of the radius at the corner and the maximum Von Mises stress occurring at the corner is conducted to determine the effect of the radius at the corners. The results can be seen in Figure 4.6. The stress decreases as radius increases up to approximately 600mm, and the curve levels out from 600-1000mm. A value of 750mm is selected for the radii. The effect of rounding the corners of the beam can be seen in Figure 4.7.

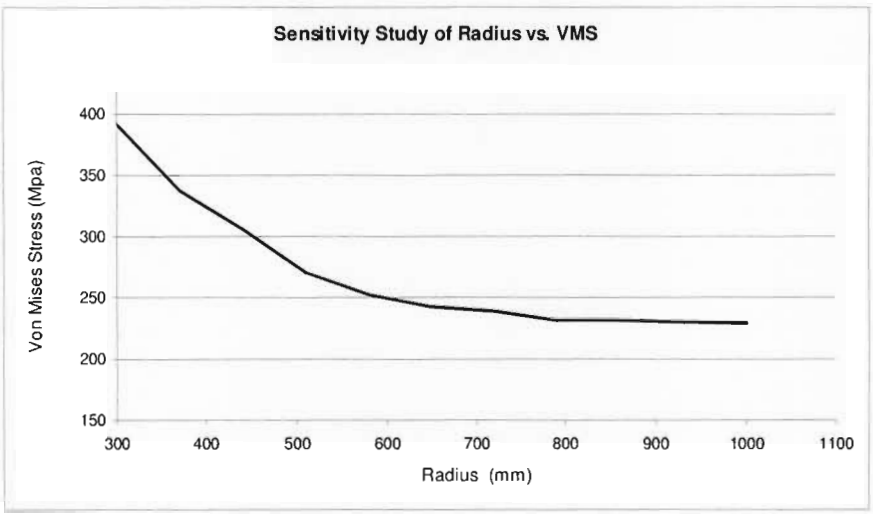

Figure 4.6 Graph showing the effects of radius on maximum Von Mises stress.

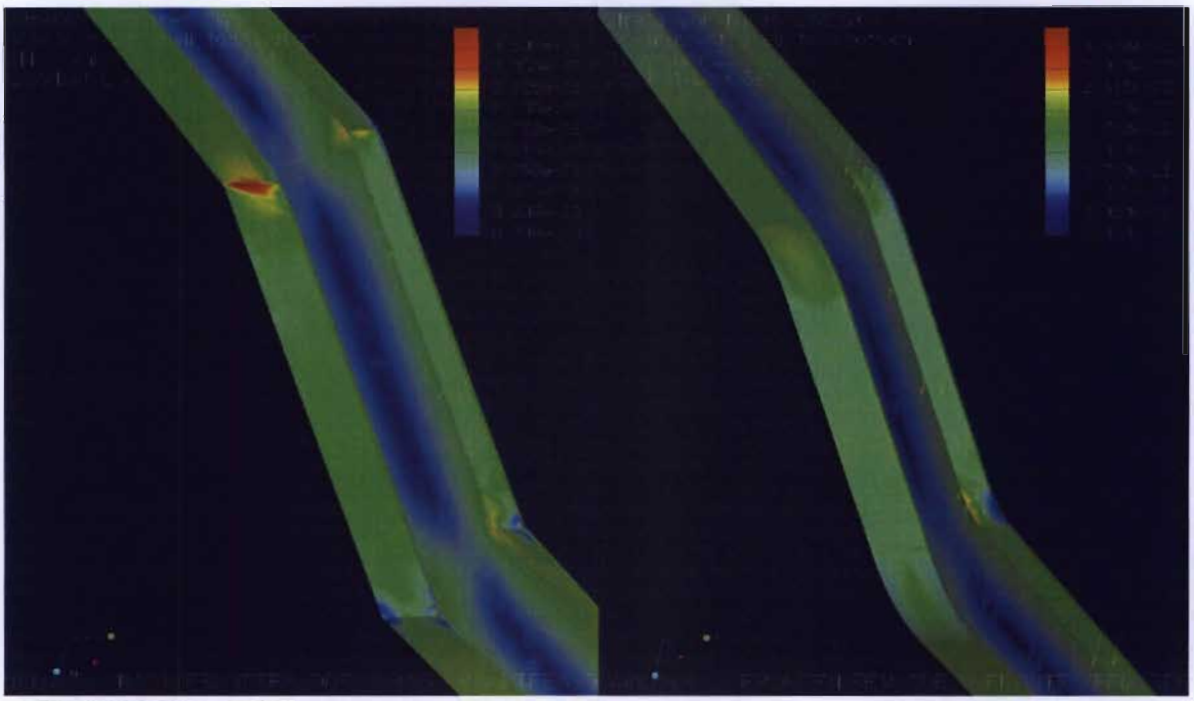

Figure 4.7 Fringe plot of Von Mises stress showing the effect of rounding the corners.

The stress at the corner is initially above 350 MPa, indicated by the red area. After rounding the corners with a radius of 750 mm, the stress at the critical regions decreases to below 230 MPa.

4.3.2 Mesh Density Refinement

To investigate the effect of mesh density on the results obtained from the finite element analysis, a comparison to the initial mesh results is conducted. A new mesh with a higher density is created by reducing the maximum allowable edge and face angles from 175 to 160 degrees, and increasing the minimum allowable edge and face angles from 5 to 10 degrees. In addition to this, mesh controls are placed on the web/flange interface to limit node spacing.

The resulting mesh contained 4179 solid tetrahedral, 139 quad shell and 104 tri elements, almost tripling the average mesh density. Models with the initial mesh and refined mesh are subjected to the same loads and boundary conditions. The result is shown in Figure 4.8.

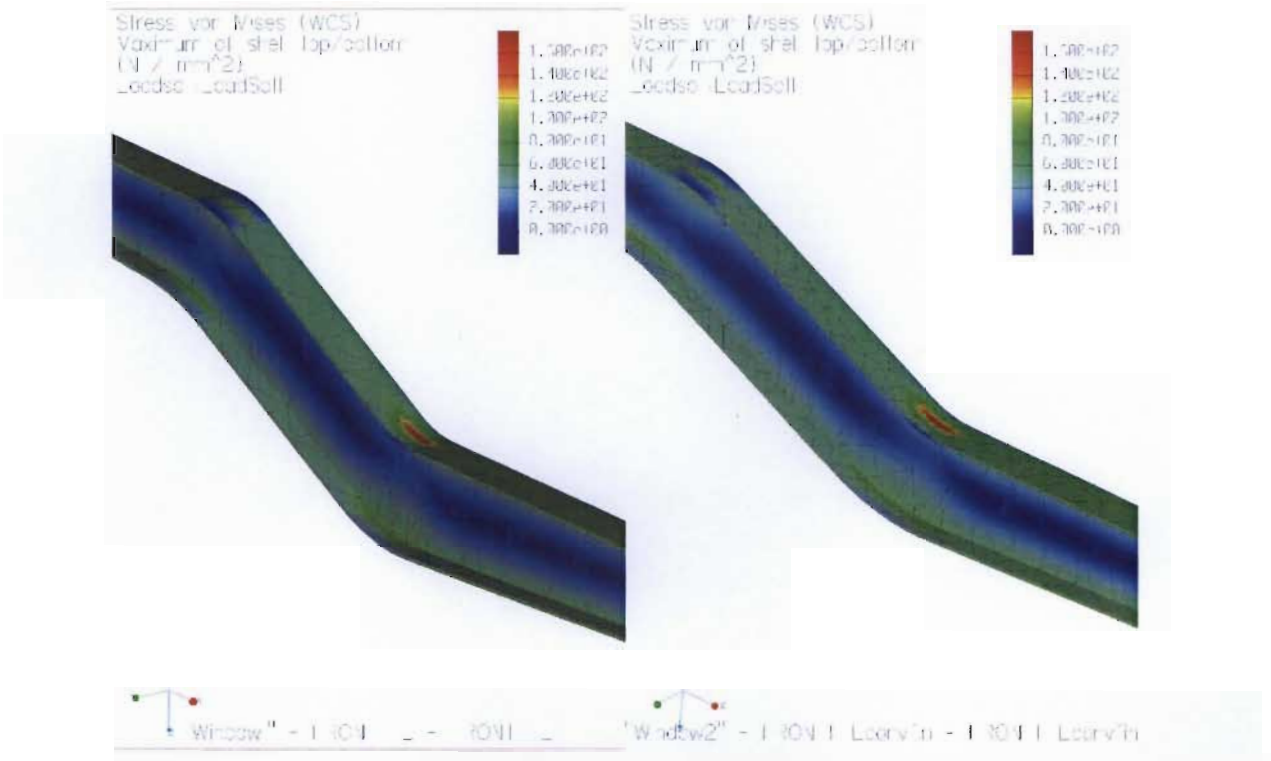

Figure 4.8 Fringe plots of Von Mises Stress showing comparison between initial and refined mesh.

The results are not significantly affected by mesh density. The two analyses produced

identical stress contours (see Figure 4.8), and the maximum stresses of the analyses corresponded to within 1.5%.

4.3.3 Convergence

The front trailer analysis converged after 5 passes, with a maximum polynomial level of six. The polynomial level of the elements in the model varies from 2 to 6 (see Figure 4.9), with a higher level occurring at the supports and in the regions where the beam curves. These are areas of greater stress gradient, in comparison to the rest of the model.

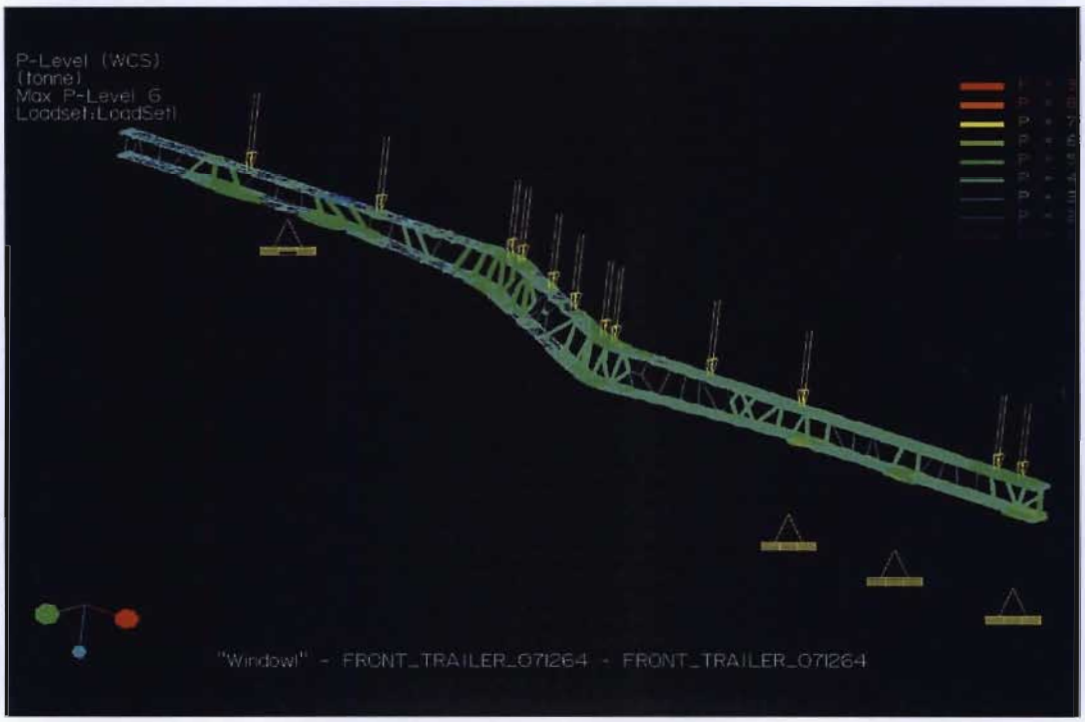

Figure 4.9 *P*-level of the front trailer model.

The graphs showing the convergence of the measures for the front trailer with loading of 1g in the vertical direction can be seen in Figure 4.10 (see Appendix V for convergence reports). The graphs of maximum Von Mises and principle stress in the web and flange all display similar trends. The value of the measure corresponding to first *p*-loop is high. The measures reach lower values for the second loop, then increase and converge to within 5%. The strain energy increases after the low value

of the initial loop, and then converges upwards to within 5%.

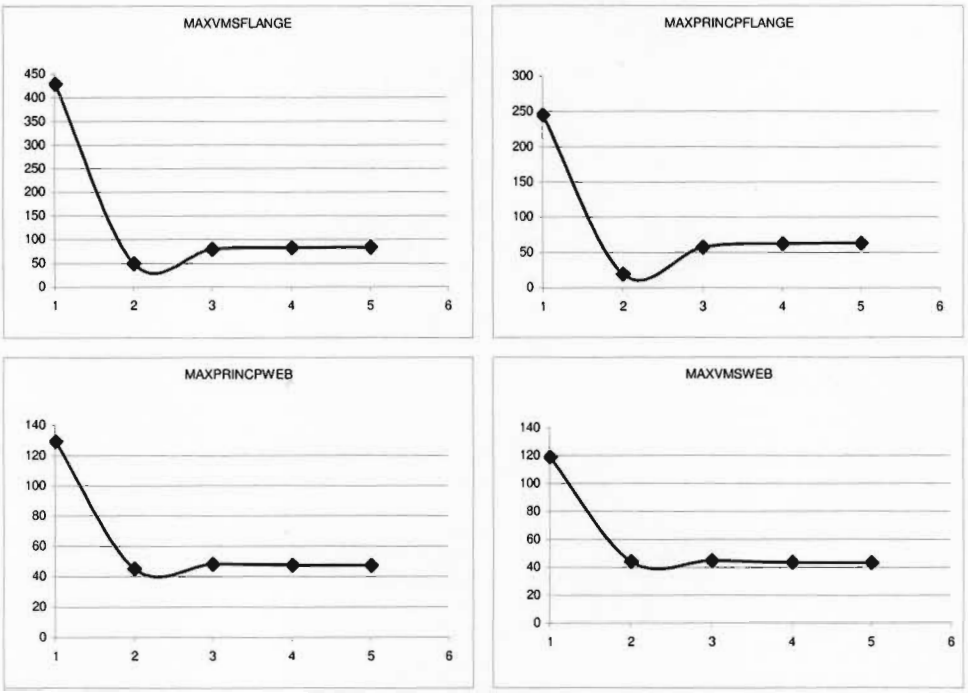

Figure 4.10 Graphs showing convergence of Von Mises and maximum principle stress in MPa for the front trailer web and flange vs. *p*-loop.

The back trailer converged after 6 *p*-loops, and displayed identical behaviour with regard to convergence of stresses and strain energy. The convergence of analyses with a load equivalent to the payload multiplied by the DDF also displayed identical behaviour, and the front and back trailer analyses converged after 5 and 6 *p*-loops respectively.

4.4 Results

Static Loading

A fringe plot of Von Mises stress for the front trailer under loads of the payload and payload multiplied by the DDF can be seen in Figures 4.11 - 4.12. Results for both back and front trailers are included in Appendix VI. The maximum Von Mises stress over the model is over 5000 MPa, and occurs at the location of the point constraints of the fifth-wheel attachment. The unrealistically high stress is a result of singular stress concentrations at the corners where the spring elements link to the fifth-wheel plate,

and is a fictitious critical region induced by the applied boundary conditions [102]. This highly stressed zone is localised and, does not affect the overall structure.

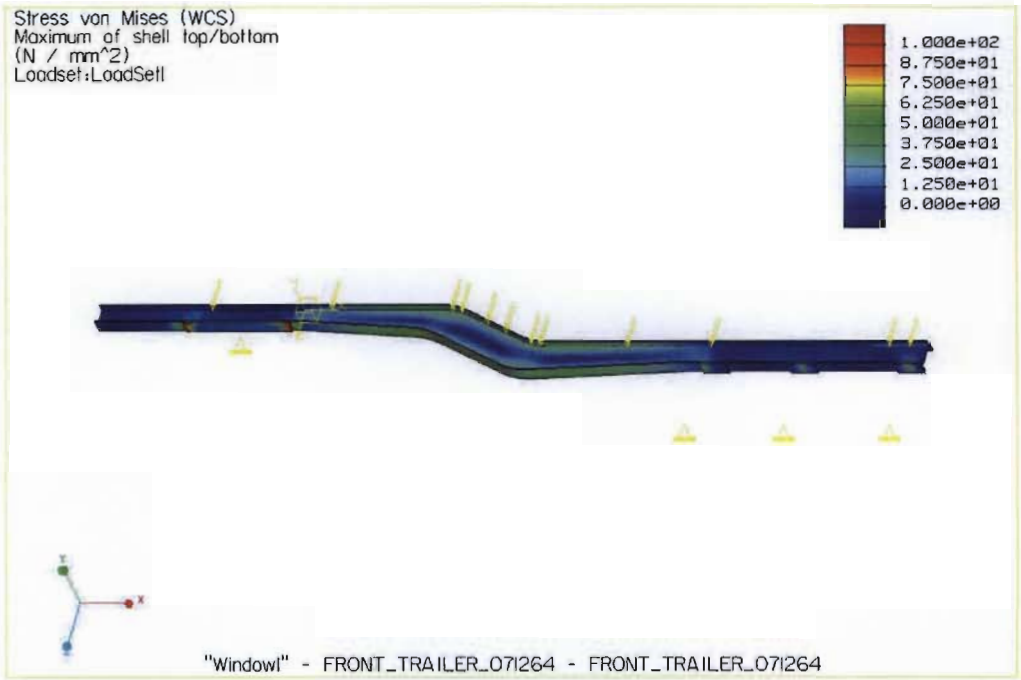

Figure 4.11 Fringe plot of Von Mises stress for front trailer under normal loading

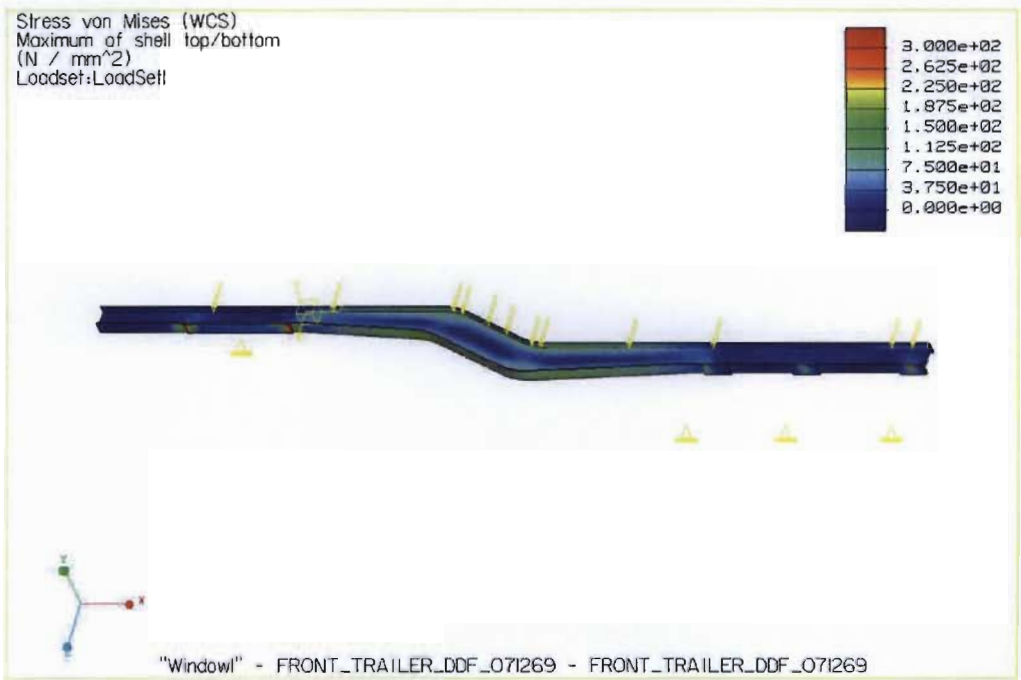

Figure 4.12 Fringe plot of Von Mises stress for front trailer under DDF loading

The stress distribution in the beam and flanges are identical for both cases with the exception of the scale. The stress for the DDF load case is higher by a factor of within 1% of 2.75. The middle section of the beam is more stressed than the front and rear section. This is due to the initial optimisation of the cross-section. The depth of the web of the front and rear sections are limited to a minimum by manufacturing and assembly requirements rather than stress requirements, and are thus over designed in comparison to the middle section.

The maximum and minimum principle stresses in the back trailer subjected to DDF load are shown in Figures 4.13 – 4.14. As can be seen, similarly to the front trailer, the front and rear sections of the rear trailer are over designed to meet manufacturing and assembly criteria.

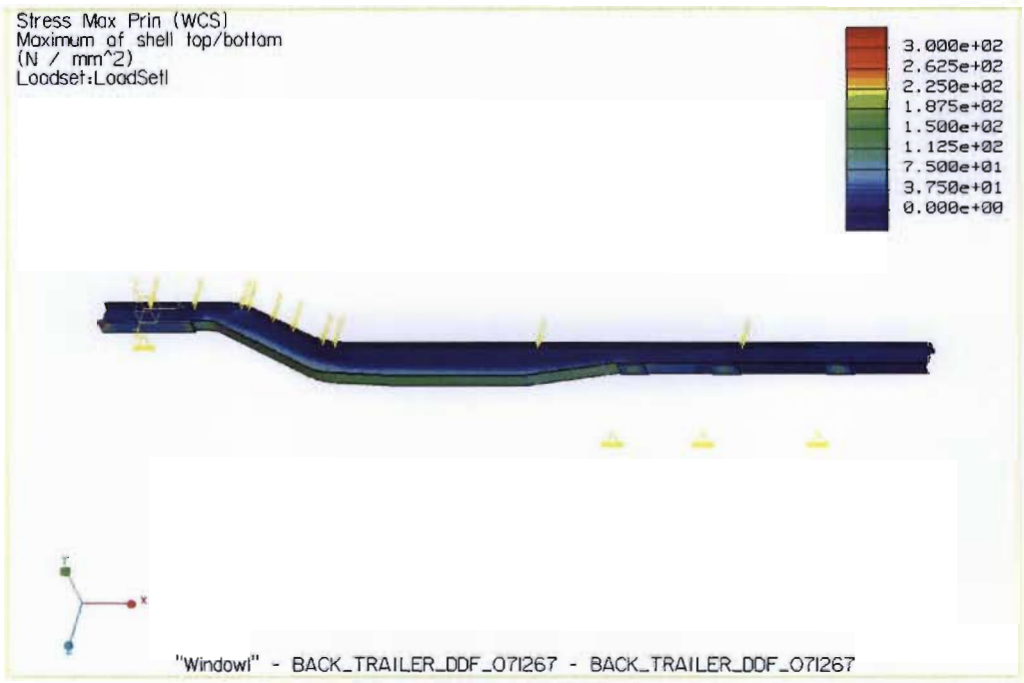

Figure 4.13 Fringe plot showing the maximum principle stress in the back trailer

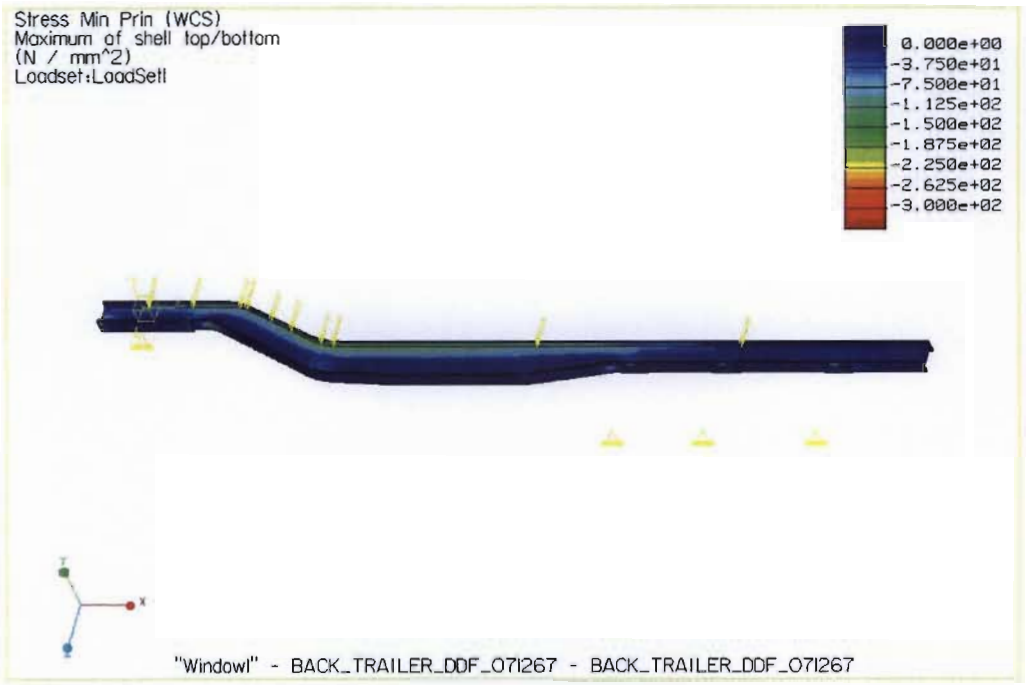

Figure 4.14 Fringe plot showing the minimum principle stress in the back trailer

The maximum and minimum principle stresses occur on the bottom and top sides of the main chassis beam. This is consistent with a beam under a downward acting force, with the top flange in compression and the bottom flange in tension. The maximum stresses in the web and flanges of both trailers are presented in Table 4.1.

Table 4.1 Maximum stresses in the web and flanges for static and static DDF load

Stress (MPa) DDF Load	Front Trailer	Rear Trailer
Web Maximum Principle	144.18	145.25
Web Minimum Principle	-130.01	-247.08
Web Maximum Von Mises	117.76	243.59
Flange Maximum Principle	171.95	190.97
Flange Minimum Principle	-231.09	-187.04
Flange Maximum Von Mises	226.38	239.26
Stress (MPa)	Front Trailer	Rear Trailer
Web Maximum Principle	52.43	52.82
Web Minimum Principle	-47.28	-89.85
Web Maximum Von Mises	42.82	88.58
Flange Maximum Principle	62.53	69.44
Flange Minimum Principle	-84.03	-68.01
Flange Maximum Von Mises	82.32	87.00

The stresses in the trailers are all lower than 50% of the 500MPa yield strength of the

material. This confirms that the fatigue criteria used in the initial section optimisation is the dominating factor. The values of the maximum principle, minimum principle and Von Mises stresses are all within the same range, but the values vary for the front and back trailers. This is primarily due to the geometric differences between the trailers. Figures 4.15 and 4.16 show views of the maximum and minimum principle stress of the top and bottom flanges of the front trailer.

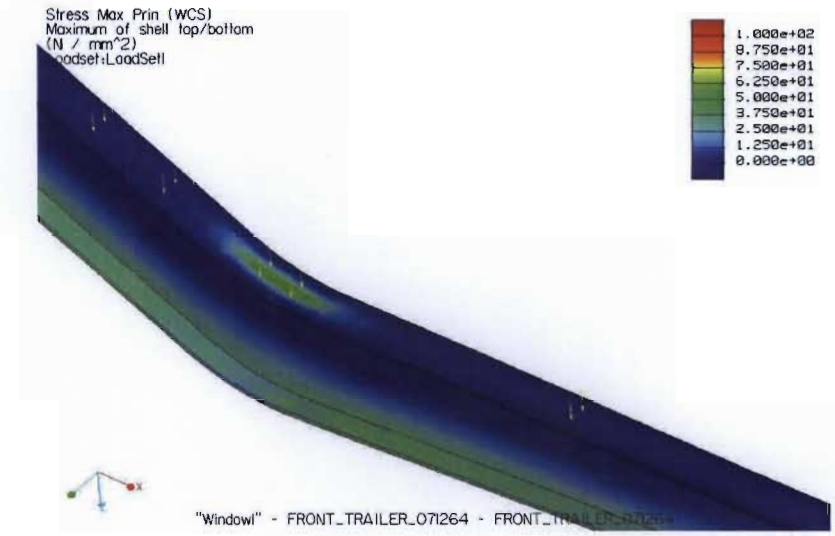

Figure 4.15 Maximum principle stress of the top flange

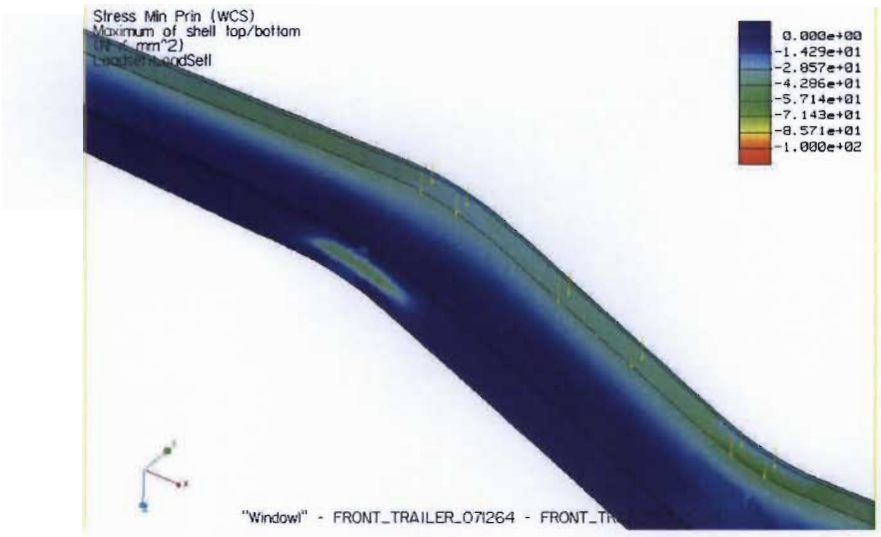

Figure 4.16 Minimum principle stress of the bottom flange

Although generally the areas of highest and lowest principle stresses are on the bottom and top parts of the beam sections, other areas are also subjected to significant

principle stresses. In Figures 4.15 and 4.16, significant areas of tension on the top flange and compression of the bottom flanges can be observed. This is the complex geometry of the beam. Substantial areas of compressive stress also occur in the regions of the supports.

Figures 4.17 and 4.18 show the displacements of the front and back trailers respectively. The displacement includes the deflection from the bending of the main chassis beam and the effects of the spring constraints. The maximum displacement for both trailers occurs at the rear of the beams. This is due to the suspension stiffness in comparison to the higher vertical stiffness of the fifth-wheel constraint.

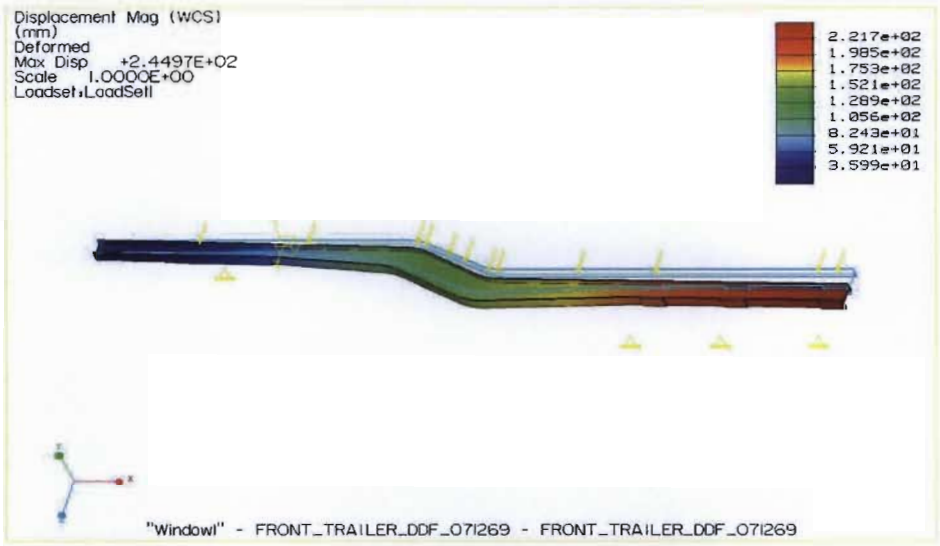

Figure 4.17 Displacement of the front trailer

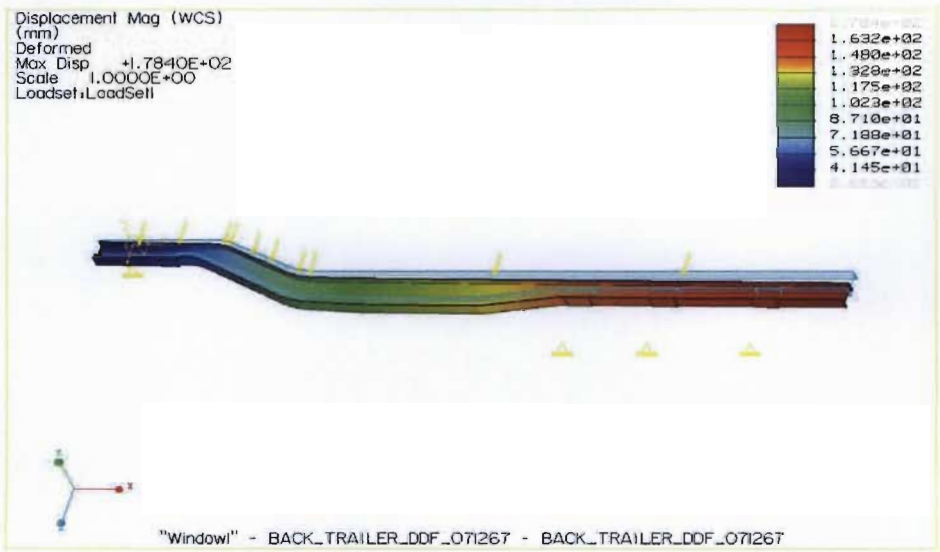

Figure 4.18 Displacement of the rear trailer

The maximum deflections are 245.97 mm and 178.40 mm for the front and back trailers respectively. This value is high with respect to normal suspension deflections due to the DDF load. The analyses with a load of 1g resulted in deflections of 89.14 mm and 64.57 mm, which equate into axle loads of 17.4 tons and 14.6 tons, which are consistent with the initial design optimisation.

Accelerating and Braking

Fringe plots for Von Mises stress for the front trailer under braking load and the rear trailer under accelerating load are shown in Figures 4.19 and 4.20, and the maximum principle, minimum principle and Von Mises stresses are shown in Tables 4.2 and 4.3.

The stress distribution in the front trailer under braking load differs from that obtained from static loading. The main contributing factor to this is the load from the rear trailer in combination with the braking load.

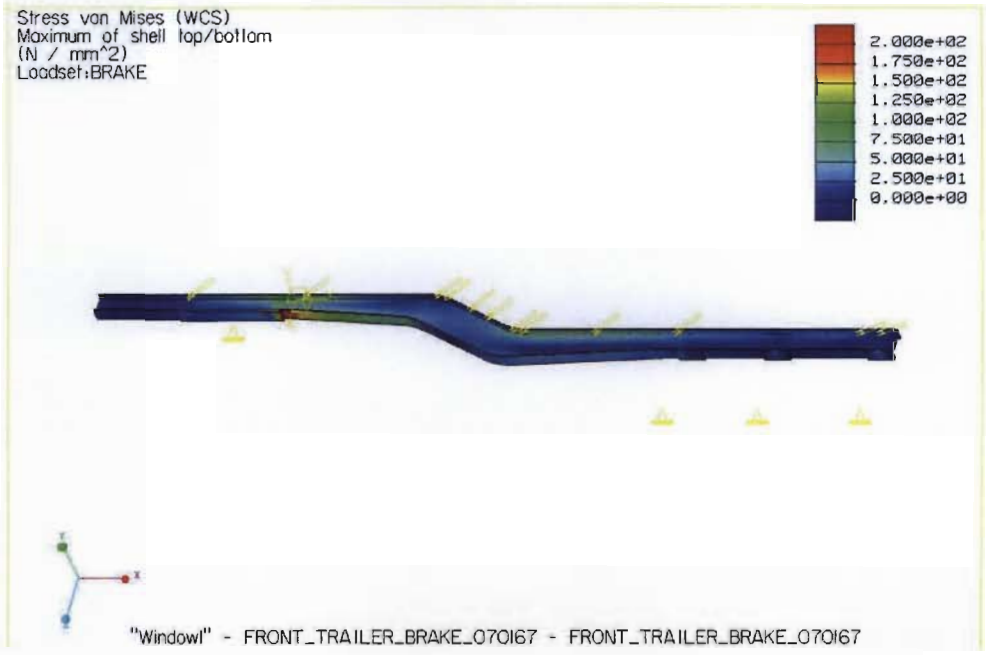

Figure 4.19 Fringe plot of Von Mises stress of front trailer under braking load.

The highest Von Mises stress in the front trailer under breaking load occurs in the region behind the fifth-wheel plate. This is due to a combination of the reactions from

the vertical and horizontal components of force at the fifth-wheel constraint. The top flange is also stressed (although to a lesser degree) in this region.

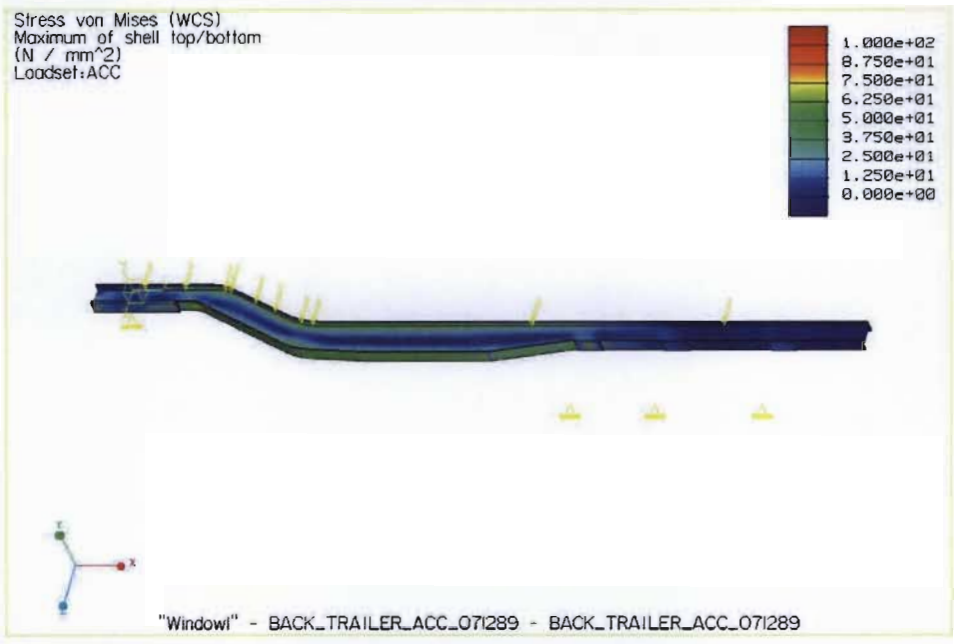

Figure 4.20 Fringe plot of Von Mises stress of rear trailer under accelerating load.

The stresses resulting from the accelerating loads are all lower than 100MPa, and a stress distribution similar to static loading is expected as the load is similar to the static loading, with the addition of a small component in the horizontal direction.

Table 4.2 Maximum stresses in the web and flanges for accelerating load

Stress (MPa) Acc. Load	Front Trailer	Rear Trailer
Web Maximum Principle	61.58	51.71
Web Minimum Principle	-48.21	-90.78
Web Maximum Von Mises	56.37	89.51
Flange Maximum Principle	71.87	70.82
Flange Minimum Principle	-62.60	-68.37
Flange Maximum Von Mises	82.12	86.87

Table 4.3 Maximum stresses in the web and flanges for braking load

Stress (MPa) Brake Load	Front Trailer	Rear Trailer
Web Maximum Principle	110.59	43.77
Web Minimum Principle	-240.56	-74.45
Web Maximum Von Mises	189.37	65.61
Flange Maximum Principle	125.51	73.59
Flange Minimum Principle	-208.11	-89.24
Flange Maximum Von Mises	133.27	107.21

The stresses from the accelerating load are similar for the front and back trailers, with the exception of the minimum principle stress in the web, which is significantly smaller for the rear trailer. This stress occurs in the upper section of the web, in the region of the step geometry, and is a result of the change in direction of the beam. The maximum Von Mises stress also occurs in this region in correspondence with the minimum principle stress.

The braking load significantly increases the stresses in the model in comparison to the static model, and is due to the addition of a horizontal force component almost of the same magnitude as the vertical component. The braking load produces the most noticeable effect on the stresses of the front trailer. This is due the additional load of the rear trailer as previously discussed.

4.5 Web Stiffeners

Web stiffeners are added to avoid buckling of the web, and are commonly found on structures of this sort. Transverse web stiffeners will be used on the main chassis beam. Initial attempts to conduct buckling analyses resulted in very large lateral deflections as a result of the limited transverse resistance of the spring element model of the suspension unit. The problem was resolved by using an additional constraint. The horizontal surfaces on the sides of the bottom flange are limited to movement in the XZ-plane.

Figure 4.21 shows views of the most significant deflections for the first four buckling modes of the front trailer under DDF loading.

Buckling modes 1 and 3 result in large deflections of the corners of the upper flange. Buckling modes 2 and 4 are more complex, with mode 4 affecting the region at the rear of the trailer where the suspension unit attaches. The area is prone to buckling due to the high compressive force resulting from the load on the top flange and supports on the opposite flange. For this reason, the spacing of stiffeners should be smaller in this region.

Figure 4.21 Views of the deflection for the first four buckling modes of the front trailer beam

Figure 4.22 shows a plot of the Von Mises stresses for the front chassis beam under DDF loading.

The addition of stiffeners does not significantly change the stress distribution in the main chassis beams, and the maximum principle and Von Mises stresses in the webs and flanges are the same as with the static analyses. Subsequent buckling analyses showed that stiffened beams are not prone to web buckling.

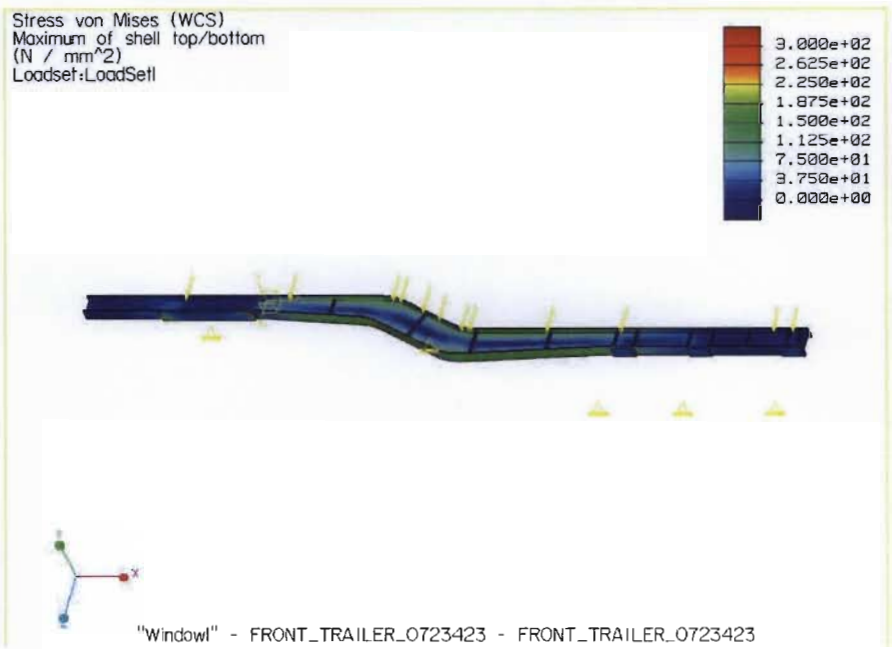

Figure 4.22 Fringe plot of the front chassis beam under DDF loading with stiffeners

4.6 Conclusion

Finite element analysis of the main chassis beams of a semi-trailer has been performed. A method of constraining the model with spring element representations of the fifth-wheel and suspension unit was developed. This resulted in more realistic stress distributions and deflections as opposed to constraining the model with fixed surfaces. The effect of mesh density did not have a significant impact on the results. This is primarily due to the nature of *P*-version finite element techniques.

Load cases for the chassis have been analysed, and the effect of static, accelerating and braking forces on the main chassis beam have been examined. The highest stress in the model occurs at the points where the spring elements attach to the fifth-wheel plate. This localized and unrealistically high stress caused by the boundary conditions imposed and does not affect the overall stress distribution in the flanges and web of the beam. The results showed that the Von Mises and principle stresses in the main chassis beam are relatively low. Although the top and bottom flanges are generally in compression and tension respectively, areas of tension and compression are located on the top and bottom flanges due to the complex geometry of the beam.

A global sensitivity analysis showed that by rounding the corners in the region of the step geometry, the stress at these locations can be substantially reduced. In this particular example, the local stress is reduced by 37.78 %. The accelerating and braking loads showed that the braking load results in significantly higher stresses than the static and accelerating load cases. Stiffeners are added in the design to prevent web buckling. The addition of stiffeners did not significantly affect the stresses in the beams under static loading, but reduced the effect of web buckling.

Finite element studies presented in [15] and [54] resulted in maximum Von Mises stress ranges of 94.7– 184.8 MPa and 42.9 – 82.8 MPa. The stress range in [54] is larger as these stresses occurred in the region of the pinned support of the fifth-wheel. The results in [15] correlate well with the Von Mises stress range obtained for static loading of 42.82 – 87.00 MPa. The measured stresses for a semi-trailer travelling over a variety of surfaces in [69] range from 99 – 185 MPa, which the author relates to a range of design factors of 1.2 – 2.4. This data also agrees well with the results obtained in this study, with the maximum Von Mises stress of 243.59 MPa corresponding to a design factor of 2.75.

Chapter 5 – Assembly and Component Design

5.1 Introduction

The purpose of this chapter is to investigate the design of bolsters and cross-braces, and to analyse the entire structure of the front and back trailers. The design of the cross-braces is based on research presented in [127]. The bolsters are designed using recommendations from experienced designers in conjunction with FE analyses. The trailer structure is analysed using a beam frame model that includes all the main structural members of the trailer. The purpose of the analysis is to investigate the performance of the structure, under normal vertical loading, as well as load cases IV and V (see Section 4.2). Another important aspect of the beam model is to review the main chassis rail design, and investigate possibilities for further mass reduction.

5.2 Cross-Brace Design

The function of a cross-brace in a semi-trailer structure is to maintain the shape of the structure under lateral and torsional loading. Different types of cross-sections have been used in semi-trailer cross-brace design, including channel and tube sections.

A study of the effect of the type and number of cross-braces in this type of structure in [127] showed that for lateral loading, the torsional shear stress in the cross-braces initially increases, then decreases with the total cross-sectional area and number of cross-braces. The bending stress in the main chassis rails decreases with total cross-sectional area and increases with the number of cross-braces. The author concludes that, for a ladder-frame design, the best design with regard to minimum weight, shear stress and torsional stiffness, between 8 and 10 cross-braces are required.

It is also shown in a separate study in [127] that thin-walled tube sections result in the least mass and stress for a given torsional stiffness.

The cross-braces used in this design are thin-walled tube sections, and attached to the inner sides of the main chassis rail through bolted connections. The tubes are welded to connection plates, which are profiled so that there is only material where it is required; at the bolt holes and the weld around the perimeter of the tube.

The forces that act on the cross-braces arise from load cases IV and V (Section 4.2), therefore analysis of the bolsters is integrated with the analysis of the entire structure using the beam frame model in Section 5.4.

5.3 Bolster Design

5.3.1 Loading Conditions

The purpose of bolsters is to retain the raw sugarcane during transportation. To ensure that the sugarcane is effectively retained without the need for substantial additional support between the bolsters, six main bolsters and two end bolsters are used.

The loads on the bolsters are determined from [24]. The static loads consist of three main load cases; vertical, transverse and longitudinal. The rated bolster load is defined as the total payload divided by the number of bolsters.

The rated bolster load is increased to allow for maldistribution within the payload by a maldistribution factor $M = 1.2$, such that:

$$L_{DS} = L_R M + D$$

where

L_R is the rated bolster load (kg)
L_{DS} is the static design load (kg)
M is the maldistribution factor
D is the mass of the bolster and attachments (kg)

The vertical loads are applied as a uniformly distributed load across the top of the bolster bed. The bolster attachment code states that the transverse load is applied at the load centre and longitudinal load loads are applied at points 300 mm above the bed height and

at the bed height. To avoid stress singularities associated with 3D FE models and point loads, the loads are applied to surfaces on the FE model (see Figure 5.1).

The loads are:

$$P_{VD} = L_{DS}(2.5g)$$
$$P_{VU} = L_{DS}(0.5g)$$
$$P_{T} = L_{DS}(0.5g)$$
$$P_{LF} = L_{DS}(1.0g)$$
$$P_{LR} = L_{DS}(0.5g)$$

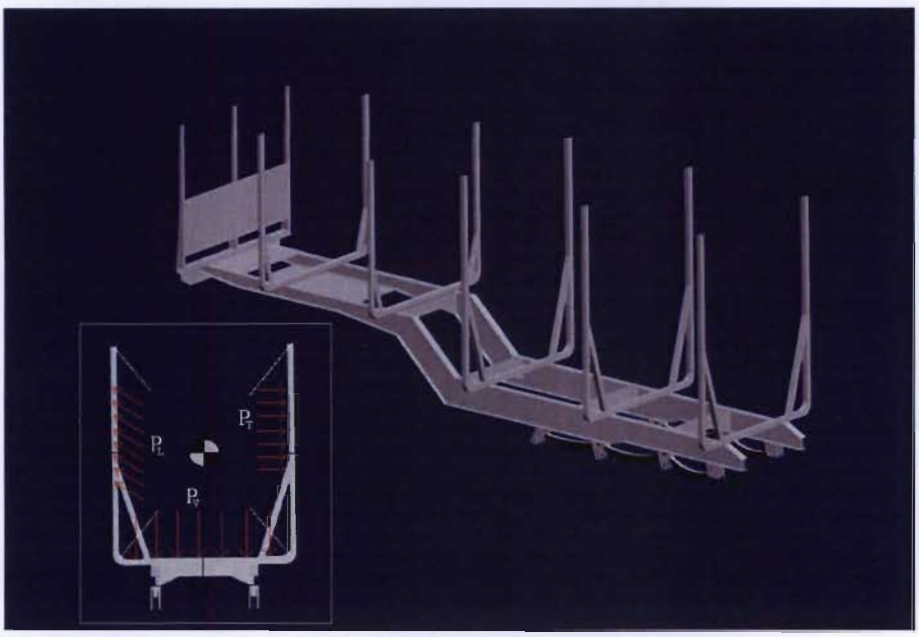

Figure 5.1 Diagram showing a typical bolstered chassis with insert showing application of loads.

5.3.2 Initial Bolster Design

The initial bolster design consisted of two sections which bolt on to the webs of the main chassis rails, at the locations of the cross-members (see Figure 5.2).

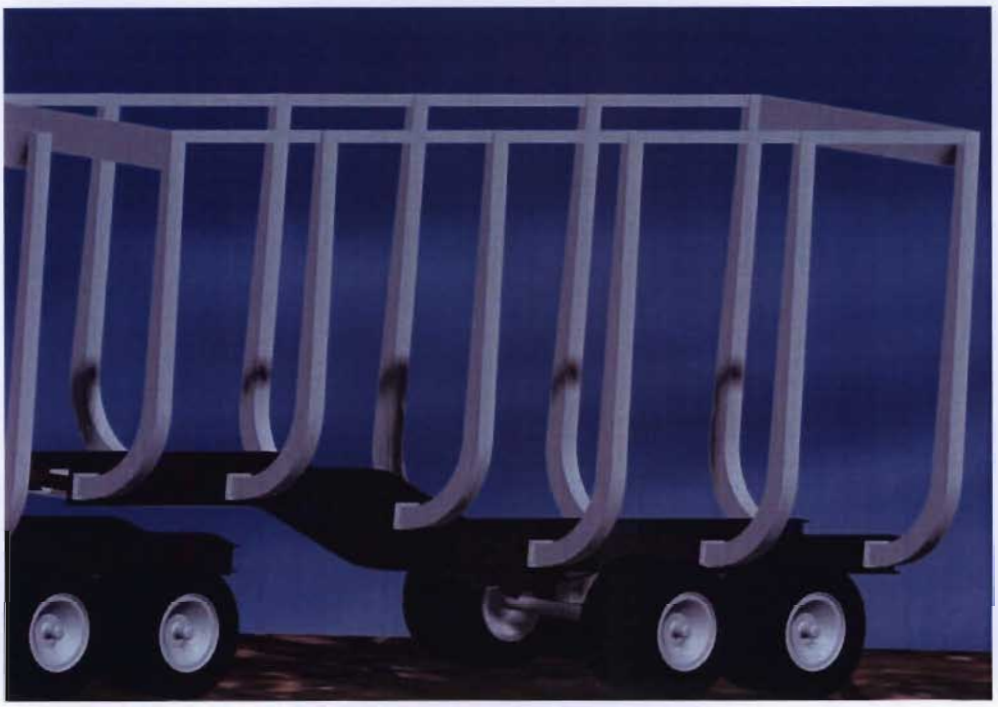

Figure 5.2 Initial bolster design

This design was initially analysed using the fastener function in Pro/Mechanica, and using a beam element fixed to circular surface regions on the outer surfaces of the joint. These methods were found to be inaccurate because of their inability to accurately model the joint. The beam element approach did not produce accurate results due to difficulties in obtaining the correct pre-tension in the beam element. Although it is possible to include pre-tension with the fastener function, the complex nature of the joint limited the value of this method.

5.3.3 Nonlinear Contact Analysis

A nonlinear contact model was created to analyse the joint. The model includes a section of chassis beam, the connection plates of the cross-brace and bolster, the bolster and the bolts (see Figure 5.3). The model simulates contact between the various components instead of having a single solid model. Contact regions are defined between the surfaces

of the chassis and the cross brace, the chassis and the bolster, and between the bolts and all other parts. The bolts are modelled using the equivalent stressed area and material properties of an M16 class 10.6 fine thread bolt, and are pre-stressed to the level obtained from correct torque tightening. The model is similar to that used in [129] for analysing truck joints.

Figure 5.3 The geometry of the bolster joint

The ends of the chassis rail section are fixed, and a symmetry constraint is applied to the cut surface of the cross-brace. The bolster is loaded with the transverse load.

The analysis showed that the stress on the connection plates around the bolts followed the contours of the elements (Figure 5.4). To reduce this effect, the mesh was locally refined by creating mesh controls in the regions of high stress gradient (see Figure 5.5).

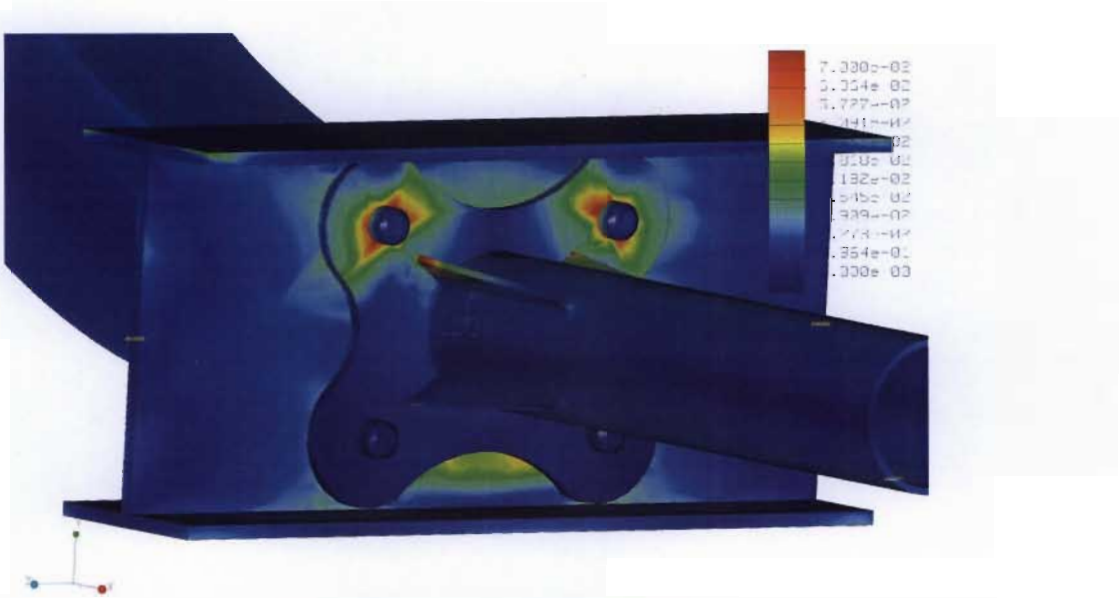

Figure 5.4 Contour plot of Von Mises stress

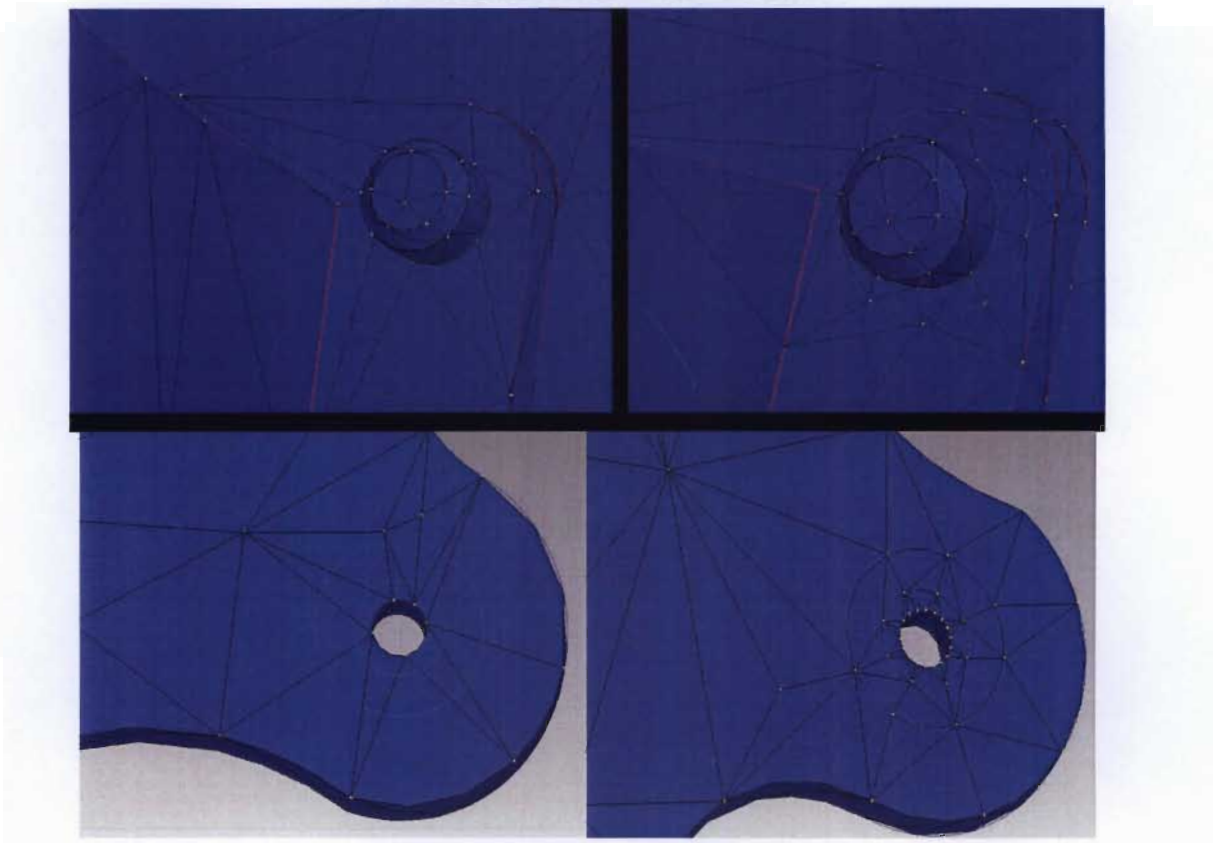

Figure 5.5 Initial and refined meshes of the connection plates

The refined mesh produced a stress contour with no influence of element boundaries (see Figure 5.6). The results from the nonlinear contact analysis showed that a high stress concentration occurs at the corners of the bolster/connection plate interface.

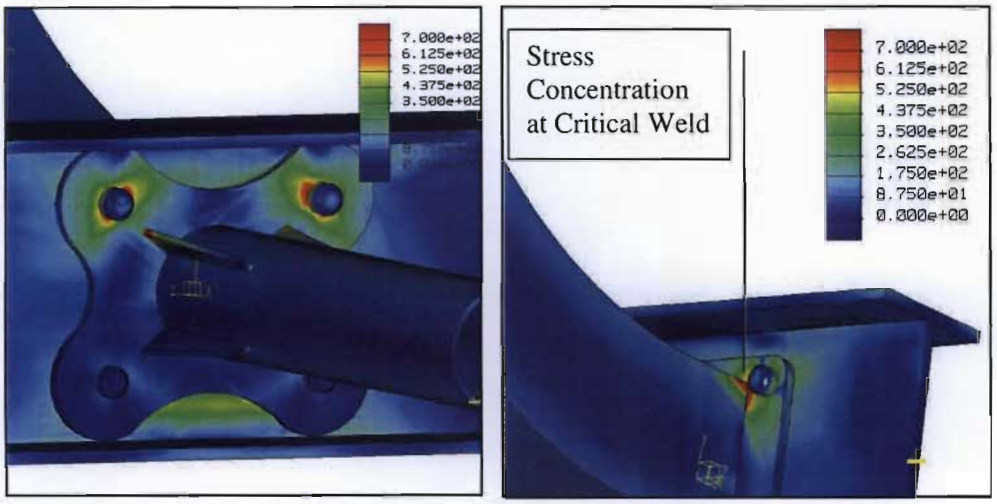

Figure 5.6 Fringe plot of the Von Mises stress of the connector plates on both sides of the chassis beam.

This is the location of a critical weld, therefore a new design concept is proposed. The new design is similar to the initial design, except the bolster is continuous through to the opposite side, and is attached on top of the upper flange (see Figure 5.7).

5.3.4 Refined Bolster Design and Design Optimisation

The new bolster design eliminates the high stress concentration in the region of the critical weld. The refined design is inherently heavier than the initial design due to the addition of the added material linking the two uprights, but the continuous nature of the geometry results in a stronger structure.

Figure 5.7 The refined bolster design

A series of local sensitivity studies on the parameters that define the shape of the bolster are conducted to determine the parameters that most significantly affect the mass and stress in the bolsters. A sample result is presented in Figure 5.8.

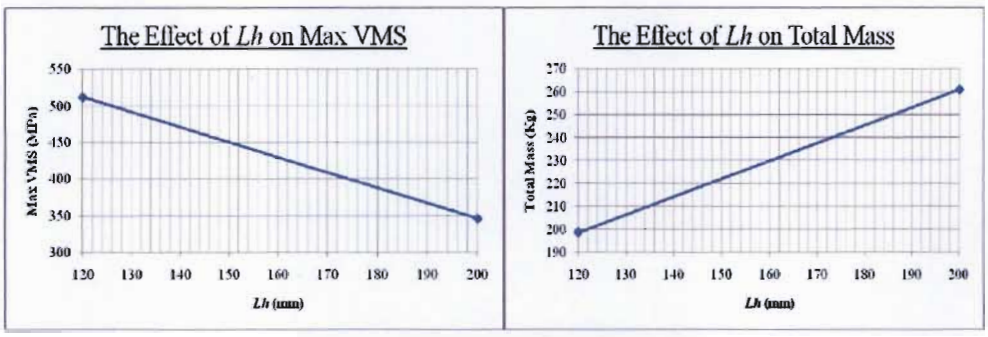

Figure 5.8 Sample result from sensitivity analysis

From Figure 5.8, it can be seen that increasing *Lh* (see Figure 5.9) results in a decrease in the maximum Von Mises stress, with a corresponding increase in the total mass of the

bolster. The results of the local sensitivity analyses revealed that the parameters that have the greatest effect on the maximum Von Mises stress and the mass of the bolster are the inner and outer radii of the corner, *Ro* and *Ri*, the height of the base, *Lh*, the width of the bolster, *wl*, and the thickness of material, *t*. A sketch showing the basic bolster shape is shown in Figure 5.9.

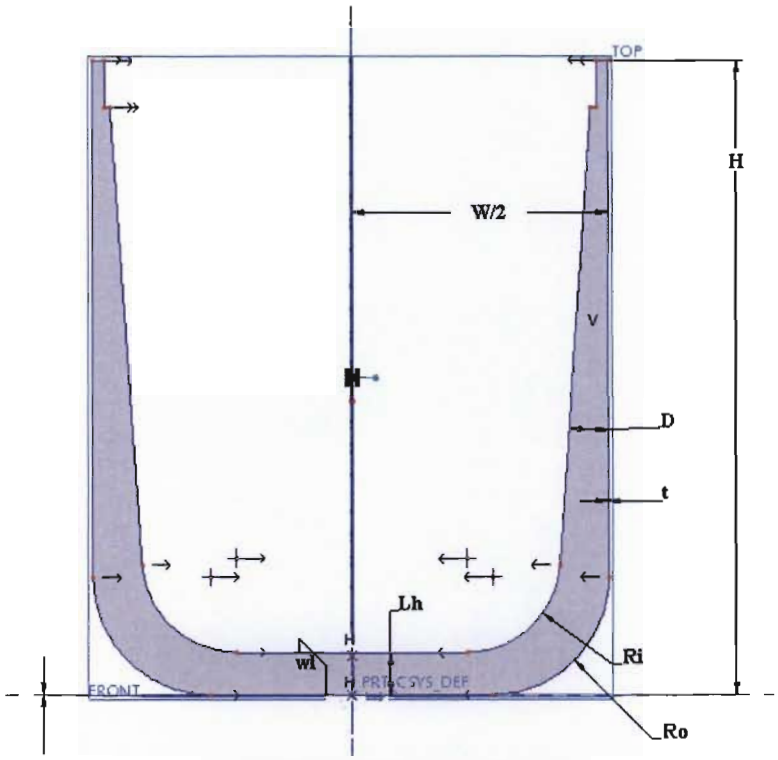

Figure 5.9 Sketch showing the design parameters of the bolster

Due to the fact that height of the chassis beam changes from front to back, the heights of the bolsters will vary. The tallest bolster can be considered as the worst case scenario because it is the longest, generating the largest moments and it is the most likely to fail. For this reason, the longest bolster will be used for optimisation. Optimisation design studies are conducted on the bolster design, using the design optimisation function in Pro/Mechanica. The function uses a sequential quadratic programming algorithm [111]. The design parameters in the optimisation are the inner and outer radii of the corner, *Ro* and *Ri*, the height of the base, *Lh*, the width of the bolster, *wl*, and the thickness of material, *t*. The limits on the values of the design parameters are shown in Table 5.1.

Table 5.1 Design parameter values

Parameter	Symbol	Min Value (mm)	Init Value (mm)	Max Value (mm)
Outer Radius	*Ro*	300	600	700
Inner Radius	*Ri*	300	500	700
Base Height	*Lh*	100	180	200
Base Width	*Wl*	100	180	200
Thickness	*t*	4	8	12

The height, H, width, W, and angle between the sides, D, are fixed. The value of H and W are determined by the maximum height and width of the vehicle. The value of D is 3 degrees (which allows the cane to slip out easily during offloading), and is obtained from recommendations by experienced designers. The goal function of the optimisation is the minimisation of the mass of the bolster, within the bounds of a maximum Von Mises stress of less than 450 MPa and a maximum deflection of 40mm. A design optimisation study is conducted for transverse, longitudinal, vertical and offloading load cases.

The forces generated during the unloading process are difficult to determine. Efforts to calculate the forces using the differential equations that describe an inextensible, flexible string (modelling the chains that spill the cane) in conjunction with the forces measured at the offloading station did not yield results. This is due to uncertainties with respect to the bulk modulus of the cane, friction between the chains and the bolsters, and other parameters. An estimation of the forces generated during the unloading process is made, with 13.92 kN force acting in the direction of the chains at the top of the bolster, a 19.62 kN downward acting vertical load on the load bed. The reaction of the spill wall and the force of the cane on the opposite bolster are taken into account, with forces of 5.00 kN and 9.81 kN respectively. The offloading load case is shown on the bolster model in Figure 5.10.

The model consists of 206 shell elements for the main section, and 1124 solid tetrahedral elements for the mounting blocks. The model is constrained with fixed surface constraints on the underside of the mounting blocks.

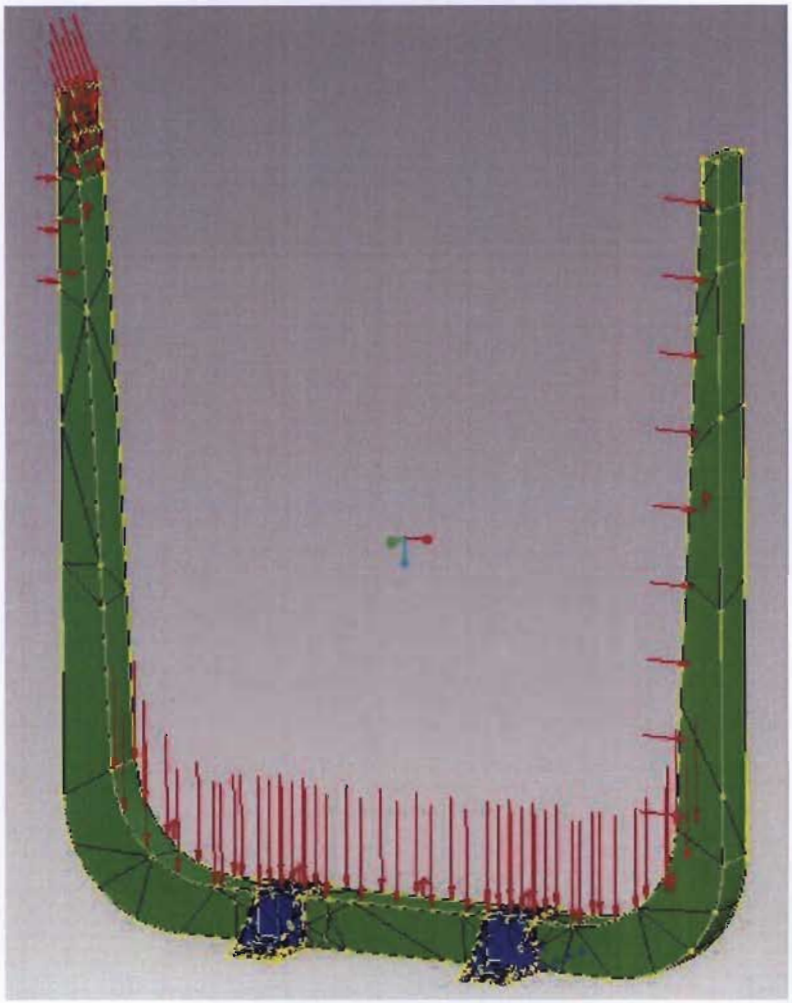

Figure 5.10 A view of the bolster model with the offloading load set.

The results of the optimisation are shown in Figure 5.11.

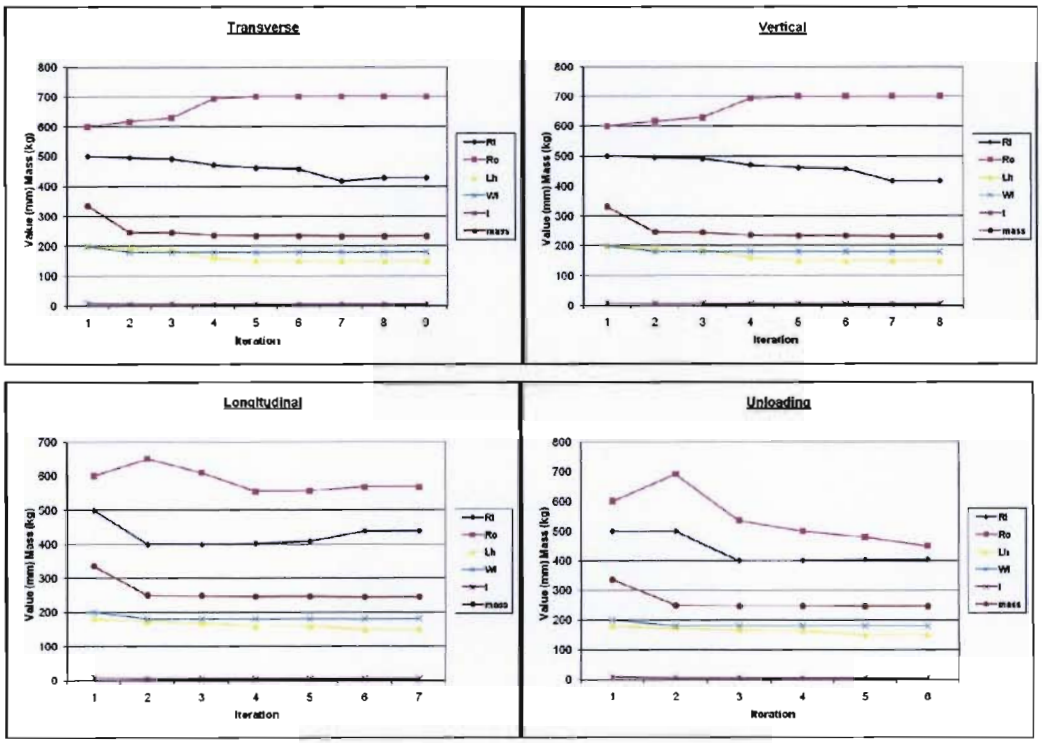

Figure 5.11 Results from optimisation design study of bolster

Figure 5.11 shows the changes in the design variables and the goal function (the mass of the bolster) for each iteration during the optimisation design studies, for each load case.

The different load cases result in a different optimum designs, but the results showed some general trends. After iteration 1, a noticeable decrease in mass is obtained due to the thickness of material decreasing from 8mm to 5mm. The values for the height and width of the bolster base are similar for all the load cases.

The final parameters determined for the bolster can be seen in table 5.2. The value for the thickness of the material is selected as 5mm, as this is the optimum value for all the load case design studies. The values for *Lh* and *wl* are similar for all load case design studies and a value of 180 mm is selected for both variables as an average of the optimum values obtained. The values for the inner and outer radii are selected from the unloading load case as the unloading case is expected to be the most frequent and severe load case

occurring in operation of this particular type of vehicle. The initial mass of the bolster is 295 kg, and the mass of the final optimised design is 247 kg, resulting in a mass saving of 16.27%

Table 5.2 Design parameter values for the bolster

Parameter	Symbol	Value (mm)
Outer Radius	Ro	450
Inner Radius	Ri	400
Base Height	Lh	180
Base Width	Wl	180
Thickness	t	5

5.3.5 Analysis of Final Bolster Design

The final design is analysed under transverse, vertical, longitudinal and unloading load sets. A view of a fringe plot of Von Mises stress for the unloading case is shown in Figure 5.12, and results for the maximum Von Mises and deflection are presented in Table 5.3. The maximum Von Mises stress occurs in the region where the mounting blocks attach to the bolster. The longitudinal load set produced the highest stress overall, and the unloading case resulted in the highest deflection. All the results are within the constraints of the design optimisation study.

Figure 5.12 Fringe plot of maximum Von Mises stress for unloading bolster analysis

Table 5.3 Von Mises stresses and deflections for the bolster analysis

Load Case	Von Mises Stress (MPa)	Deflection Magnitude (mm)
Transverse	395.92	22.77
Longitudinal	413.46	20.98
Vertical	220.43	02.11
Unloading	344.09	36.47

Due to the long, slender geometry of the bolster, buckling analyses are conducted. The first four bucking modes for each of the load cases are calculated. The vertical load case resulted in no significant buckling. The transverse and longitudinal cases resulted in local buckling occurring in the region corners of the bolster. Negative buckling load factors were calculated in each case. This occurs when the elements in the region where the buckling is occurring are in tension as opposed to compression. This is as expected because the loads on the bolsters are not directly axial, and cause bending about the mounting blocks; when one side of the bolster in compression, the other is in tension. Buckling would occur for that specific mode if the direction of the force is reversed. The results for the unloading case are shown in Figure 5.13.

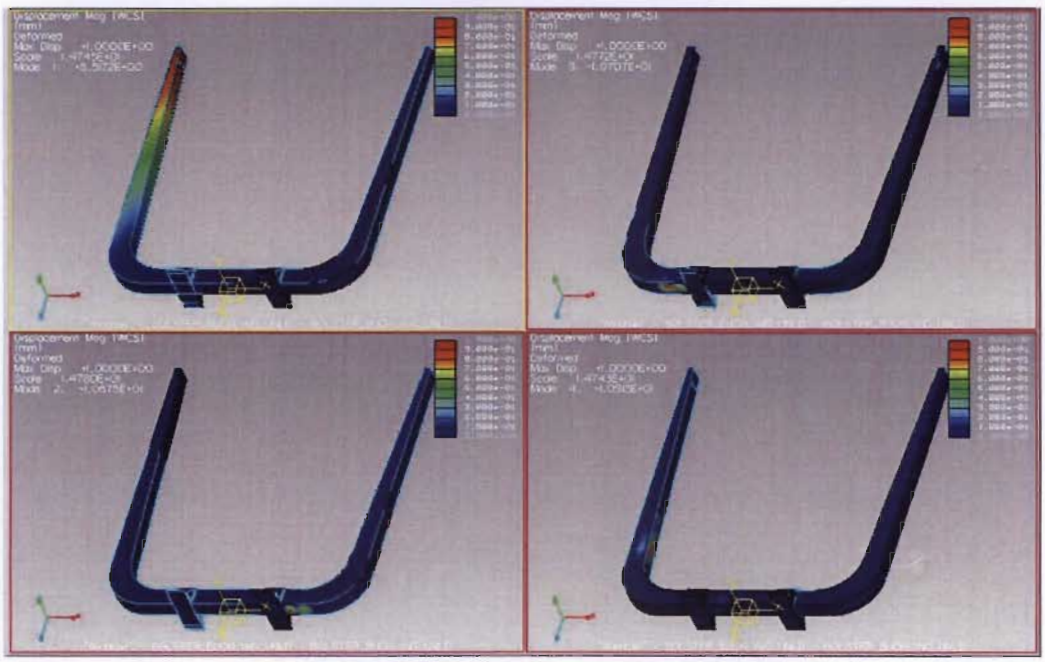

Figure 5.13 Plots of displacement for the first four buckling modes of the unloading case

The unloading case results in varied buckling modes due to the combination of forces acting on the bolster. The buckling analyses showed that the loads on the bolsters cause local buckling, but the extent of the local buckling and the stresses induced are low enough to exclude buckling as a mode of failure for the bolsters.

5.4 Beam Frame Model Analysis

5.4.1 Introduction

The purpose of the beam frame model analysis is to investigate the performance of the structure. The advantage of this type of analysis is that it includes the all the main structural members of the trailers, rather than single components, and allows for the investigation of various structural permutations. This analysis also allows for the analysis of the performance of the structure under normal vertical loading, as well as load cases IV and V (see Section 4.2). The beam model does not take details such as joint geometry and stress concentrations due to re-entrant corners, but rather provides an overview of the general stress distribution in the structural members.

Another important aspect of the beam model is to review the main chassis rail design, and investigate effects of load cases IV and V. The effects of altering the section parameters of the main chassis beam will be investigated, and modifications with the aim of mass reduction will be considered.

5.4.2 Frame Design

An initial simple beam frame is used to investigate the effects of various structural permutations of the trailer frame. Analyses, with transverse loads acting on the bolsters and downward DDF load acting on the load bed, are run to determine the interactions of the various members.

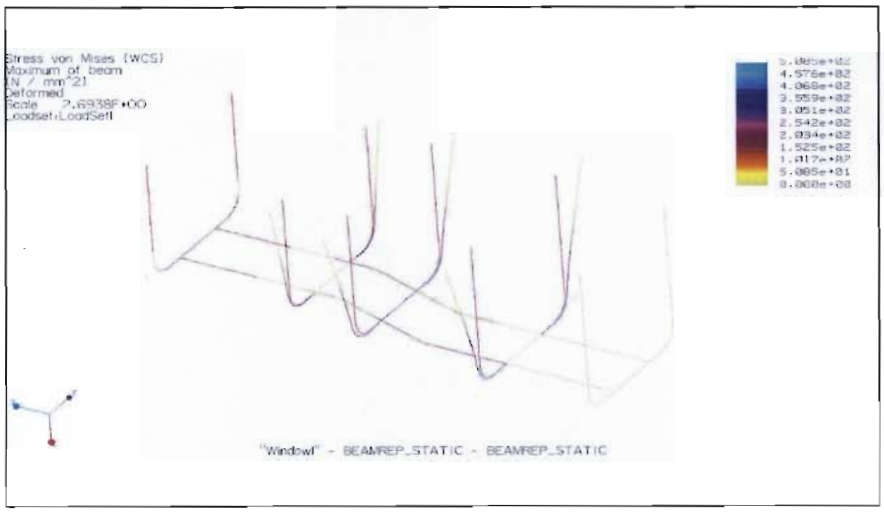

Figure 5.14 Beam model with no support at the tops of the bolsters

Figure 5.14 shows the results for analyses of the frame with no support at the tops of the bolsters. The beams deflect considerably and the maximum Von Mises stress occurs in the corners of the bolsters, with a value of 508.51 MPa. Figure 5.15 shows the same analysis with the addition of a longitudinal support member running through the tops of the bolsters. The result is more evenly distributed stress, with a maximum value of 420.20 MPa.

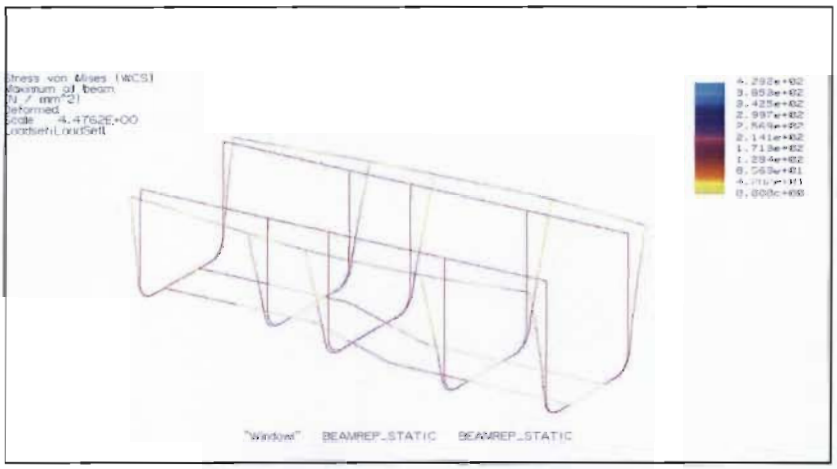

Figure 5.15 Beam model with longitudinal bolster supports

The effect of adding a member between the tips of the end bolsters is shown in Figure 5.16. The structure is generally more rigid and the stress is evenly dispersed. The stresses on the cross brace members and the corners of the bolsters are lower than in the initial beam model.

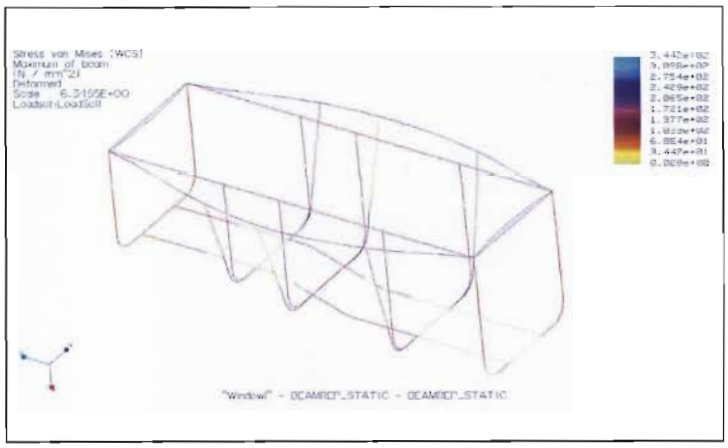

Figure 5.16 Beam model with longitudinal supports and member between end bolsters

After repeated iterations of various beam placements, it is found that the ideal trailer must have longitudinal supports, as well as a transverse member linking the top two points of the end bolsters.

5.4.3 Beam Frame Model.

The beam frame models of the front and rear trailers consist of 231 beam elements and 14 spring elements each (Figure 5.17 shows a view of the front trailer beam model). The main chassis beams do not have a continuously variable section, but are composed of beam elements with the average dimensions of that particular section of the main chassis rail.

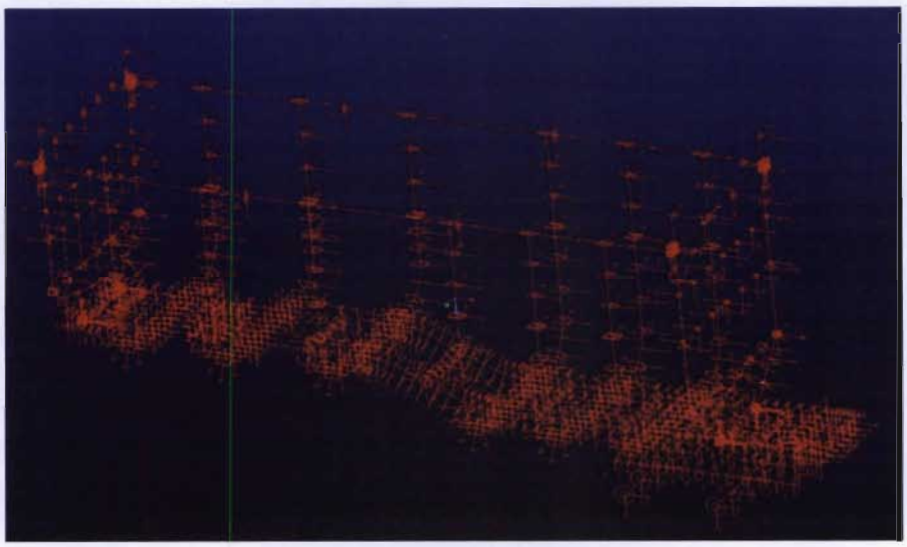

Figure 5.17 Front trailer beam frame model.

The models include the main chassis beams, bolsters, cross-braces, fifth-wheel mountings, the beams which link the top of the bolsters and the end bolsters. The size of the cross-braces is determined by the maximum size of round hollow tube that can be mounted to the main chassis rail.

The beam models are constrained using the same method as in the main chassis beam models, although in this case the stiffness of the wheels is included. The suspension assembly and wheels are modelled using a combination of beam and spring elements (see Figure 5.18).

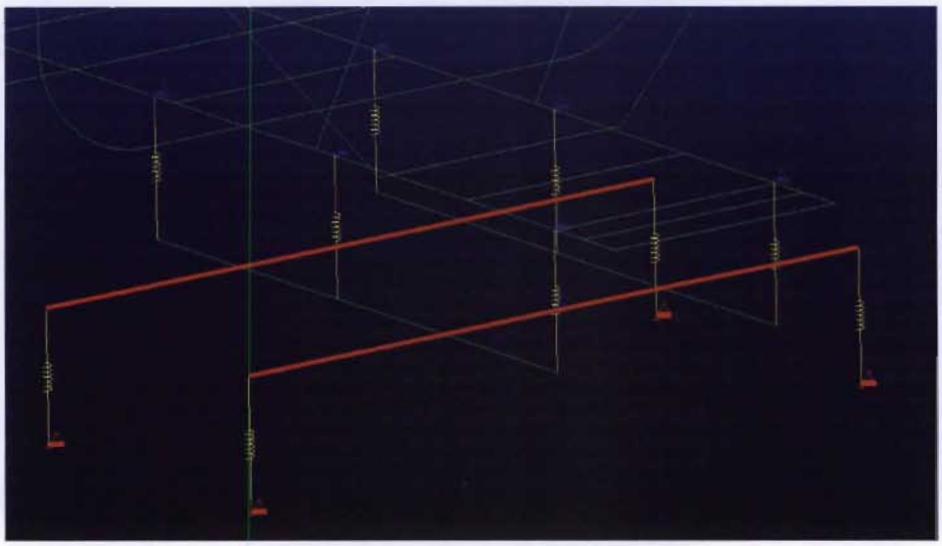

Figure 5.18 Suspension model of the beam frame model

The main chassis beams are linked to a beam element with three spring elements per side, which is the same simple leaf spring model used in the main chassis beam analyses. The beam elements are linked to the axles (highlighted in red), which are in turn fixed to ground with spring elements that have the same stiffness as dual truck tires obtained from [129]. At the front ends, the models are constrained with the same spring element fifth-wheel representation as the main chassis beam models.

Load cases I, IV and V (Section 4.2) are investigated. Load case I is realised a UDL equivalent to the force generated by the payload, distributed over the load bed (highlighted red in Figure 5.19). Load case IV consists of the UDL of case I in combination with a 0.3g force acting on the right side bolsters (highlighted yellow in Figure 5.19).

Load case V is achieved through the use of a prescribed displacement of 400mm in the downward direction, on the points where the wheel springs attach to the ground. The prescribed displacement is imposed in conjunction with the UDL of case I, and represents a worst case scenario of a fully loaded vehicle travelling over terrain such that both of the contact points of the tires on one side are 400 mm lower than the other side. The load of

the rear trailer on the front trailer fifth-wheel is also taken into account, with an equivalent load acting on the fifth-wheel mounting at the back of the front trailer.

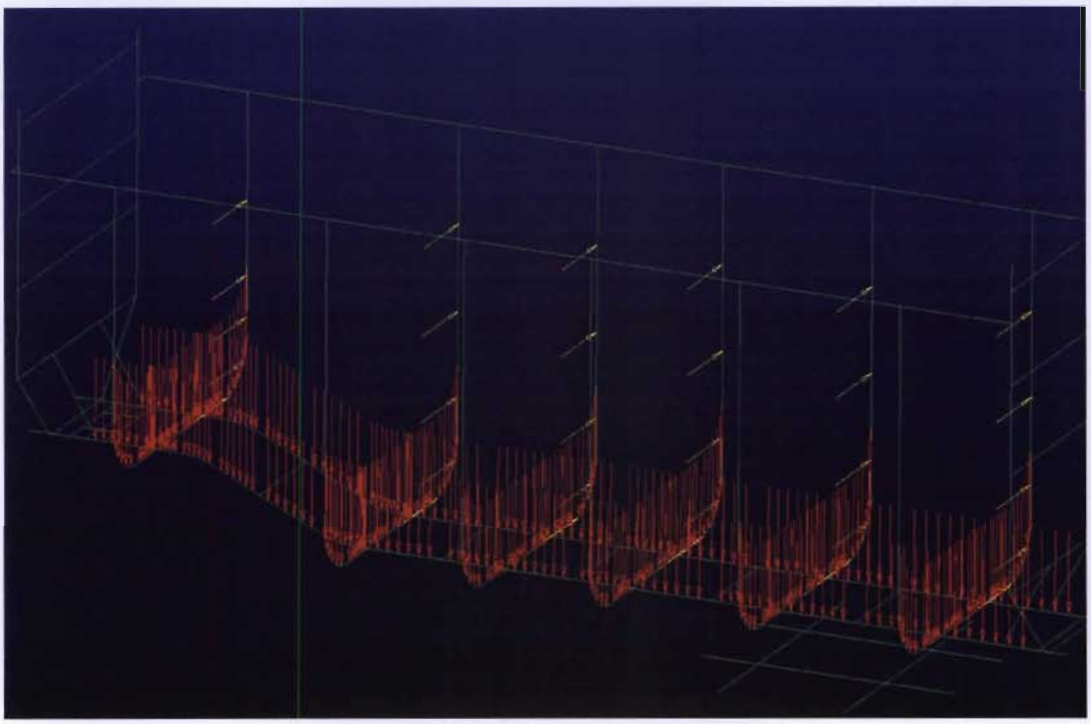

Figure 5.19 A view of the loads on the beam frame model of the rear trailer.

5.4.4 Results

The results showed that the load case IV resulted in the highest stress in both the front and back trailers. The maximum Von Mises stress for load cases IV and V respectively are 252.08 MPa and 128.74 MPa for the front trailer, and 225.23 MPa and 93.65 MPa for the back trailer.

The stress distribution for the front trailer under load cases IV and V are shown in figures 5.20 and 5.21 respectively.

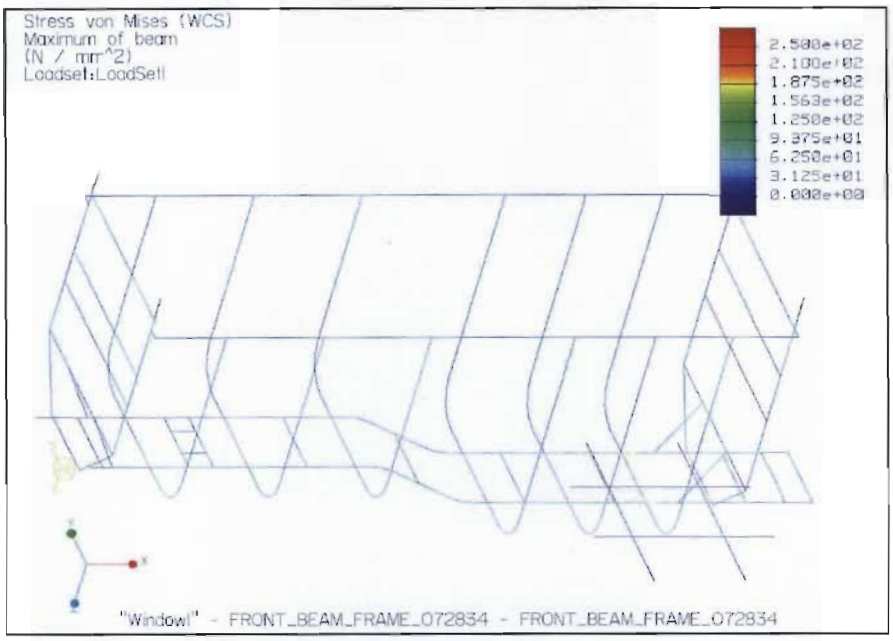

Figure 5.20 Stress distribution of the front trailer for load case IV

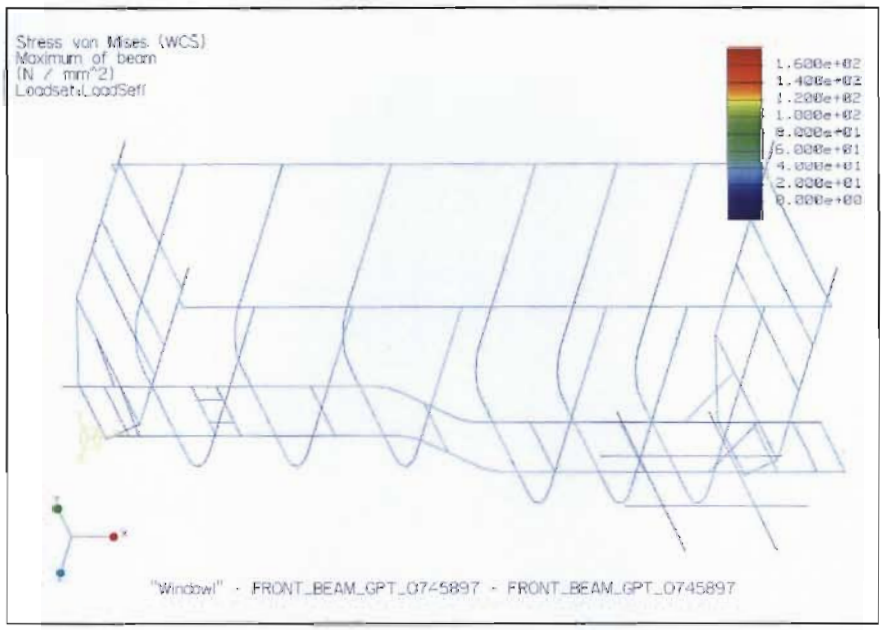

Figure 5.21 Stress distribution of the front trailer for load case V

The general Von Mises stress for load cases IV and V in the front and back trailer is relatively low, and ranges from 30 – 90 MPa. The maximum Von Mises stress for load case IV occurs at the points where the suspension spring element model attaches to the main chassis beam, and is probably slightly exaggerated due to the nature of the point connections. The maximum Von Mises stress for load case V occurs at the front end of the trailer, at the location where the end bolster attaches to the main chassis beam.

A study of the effect of altering the flange and web thicknesses is also conducted. The purpose is to investigate if any possible mass savings can be made without significantly affecting the structural integrity of the trailers. It was found that by reducing the flange and web thicknesses to 10 mm and 8 mm respectively (which reduces the mass of the beams from 514.5 kg to 428.2 kg for the front trailer beam, and 495.9 kg to 410.1 kg for the rear trailer beam), the maximum Von Mises stresses for load case IV increased marginally to 267.02 MPa and 237.70 MPa for the front and rear trailers, and the general stress range of the structural members increased marginally (see Figure 5.22).

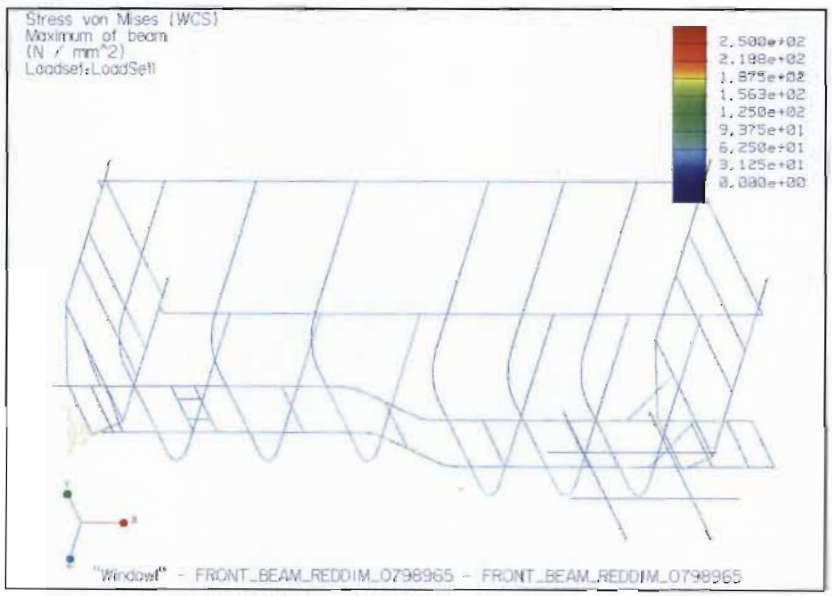

Figure 5.22 Stress distribution for load case IV of the front trailer with reduced main chassis beam section

Further reducing the dimensions (8 mm and 6 mm for the flanges and web respectively) resulted in a much higher maximum Von Mises stress (325.44 MPa for the front trailer with load case IV), and resulted in large deflections of the trailer under torsional loading.

Analyses of the main chassis beams of the front and back trailers with flange and web thicknesses of 10 mm and 8 mm rerun. The static UDL DDF and braking loads (load cases I and II) are investigated as these resulted in the highest stresses in the initial chassis beam analysis. The results are summarised in Table 5.4.

Table 5.4 Results from analysis of load case I with reduced section dimensions

Stress (MPa)	Front Trailer	Rear trailer
Web Maximum Principle	151.71	183.41
Web Minimum Principle	-154.91	-276.35
Web Maximum Von Mises	141.76	281.00
Flange Maximum Principle	215.40	293.37
Flange Minimum Principle	-241.51	-239.68
Flange Maximum Von Mises	283.24	317.97

The stresses for the front and rear trailers with reduced section dimensions are on average 17.4 % higher, and still lower than the yield strength of the material. The mass reduction obtained by reducing the section dimensions is significant (approximately 20%), and the maximum and minimum stresses, although higher than the initial main chassis beam are still at an acceptable level.

5.5 Conclusion

The initial design of the bolster was found to be inadequate, and a new design is developed and analysed. The parameters that affect the mass and stress most significantly are identified with local sensitivity studies. The bolster design is optimised using the Pro/Mechanica optimisation tool. Although the optimisation results are different for each load case, several general trends are identified. The optimised design resulted in a 16.27% reduction in mass.

The optimised bolster design is analysed using a finite element model, with 206 shell elements and 1124 solid tetrahedral elements. The results showed that the stresses and deflections of the bolster are all within the constraints of the optimisation when subjected to the transverse, longitudinal, vertical and offloading load cases. The longitudinal and offloading cases resulted in the highest Von Mises stress and deflection respectively. Buckling analyses showed that failure due to buckling is not likely to occur.

A beam frame model is used to investigate various structural permutations, and analyse the trailer when subjected to load cases IV and V. The beam frame model is also used to investigate the entire structure (as opposed to individual components), and to review the main chassis beam design.

The beam frame model is constrained in a similar manner to the main chassis rail analyses, but includes the effect of the tyre stiffness through a simple spring and beam element model of the tyre and suspension assembly. A series of analyses showed that the optimum configuration for the structure is to have supports linking the top of the bolsters, and linking the opposite sides of the end bolsters.

The results for load cases IV and V showed that the lateral cornering load (load IV) resulted in the highest stress. The stress is possibly slightly exaggerated due to the nature of the point connections of the suspension unit spring element model. The stress in the structural members for both load cases generally ranges from 30 - 90 MPa, which is relatively low. This prompted the investigation into further mass reductions. A study of the effect of adjusting the flange and web thickness revealed that a significant mass reduction can be achieved (approximately 20%), with a marginal increase in stress in the structure, by reducing the flange and web thickness to 10 mm and 8 mm respectively. Further reduction in the flange and web thickness resulted in significantly increased stress levels, and a large decrease in torsional rigidity.

The analysis showed that further mass reduction is possible, and the beam is re-analysed using the same methods as Chapter 4. The stresses are higher than the initial beam, but still lower than the yield strength of the material. This indicates that the block loading diagram used for the fatigue criteria in the initial section optimisation is possibly an over-estimation of the loading that occurs in the trailers lifespan. A more accurate way to analyse fatigue loading would be to fit strain gauges to strategic locations on the chassis, and calculate the fatigue loading using the rain-flow method from the strain history.

Chapter 6 - Discussion and Conclusion

6.1 Discussion

The initial investigations into sugarcane transportation revealed that in most areas where sugarcane is cultivated in South Africa, road transportation is the most appropriate means. This is mainly due to the topology of the land, with steep terrain limiting rail access. The cost associated with replacing the unloading equipment and apparatus at the sugar mills resulted in the focus shifting to reducing the tare mass of the vehicle, as opposed to designing a new offloading system.

The ten vehicles analysed in the vehicle mass analysis showed that the average payload index is 1.71. The two timber vehicles included for comparison had notably higher payload indices. This indicates that sugarcane haulage vehicles are inherently heavier than other similar haulage vehicles due to the nature of the cargo. Although rigid drawbar vehicles have (on average) a higher payload index, a tandem/tandem interlink is selected as the basis of the design. This is primarily due to the flexibility and stability associated with this type of vehicle. The prime mover can be easily disengaged and replaced for maintenance and repair, as can the trailers. In addition to this, the trailers can be adapted to carry alternative cargo when the vehicle is not being used for sugarcane haulage. Previous rigid drawbar designs have been known to be unstable, especially on downhill turning manoeuvres.

An investigation into the force required to offload the cane was conducted to compare two types of tandem/tandem interlink. Readings from load cells situated on the offloading apparatus structure were taken for bolster-type and frame-type trailers. The results showed that a bolster-type trailer requires a lower force to offload the cane. This is primarily due to the geometry of the structure of the two types of trailers. The bolster structure allows the cane to easily slip out, while cane tends to get stuck against the horizontal and diagonal members of the frame structure, increasing the force required to

offload the cane. A higher offloading force results in unnecessarily high forces acting on the chassis and supporting structures during offloading; therefore, the configuration that forms the basis of the design is a bolster-type tandem/tandem interlink.

Research into trailer design methods was conducted to investigate trailer design methodologies, and determine required structural capacity and load cases. A review of standards related to trailer design showed that there are many standards that deal with various components and the geometric limits of the overall size of trailers, but general standards that explicitly state the required structural capacity for a given load, reserve factors and load cases, are lacking.

Research related to heavy vehicles was reviewed, with the aim of determining design methods and loads acting on the vehicle. The topics addressed are static and dynamic chassis frame simulation, ride quality assessment and vehicle-infrastructure interaction. The publications regarding static and dynamic chassis frame simulation showed that while various methods for modelling heavy vehicles exist, data regarding general load cases (especially dynamic loads) and reserve factors is not available. The main area of focus for ride quality assessment research is force and vibration acting on the truck cab or driver. Although these forces arise from irregular road surfaces, the chassis response to these forces, and forces generated by dynamic movement of the payload, are not comprehensively discussed. Publications regarding vehicle-infrastructure provided wheel forces for various road surfaces, but it is difficult to relate the wheel forces to forces acting on the chassis due to the complex nature of tyres and suspension systems. In general, the research regarding heavy vehicle simulation did not provide thorough quantification of the loads acting on the chassis, but focused on the particular measures relevant to each field.

Experimental measurements of the strain history of heavy vehicle chassis proved to be useful. The statistical analysis of the recorded dynamic strain in [71] showed that design factor depends on the surface on which the vehicle is travelling. The factors range from 1.2 for a smooth surface to 2.4 for a paved surface. Although the results of the

experimental measurements do provide some insight into the dynamic forces acting on the vehicles chassis, it must be noted that the force generated in a dynamic situation also depend on particular vehicle parameters (such as the span between the supports, chassis flexibility, suspension and tyres), and the particular road on which it is travelling. This suggests that the most accurate way to determine the forces acting on the chassis and strain history for fatigue analysis, is to manufacture a prototype of the vehicle and fit it with strain gauges to record the response of the chassis during operational conditions.

Discussions with various manufacturers revealed that trailers are generally manufactured in a trial and error manner. Some manufacturers use dynamic models to determine a design factor and fatigue life for specific cases, but generally a design factor of between 2.0 to 3.0 is used. This factor is applied to the static case, and is high enough to account for fatigue failure. A dynamic design factor of 2.75 is used for this design, and is selected from the upper section of the range due to the harsh operating conditions often experienced by this type of vehicle.

The load cases consist of the load cases outlined [52], and the bolster loads from [24]. In [127], the author showed that the most critical torsional loads are lateral cornering loads and torsion from twisted ground plane. The resulting loads for the chassis are the static load of the stationary vehicle multiplied by the dynamic design factor, braking and accelerating loads, and loads from cornering and ground plane twist. The braking and accelerating loads are taken as the most severe operating conditions for this type vehicle (emergency braking and hard acceleration with a factor of 2.0), which the vehicle is unlikely to experience often in its lifespan. The cornering load is taken as 0.3g as in [127]. The ground plane twist is achieved by imposing a displacement of 400mm on the ends of the springs which constrain the model. This is equivalent to one side of the trailer travelling over a 400mm high obstruction in the road. Both the cornering and twisted ground plane load cases are, like the braking and accelerating loads, generally conservative, and not likely occur frequently.

A comparison of materials is conducted to determine the best suited material for the

semitrailer design. The materials considered included various aluminium alloys, composite materials, and various steels.

Aluminium alloys generally have good strength to weight ratios and corrosion resistance. Poor fatigue life, especially around welded connections, coupled with the harsh operating environments of cane haulage vehicles excluded aluminium alloys as a possibility.

Composite materials generally have good strength to weight ratios and corrosion resistance, and have the potential to result in large tare mass savings. The high cost and complexity of manufacturing eliminated composite materials as a possibility.

Steel has been widely used in automotive and heavy vehicle applications. The properties of steel vary according the particular type. The steels investigated in this study range from mild steel to high-strength, low-alloy steel. Although all the steels generally scored well in the comparison, DOMEX 700 MC scored the highest due good strength and adequate corrosion and fatigue properties. DOMEX 500 MC and ROQtuf scored almost on par with DOMEX 700 MC, the only reason being lower yield strength.

The axles and suspension unit specified for the trailer are solid round axles and spring leaf suspension. These are selected on the basis of low weight, low cost and simplicity. Although aluminium rims are more expensive than steel rims, they are specified due to the substantial mass saving obtained through their use.

To determine the optimum lengths for the various sections of the chassis, an optimisation problem is formulated. To reduce the tare mass of the chassis, the bending moment of the front trailer (which is generally greater than that of the rear trailer) is minimised, with the lengths of the sections as design variables. This results in a smaller required cross-section, hence a reduced mass. The initial model did not take the position of the kingpin on the prime mover and front trailer, or the reactions at the suspension units into account. A more complex model involving these parameters was utilised.

The optimisation problem has constraints relating to road regulations, payload requirements and swing clearance. The swing clearance constraints are linearised using least squares method. The reaction constraints are linearised using an iterative process that recalculates the linear approximations every loop.

The optimisation problem is solved using a program written in SCILAB. The results indicate that the feasible domain is tightly bounded. The optimisation resulted in a feasible design, meeting all the constraints. The bending moment decreased from the initial design by 30.04%, but the resemblance of the optimal design to current designs indicates that, through the process of trial and error, the current designs, within the bounds of present road regulations and other constrains, are close to optimal.

The size of the cross-sections of the various lengths of the main chassis beam are optimised by calculating the minimum web depth required for varying flange and web thicknesses. The required web depth is calculated using elastic moment capacity, shear moment capacity, shear-buckling, and shear, normal and combined fatigue of the welds.

Due to the lack of design data, the fatigue loading is approximated using a block loading cycle. The block loading cycle is probably an overestimation of the forces encountered in a typical cane haulage vehicles lifespan. A more accurate method would be to manufacture a prototype and record the strain at various points on the chassis; however this is beyond the scope of this study.

The results showed that the limiting factor for the required web depth is fatigue loading. Due to the independence of weld fatigue strength and yield strength, the high yield strength of DOMEX 700 MC does not improve the materials applicability. For this reason, DOMEX 500 MC, which scored identically to DOMEX 700 MC except for the higher yield strength, is used in the design.

The web and flange thickness combination that resulted in the lowest mass within the constraints is 10mm and 12mm respectively. However these values are reviewed during

further analysis of the design.

The main chassis beam is analysed using a three-dimensional, *p*-type finite element model. Constraining the model with fixed surface constraints was found to be inadequate due to unrealistic deflection and stress concentrations occurring in the regions of the fixed surfaces. A method of constraining the model using spring elements was developed. The model is constrained through the use of simple spring element models of the suspension units, and a group of spring elements simulating the fifth-wheel connection. The spring constraints resulted in a more realistic deflection, and the behaviour of the chassis beam model generally reflected that of a chassis beam in operation more accurately than the fixed surface constraints. The spring constraints did produce a high stress concentration in the region where the spring elements attach to the beam. This effect is localised, and does not significantly influence the results.

The main chassis beam is subjected to static, braking and acceleration loads (load cases I-III). It was found that a stress concentration occurred at the step in the neck of the beams. A sensitivity analysis showed that the stress in this area can be reduced by rounding the corners. The analyses generally converged after 5-6 *p*-loops, and mesh density was found to be insignificant with respect to the stress distribution in the main chassis beam. This is due to the nature of the *p*-type method, where the elements increase in polynomial value in areas of high stress gradient, as opposed to local mesh refinement. The polynomial value of the elements generally varied form 2 - 6.

The stresses in the main chassis are relatively low for all the load cases, with the static DDF and braking load cases resulting in the highest stresses. The low stresses indicate that there is a possibility for further mass reduction, which is investigated with the beam frame model.

Web stiffeners are added to prevent buckling of the web. The addition of stiffeners did not significantly affect the stress distribution for load cases I-III, but significantly reduced the tendency of the main chassis beam to buckle for the first four buckling modes.

The initial bolster design, which bolts onto the main chassis beam web, is analysed using a non-linear contact model. In this case, the mesh density did affect the results. The stress contours where influenced by the shape of the elements of the connection plates in the region of the bolt holes. Refining the mesh through the use of mesh controls on concentric circles around the holes resulted in an improved stress contour, with no influence from the elements boundaries. One of the principal results from the non-linear contact analysis is the identification of a high stress concentration in the region of a critical weld. This resulted in the redesign of the bolsters.

A new bolster design, which is continuous through to both sides, and is bolted on top of the main chassis beam, is developed. The parameters that affect the stress and mass are identified using local sensitivity studies. The bolster design is optimised using the Pro/Mechanica optimisation tool. The results varied for different load cases but several general trends where identified. The final bolster design is a combination of the results of the individual design studies. The optimisation resulted in a mass saving of 16.27%.

The bolster design is analysed using a finite element model. The transverse, longitudinal, vertical and unloading load cases resulted in Von Mises stresses and deflections that are within the bounds of the initial optimisation. The buckling analyses showed that the loads on the bolsters cause local buckling, but the extent of the local buckling and the stresses induced are low enough to exclude buckling as a mode of failure for the bolsters.

A beam frame model is used to investigate structural permutations, and to analyse the response of the trailers to load cases IV and V. Another aspect of the beam frame model is to review the main chassis rail design, with the aim of investigating possibilities for further mass reduction.

It was found that the optimum configuration for the structure is to have supports linking the top of the bolsters, and linking the opposite sides of the end bolsters. This creates a rigid frame with more evenly dispersed stress.

The beam frame model is constrained in a similar manner to the main chassis rail analyses, but includes the effect of the tyre stiffness. The results for load cases IV and V showed that the lateral cornering load (load IV) resulted in the highest stress. The stress is possibly slightly exaggerated due to the nature of the point connections of the suspension unit spring element model. The stress in the structural members for both load cases generally ranges from 30 - 90 MPa, which is relatively low. This prompted the investigation into further mass reductions. A study of the effect of adjusting the flange and web thicknesses revealed that a mass reduction of approximately 20% can be achieved, with a marginal increase in stress in the structure, by reducing the flange and web thicknesses to 10 and 8 mm respectively. Further reduction in the flange and web thicknesses resulted in significantly increased stress levels.

The final design is shown in Figure 6.1. The two main chassis beams are connected with cross-braces, and the bolsters are bolted on top of the upper flanges of the main chassis rails.

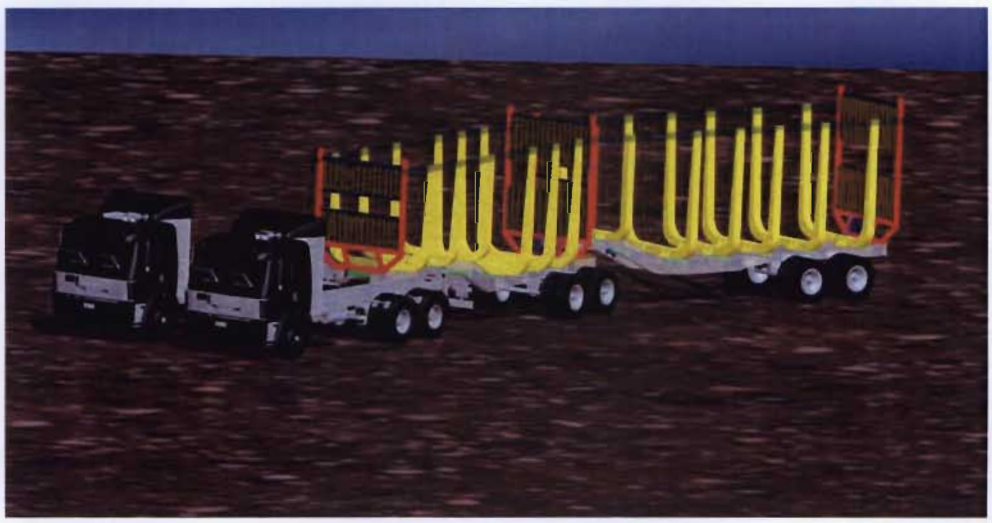

Figure 6.1 The final design

The end bolsters are lighter than the main bolsters, with the primary function of retaining

the cane in the longitudinal direction. The bolsters are linked along their tops, and the end bolsters are linked between the opposite sides. This results in a rigid frame structure.

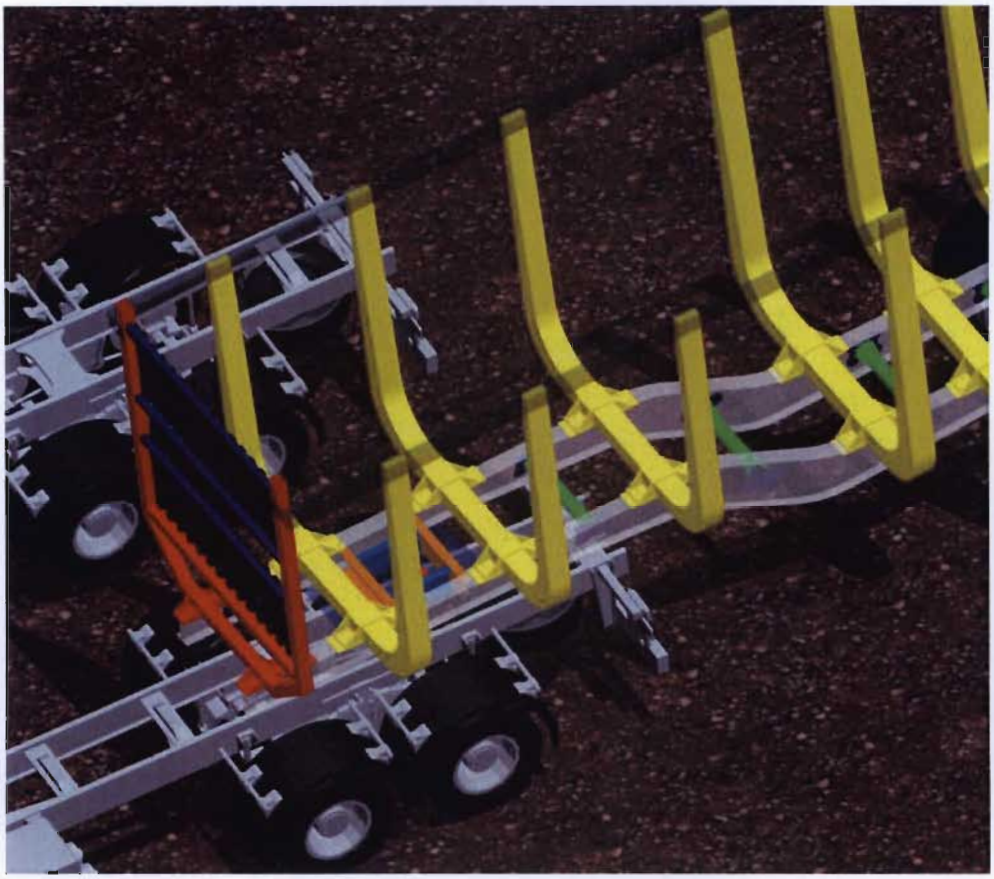

Figure 6.2 The trailer hitch point

The kingpins are the flange-type bolted type, and are attached to a reinforced skid plate as per manufacturers' recommendations (see Figure 6.2).

It is difficult to determine the exact tare mass of the vehicle prior to manufacture, but the estimated chassis tare mass is 6900 kg. This mass does not include the spiller bars and chains, but using nylon strapping and high-strength steel, or possibly a glass fibre composite spiller bar, could result in an overall chassis tare mass of 7900 kg.

The average chassis tare mass of the tandem/tandem interlinks considered in the mass breakdown analysis (see Chapter 1) is 9579.7 kg. The optimised design results in a mass saving of 17.53%, and maximum payload of between 38 - 39 tons, which is substantial when considering the TransSolve simulation in Chapter 1, where an 8.54% tare mass reduction resulted in a 5.8% reduction in transport costs. It must be noted that the cost of cane transportation is a complex issue, and the overall cost is governed by many parameters which include distance, cane density, vehicle finance and offloading time, in addition to the tare mass of the haulage vehicle.

Cane haulage vehicles generally tend to operate under harsh conditions, carrying large payloads on rough terrain. The vehicle in this study has been designed conservatively, with the worst case scenario considered for load cases, and relatively low stresses occurring in the chassis under these loads. This, in conjunction with the additional structure required to retain the cane, results in cane haulage vehicles being inherently heavier than other haulage vehicles (such as timber vehicles).

The information obtained from industry suggests that using static design methods with a safety factor of over 2.0 ensures that fatigue failure will not occur. The majority of cane haulage vehicles are designed using similar methods, and have displayed reasonable structural performance. The opposite aspect of this is that trailers which operate for long periods (up to ten years), are inefficient as they are obviously over designed; a lighter trailer which lasts five years will be more cost effective over its lifespan.

An important aspect of the design is fatigue failure, especially with respect to welded connections. This is taken into account with the initial section optimisation, using an estimated block loading cycle. The block loading cycle is probably an overestimation of the forces that the trailer is subjected; this is substantiated by the low stresses calculate in the analyses and the investigation of the effect of reducing the flange and web thicknesses in Chapter 5. To accurately determine the exact fatigue loading that the vehicle is subjected to, a study involving strain gauges fitted to the chassis is required. Fitting strain

gauges to the vehicle at critical locations (such as the welds on the main chassis beam in the region of the step and the cross braces) would enable the strain history for typical operating conditions to be plotted. From this, an accurate fatigue loading cycle can be obtained using the rain-flow cycle counting method. This would allow for accurate fatigue life prediction, and give more insight into the loads to which the trailers is subjected.

The current trailer designs have reached a state of optimisation through trial and error methods. This is evident from the similarity in appearance of the current designs and the optimised design. The mass tare mass saving achieved through the optimisation of the design, while fairly substantial, is not a leap forward. To further increase the efficiency of sugarcane transportation, developments such as performance based standards, onboard weighing systems and central tyre inflation, will have to be considered.

6.2 Conclusion

The various vehicles used for sugarcane haulage are investigated and compared. The bolster-type tandem/tandem interlink configuration is chosen as the basis for the design. An investigation into trailer design methodologies is conducted. The geometric vehicle parameters were optimised, and resulted in a 30.04% decrease in bending moment.

A method of constraining the trailer models with spring elements was developed. This method resulted in more accurate results from the analyses. The stresses and deflections of the structural components of the chassis are analysed. The bolsters are optimised using an FE based optimisation tool, which resulted in a 16.27% mass saving. An investigation into altering dimensions of the main chassis beam revealed that by reducing the flange and web thicknesses, a 20% mass reduction over the initial beam design can be achieved, with a marginal increase in stress.

The optimised trailer results in a tare mass saving of 17.53%, which in turn results in more efficient sugarcane transportation. Future studies would involve the manufacture of

a prototype and recording of strain histories. This could provide accurate fatigue life data and provide further insight into the loads to which the trailers are subjected.

To gain further savings in transportation costs, the implementation of performance based standards and other developments in heavy vehicle and transportation fields of research must be considered, as the limitations of the current system are close to being reached.

Although the research in this study revealed that the current designs are, in some senses, close to optimal, a mass saving of 17.53% over the average tare mass of 9579.7 kg has been achieved. The actual impact in terms of transport cost and efficiency of this mass saving is difficult to determine. This is due to the many variables affecting the overall cost of sugarcane haulage. However, referring to the TransSolve simulation in Section 1.1.2 (in which an 8.54% reduction in tare mass resulted in a 5.8% reduction in transport costs), a 17.53% reduction in tare mass will definitely reduce the costs of sugarcane transport significantly.